Synthesis of Mesoporous Silica Derived from Layered Sodium Disilicates

層状ジケイ酸塩からのメソポーラスシリカの合成

THESIS SUBMITTED TO WASEDA UNIVERSITY

Tetsuro SHIGENO

March, 2004

CONTENTS

Chapter 1

General Introduction

1.1 Mesoporous Materials Overview

Ordered mesoporous materials have attracted much attention for years because of the excellent physical properties including a huge specific surface area, nanometer scale-fine pores and high stability that are merits for use as a catalyst, catalysis support, inclusion vessels, and an adsorbent. Nowadays, more than 1000 reports on mesoporous materials are published a year.

In the early 90's, Yanagisawa *et al.* discovered mesoporous silicas (denoted as KSW-1 in the thesis) by the reaction of a layered polysilicate kanemite with alkyl-trimethylammonium ($C_nH_{2n+1}(CH_3)_3N^+$, C_nTMA) surfactants.[1] The surfactant assembly plays a role in the formation of ordered mesopores because the pore sizes varying from 2 to 4 nm are dependent on the alkyl chain lengths of C_nTMA ions (n = 12–18). On the other hand, Mobil researchers expanded the availability of surfactant assemblies into the synthesis of ordered mesoporous silicas and aluminosilicates.[2,3] The materials, designated as M41S, have been prepared using the hexagonal, cubic and lamellar liquid-crystal phases of C_nTMA surfactants. The variation in the pore sizes up to 10 nm can also be achieved by changing the amount of 1,3,5-trimethylbenzene (TMB) as an auxiliary organic additive into the C_nTMA micelles. Except for the thermally unstable lamellar mesophase, the M41S materials possess high surface areas above 700 $m^2\ g^{-1}$, pore volumes of 0.79–1.2 $cm^3\ g^{-1}$ and great capacities of organic molecules.

From the viewpoint of the synthesis of extra-large pore molecular sieves, the discovery of KSW-1 and M41S prepared using surfactant assemblies is a breakthrough because zeolites can be usually synthesized using small organic amine molecules and ammonium ions as structure-directing agents. Several structures of the inorganic-surfactant mesophases and the mesoporous materials have been reported up to date. Thus, the reports on the mesostructured and mesoporous materials have intensely increased as the years pass.

1.2 Classification of Ordered Mesoporous Silicas

Ordered mesoporous silicas can be prepared by the reaction between uniform organic assemblies and inorganic species. Therefore, novel ordered mesoporous materials are possibly obtained by utilizing new surfactant assemblies, another organic aggregates as structure-directing agents, and silica source as a starting material. Here, these materials are classified according to the kind of organic assemblies used.

1.2.1 Alkyltrimethylammonium surfactants

C_nTMA ions are the most frequently used surfactants for the synthesis of ordered mesoporous materials.[1-3] FSM-16,[4] which has been prepared by optimizing the reaction condition for KSW-1, has been developed by the groups of both Waseda University and Toyota Central R&D Laboratory Inc. FSM-16 has hexagonal pore arrangements with a *p6m* structure. The materials are one of the most interesting mesoporous materials because the synthetic method using kanemite is unique in the field of the synthesis of mesoporous materials.

M41S family includes hexagonal (*p6m*) MCM-41, cubic ($Ia\bar{3}d$) MCM-48 and lamellar (L□) MCM-50 prepared using the liquid-crystal phases of C_nTMA ions.[2,3] The M41S materials were obtained from the mixtures of C_nTMA ions, silica sources and alumina sources by hydrothermal treatment in basic media. Both C_nTMA/Si molar ratio[5,6] and reaction temperature[7,8] are important for the synthesis of regular C_nTMA-silicate mesophases. can be synthesized in the presence of surfactants with large head groups such as alkyltriethylammonium ($C_nH_{2n+1}(C_2H_5)_3N^+$, C_nTEA) in acidic media.[9,10]

1.2.2 Gemini surfactants

The use of gemini surfactants ($C_nH_{2n+1}(CH_3)_2N^+(CH_2)_sN^+(CH_3)_2C_mH_{2m+1}$, C_{n-s-m}) is

available for the inorganic-surfactant mesostructures design, especially for the formation of surfactant spheres. Stucky and co-workers have reported SBA-2 (3-d hexagonal, $P6_3/mmm$) materials synthesized using divalent quaternary ammonium surfactants (e.g., C_{12-3-1}, C_{14-3-1}, C_{16-2-1}, C_{16-3-1}, C_{16-6-1}, C_{18-3-1}, C_{18-6-1}, C_{20-3-1}) in both basic and acidic media.[9,10] However, the pore system of SBA-2 is not clear because the mesoporous structure is collapsed if all the cages can be connected. SBA-3 ($p6m$) prepared using gemini surfactants (e.g., $C_{16-3-16}$, $C_{16-4-16}$, $C_{16-6-16}$, $C_{16-7-16}$, $C_{16-8-16}$, $C_{16-10-16}$, $C_{16-12-16}$) in acidic media is analogous with MCM-41. MCM-48 and -50 can also be synthesized using gemini surfactants if surfactants are selected appropriately.

1.2.3 Neutral surfactants

Tanev and Pinnavaia have reported a mesoporous silica HMS synthesized using neutral alkylamines ($C_nH_{2n+1}NH_2$, C_nA).[11-15] The assembly of C_nA molecules is worm-like rods and the formation of HMS occurs through self-assembly of hydrogen-bonded C_nA-silicate species. Therefore, the weaker interaction between silicates and C_nA molecules in HMS than the ionic bonds in M41S allows easy removal of C_nA molecules by solvent extraction; high-cost C_nA surfactants can be recovered.

MSU materials reported by Bagshaw *et al.* can be prepared using neutral surfactants which are non-ionic polyethylene oxide (PEO) surfactants.[16] The surfactants are low-cost, nontoxic and biodegradable in comparison with the alkylammonium and alkylamine types of surfactants. MSU-1 and MSU-2 named after the kind of PEO surfactants used such as C_nEO_m and C_nPhEO_m (C_n; alkyl chain, EO_m; ethylene oxide unit, Ph; phenyl group), respectively. Although MSU-type materials have a disordered pore arrangement, Attard *et al.* reported mesoporous silicas prepared using liquid-crystal phases of PEO surfactants.[17] The liquid-crystal phases of PEO surfactants are very sensitive to cosolvents (e.g., methanol, ethanol) formed by the hydrolysis of tetraalkoxysilanes used as silica sources. Therefore, these cosolvents must be removed

to create the well-defined liquid-crystal phases of PEO surfactants.

Zhao *et al.* have expanded the availability of PEO surfactants into the synthesis of mesoporous silicas with ordered structures in acidic media without removal of ethanol evolved from tetraethoxysilane (TEOS).[18] Periodic arrangements of mesoscopically ordered pores with cubic $Im\bar{3}m$, cubic $Pm\bar{3}m$ (or others) (SBA-11), 3-d hexagonal ($P6_3/mmc$) (SBA-12), 2-d hexagonal ($p6m$), and lamellar (L□) symmetries have been successfully reported. The structures depend on the alkyl chain lengths and the lengths of EO moieties.

1.2.4 Block copolymers

Bagshaw *et al.* have showed the availability of commercial triblock copolymer $(PEO)_{13}(PPO)_{30}(PEO)_{13}$ (PEO; polyethylene oxide block, PPO; polypropylene oxide block) for the formation of a mesoporous silica MSU-3.[16] MSU-3 has a disordered structure and can be obtained by just adding TEOS to a triblock copolymer aqueous solution; the pore size of MSU-3 was 5.8 nm.

Recently, Stucky and co-workers reported triblock copolymer syntheses of well-defined hexagonal ($p6m$) mesoporous silicas SBA-15 at appropriate temperatures (35–80 °C) according to the used triblock copolymer in acidic media.[18,19] At pH = 1, positively charged protonated silicate species interact preferentially with the more hydrophilic PEO block or blocks to promote cooperative self-assembly of a silica-block-polymer-rich mesophase from a dilute water-rich phase. Concurrent and further condensation of the silicate species in the presence of the block copolymer surfactant species results in the formation of the mesophase silicate composite and therefore the wall thicknesses were 3.1–6.4 nm, being larger than those observed for mesoporous silicas prepared using surfactant assemblies.[3] The absence of sufficiently strong electrostatic or hydrogen-bonding interactions at pH values of 2–7 leads to the formation of amorphous or otherwise disordered silicas such as MSU-3.

By using many $(PEO)_m(PPO)_n(PEO)_m$ triblock copolymers where (m, n) were (5, 70), (20, 70), (17, 85), (20, 30), (26, 39), (13, 70), and (19, 33),[18,19] hexagonal SBA-15 materials with pore sizes ranging of 4.6 to 10 nm can be obtained, especially the pore size was varied up to 30 nm by using TMB as a solubilizing agent. The assembly of $(PEO)_m(PPO)_n(PEO)_m$ possesses a greater adsorption capacity of organic molecules than those of C_nTMA surfactant assembly. A cubic ($Im\bar{3}m$) mesoporous silica SBA-16 can be prepared using triblock copolymer such as $(PEO)_{106}(PPO)_{70}(PEO)_{106}$, $(PEO)_{100}(PPO)_{39}(PEO)_{100}$ and $(PEO)_{80}(PPO)_{30}(PEO)_{80}$. A larger PEO/PPO ratio (> 1.5) tends to favor the formation of SBA-16. In addition, a lamellar mesophase silicate can be also obtained using $(PEO)_5(PPO)_{70}(PEO)_5$.

Antonietti and co-workers also reported the preparation of mesoporous silicas with new pore morphologies using assemblies of ionic block copolymers.[20,21] An anionic poly(ethylethylene)-*b*-polystylenesulfonate block was utilized as an organic aggregate. Depending on the relative block lengths and the salt content in the reaction mixture, different aggregation structures were obtained, leading to well-defined spherical pores in the range of 10–50 nm, more complex architectures (rattles) and casts of multilamellar vesicles.

1.2.5 Other organic assemblies

Schacht *et al.* reported the synthesis of mesoporous macroscale structures using surfactant assemblies at oil-water interfaces (emulsion) in acidic media.[22] Emulsions acted as a morphology-controlling agent and C_nTMA surfactants confirmly played a role in a structure-directing agent. In contrast, Impof and Pine showed the availability of emulsions as structure-directing agents for the synthesis of ordered macroporous materials.[23] The surfactant was a symmetric poly(ethylene glycol)-poly(propylene glycol)-poly(ethylene glycol) triblock copolymer with a relative molecular mass of 5,800 containing 30 % by weight of ethylene glycol monomer. The pore size of obtained

materials was greater than 50 nm.

1.3 Formation of Silicate-Surfactant Mesophases

The preparation of inorganic-surfactant mesophases is the first process for mesoporous materials synthesis. Many researches on both silicate-surfactant mesophases and mesoporous silicas have been conducted. Some of the most important factors for the formation of inorganic-surfactant mesophases are summarized here.

1.3.1 Formation mechanism of the mesophases

Both FSM-16 and MCM-41 have the same hexagonal (*p6m*) structure, however, the morphology of each material is quite different. The morphology of FSM-16 is similar to the original kanemite and that of MCM-41 is, for example, hexagonal prisms. The formation mechanisms of these two materials should be mainly described to understand the preparation of precursors of representative mesoporous materials.

1.3.1.1 Formation mechanism of FSM-16

Inagaki *et al.* have proposed "Folded Sheets Mechanism" (Figure 1-1, pathway (1)).[4,24,25] Also, higher pH over 11.5 at the reaction process and the subsequent pH adjustment at 8.5 at the condensation process were best suited for the formation of FSM-16 with high regularity and thermal stability. However, Chen *et al.* pointed out that kanemite sheets are dissolved during the reaction[26] because of the high pH condition.[25] Nevertheless, because the pH value during the synthesis of KSW-1 by Yanagisawa *et al.* was kept between 8 to 9,[1] Chen *et al.* have proposed the other mechanism (Figure 1-1, pathway (2)).[25] The framework of KSW-1 was confirmly derived from silicate sheets of kanemite, however, the silicate sheets decomposed locally

surrounded the assemblies of C_nTMA ions.

O'Brien *et al.* studied the formation process of FSM-16 obtained from Inagaki's method by *in situ* XRD.[27] A layered intermediate is present in the initial stage of the reaction. For the formation process of MCM-41, incipient peak due to the hexagonal phase was observed directly. Therefore, the formation process of FSM-16 is quite different from that of MCM-41, indicating that kanemite sheets are not dissolved during the synthesis of FSM-16 even at higher pH conditions. If "Folded Sheets Mechanism" is true, an obtained C_nTMA-kanemite complex has an orthorhombic structure and two kinds of silicate wall thicknesses (single SiO_4 sheets and double SiO_4 sheets). However, the wall thickness of the obtained C_nTMA-kanemite complex is almost constant in each product by TEM.[25,28] Then, FSM-16 can be formed from kanemite through making a domain structure with a hexagonal symmetry by condensation of silicate which might be derivative of kanemite sheets.

Formation mechanism of mesoporous silicas derived from kanemite has not been demonstrated yet, thus further research is definitely necessary for better understanding of the formation mechanism. At least, the fact that KSW-1 and FSM-16 are obtained from kanemite is confirmed based on the above reports and the materials can be formed by the different formation process from that of MCM-41.

1.3.1.2 Formation mechanism of MCM-41

The liquid-crystal templating (LCT) mechanism for the formation of MCM-41 have been proposed by Mobil researchers.[2,3] The syntheses of the M41S materials were carried out in basic media. Two formation routes (Figure 1-2) could be initially considered in order to assemble hexagonal arrays of C_nTMA surfactant rods.

Chen *et al.* determined the synthesis mechanism of MCM-41 by powder XRD, thermogravimetric (TG) and ^{29}Si MAS NMR in combination with *in situ* ^{14}N MAS NMR.[29] The results revealed that the liquid-crystal phase (pathway 1) was not present

in the synthesis medium during the formation of MCM-41. They have promoted the pathway 2 and modified as follows. Randomly ordered rod-like micelles interact with silicate species to yield approximately two or three monolayers of encapsulation around the external surfaces of the micelles. Subsequently, those composite species spontaneously assemble into the long-range ordered hexagonal structure. With further heating, the silicate species in the interstitial species of ordered organic-inorganic composite phase continue to condense.

The initial presence of surfactant liquid-crystal phases is not important for the formation of M41S. A schematic phase diagram for C_{16}TMABr in water is shown in Figure 1-3, indicating that higher concentration over 35 wt % is necessary to generate liquid-crystal phases of only C_nTMA ions. For the first reports on the synthesis of M41S, [2,3] MCM-41 was synthesized using a high concentration C_nTMA aqueous solution (26 wt %). However, MCM-41 can be also obtained using even lower concentration of C_{16}TMA ions above the critical micelle concentration.[30] Therefore, Huo *et al.* have reported that the cooperative organization of inorganic-organic interfaces in the formation of surfactant-silicate mesophases, as shown in Figure 1-4.[31,32] Depending on the concentration of the surfactant, the initial organic precursor consists of spherical or cylindrical (or ellipsoidal) micelles. There is a strong interaction between the cationic surfactant and anionic silicate species. Nucleation, growth and phase transitions may be directed by the charge density, coordination and steric requirements of the inorganic and organic species at the interface and not necessarily by a preformed structure.

On the other hand, Monnier *et al.* have proposed another formation mechanism for MCM-41.[33] The transformation of lamellar into hexagonal mesophases can be occurred through the formation of MCM-41 in basic media. Such transformation is possible based on the charge balance between inorganic and organic species as described later. Depending on the extent for condensation silicate species, the amount of surfactant molecules included in the silicate-surfactant mesophases is limited. Therefore, with the

progress in condensation of silicate species, hexagonal mesophases are likely to form because the amount of surfactant molecules decreases. However, many research groups have claimed that these transformation has never been found during the synthesis of MCM-41. Although Monnier *et al.* have showed that the hexagonal mesophase was obtained through the lamellar mesophase by hydrothermal post-treatment at pH = 7,[33] it is not clear at present whether such transformation of lamellar into hexagonal mesophases can occur in basic media during the formation medium of MCM-41 or not.

Steel *et al.* also proposed the same formation mechanism of hexagonal and lamellar mesophases.[34] By ^{14}N MAS NMR measurements, hexagonal and rod-like (and/or spheres) assemblies were observed. Then, they suggested that rod-like micelles form initially during the formation of M41S materials. However, O'Brien *et al.* investigated the formation process of MCM-41 by *in situ* XRD.[27] The result indicates that the peak at the *d*-spacing of 4 nm due to a hexagonal phase can be observed at the initial stage of the formation of MCM-41.

1.3.2 Packing parameter of surfactant molecules

Israelachvili *et al.* have demonstrated that the classical and contemporary molecular description of surfactant organization in amphiphilic liquid-crystal arrays is described in terms of the local effective surfactant packing parameter ($g = V / (a_0 l)$), where V is the total volume of surfactant chain, a_0 is the effective head group area at micelle surface, and l is the kinetic surfactant tail length or the curvature elastic energy.[35] This theory is simple and accounts for many of the observed physical properties of micelles. Depending on the g value, the geometry of surfactant assemblies can be decided. For example, when the g values are 1/3, 1/2 and 1, geometrical forms of surfactant assemblies are spheres, cylindrical micelles and planar bilayers, respectively.

Stucky and co-workers have synthesized mesophase silicates using various surfactant molecules and have some efforts to understand surfactant-silicate

mesostructures in detail by utilizing the packing parameter of surfactant molecules.[9,10] The representative results are described as follows. (1) For $C_{16}H_{33}R_3N^+$, obtained mesostructures changed from hexagonal (*p6m*) to cubic ($Pm\bar{3}n$) when R was varied from CH_3 to C_2H_5 (at room temperature for 1 h in acidic media). (2) For $(C_{16}H_{33})(C_mH_{2m+1})N^+(CH_3)_2$, lamellar mesophases can be obtained with the increase in alkyl chain lengths ($m > 4$) (at 100 °C for 1 week in basic media). (3) For $C_{16}H_{33}(CH_3)_2N^+(C_sH_{2s})N^+(CH_3)_2C_{16}H_{33}$, corresponding obtained mesostructures were varied from lamellar to hexagonal (*p6m*), cubic ($Ia\bar{3}d$) with the increase in spacer lengths (at 100 °C for 1 day in basic media). These results reveal that the use of the packing parameter of surfactant molecules is intensely available for the interpretation of obtained mesostructures.

However, this theory is not always useful for the decision of mesostructures. The mesostructures can be changed by varying the synthetic conditions such as reaction temperature, reaction time and pH of the starting mixtures.[10] Also, materials with different mesostructures can be prepared even when the same surfactants are used.[2,3,9,10] Although the description of mesostructures using the packing parameter is above all reliable for low temperature synthesis in acidic media because of weak interaction between inorganic and surfactant phases, inorganic-surfactant mesostructures must be considered not only the packing parameter but also the charge balance between inorganic and organic phases as described later.

1.3.3 Charge balance between inorganic and surfactant phases

For aluminosilicate and pure-silica zeolites, the frameworks are composed SiO_4 and AlO_4 units with complete condensation. However, SiO_4 units with both Q^4 (SiO ! *Si*–O–Si) and Q^3 (SiO ! *Si*–O^-) environments are present in C_nTMA-silicate mesophases because the charge balance between anionic silicate species and cationic surfactants must be satisfied on the whole. Therefore, cationic C_nTMA surfactants can be present in the

mesophase up to the amount of SiO_4 units with Q^3 environment in the silicate framework. Moreover, Chen *et al.* have suggested that complete condensation of the silicate species is impossible because the presence of SiO^- species are necessary for charge compensation of the occluded alkylammonium ions.[29]

Based on ^{29}Si MAS NMR results for mesophase silicates with various structures,[31] the Q^3/Q^4 ratios of lamellar, hexagonal and cubic ($Pm\bar{3}n$) mesophase silicates are 1.4, 1.1 and 1.1, respectively. Therefore, the control of condensation of silicate species possibly leads to the mesostructures design. The charge of silicate frameworks of inorganic-surfactant mesophases can be easily changed by variation in synthetic conditions such as surfactant/Si ratio of starting gel, reaction temperature, reaction time, pH of starting gel, pH adjustment of resultants, and so on. The variation in the change density leads to the structural change of obtained mesophases.

Monnier *et al.* have showed the phase transformation of hexagonal into lamellar mesophases by hydrothBrsing such hydrothermal post-treatment.[10,36-39] During the observations, condensation of silicate frameworks is developed and therefore the charge of the silicate frameworks decreases by the hydrothermal post-treatment. Fyfe *et al.* reported the phase transition from a layered complex, which was composed of double-four-ring silicates $Si_8O_{16}^{8-}$ and C_{16}TMA cations, to cubic ($Ia\bar{3}d$), to lamellar and to hexagonal ($p6m$) mesophase silicates in tune by acid-treatment. [36] In this phase transformation, the Q^3/Q^4 ratios of the products decreases, therefore the charge of silicate frameworks also decreases. In addition, the post-treatment and/or the variation in both reaction temperature and time also lead to restructuring of mesophase silicates.[40-44] During the reactions, d_{100} values of obtained products increased with the post-treatment or with higher reaction temperature and longer reaction time. It is necessary for the extension of d_{100} values that the silicate frameworks decompose, rearrange and re-bond.

From the viewpoint of the charge balance, it can be interpreted the formation of mesoporous or microporous silicas reported by Mobil researchers.[7] The MCM-41 materials were obtained at 100 °C and the crystallinity improved with increasing

surfactant chain length used. At higher temperature (150 °C) the C_{14} and C_{16} systems formed well-defined hexagonal structures. At 200 °C, MCM-41 type products were not obtained even for longer alkyl chain surfactant systems. It is quite important for the formation of MCM-type materials to form and/or to stabilize surfactant micelles. As results, condensation of silicate species is suppressed at lower temperature and complete condensation of silicate species occurs at higher temperature. After the complete condensation, silicate frameworks hardly have anionic charge and then it is not possible to make an interaction between C_nTMA cations and silicate framework.

From the facts mentioned above, the charge balance between inorganic and surfactant phases is also important for the synthesis of inorganic-surfactant mesostructured materials. That is, both the packing parameter of surfactant molecules and the charge balance on the whole is needed for the mesostructured design. To understand these two factors for the synthesis of mesostructured materials is quite important for the preparation of mesostructured materials.

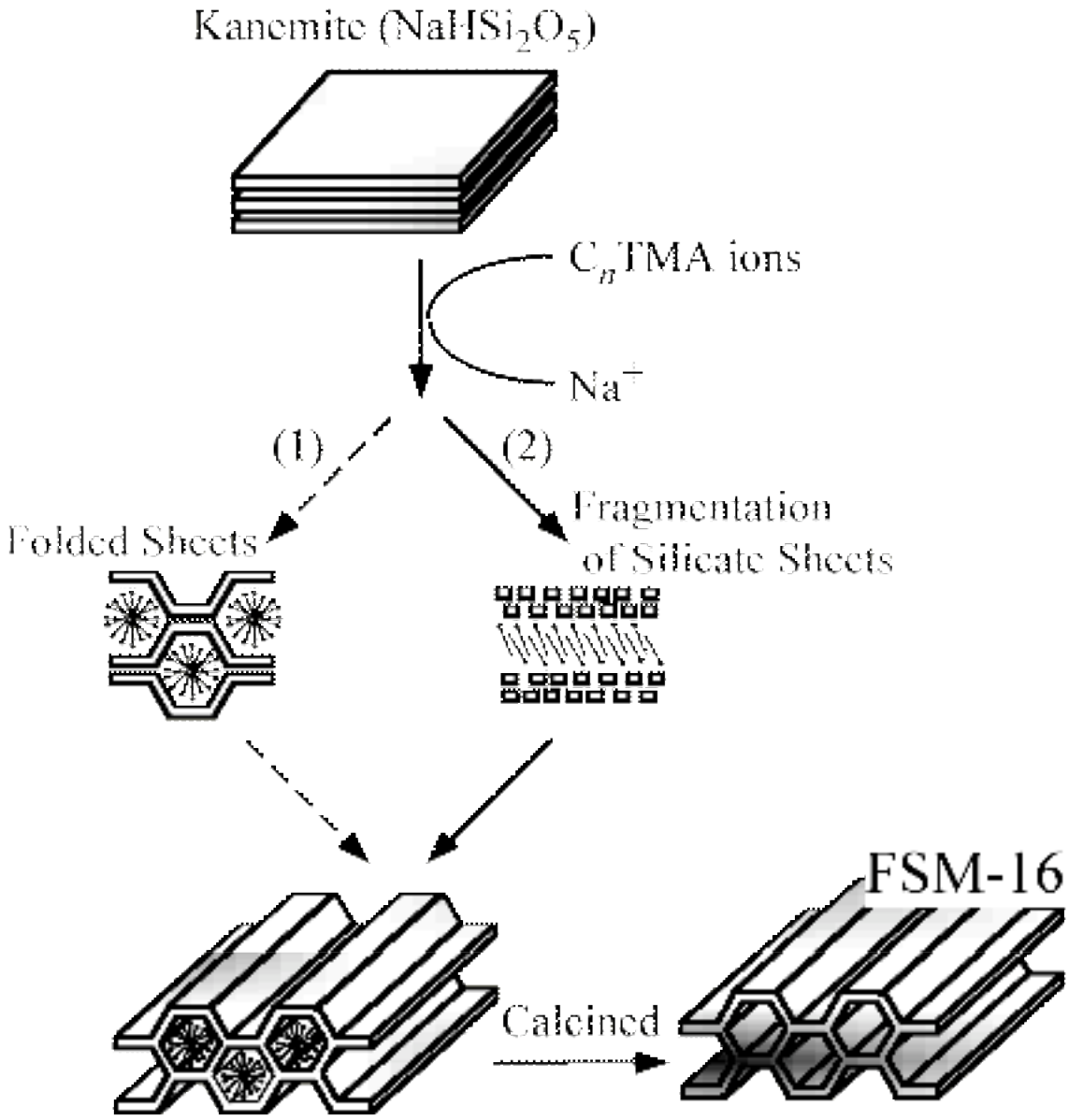

Figure1-1. Schematic model for the formation of mesoporous silicas derived from kanemite.[24,26]

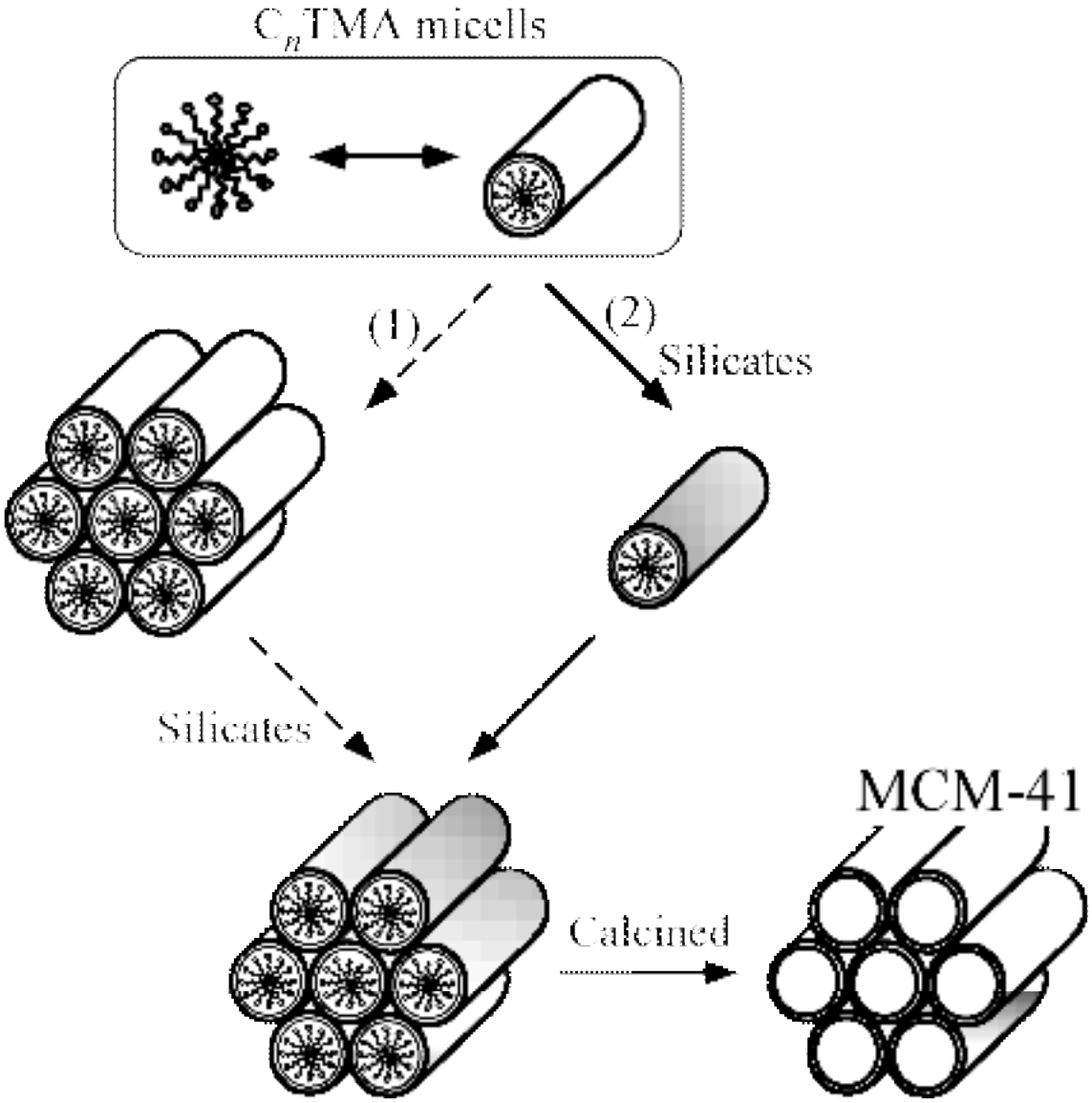

Figure1-2. Possible mechanistic pathways for the formation of MCM-41: (1) liquid-crystal phase initiated and (2) silicate anion initiated.[3]

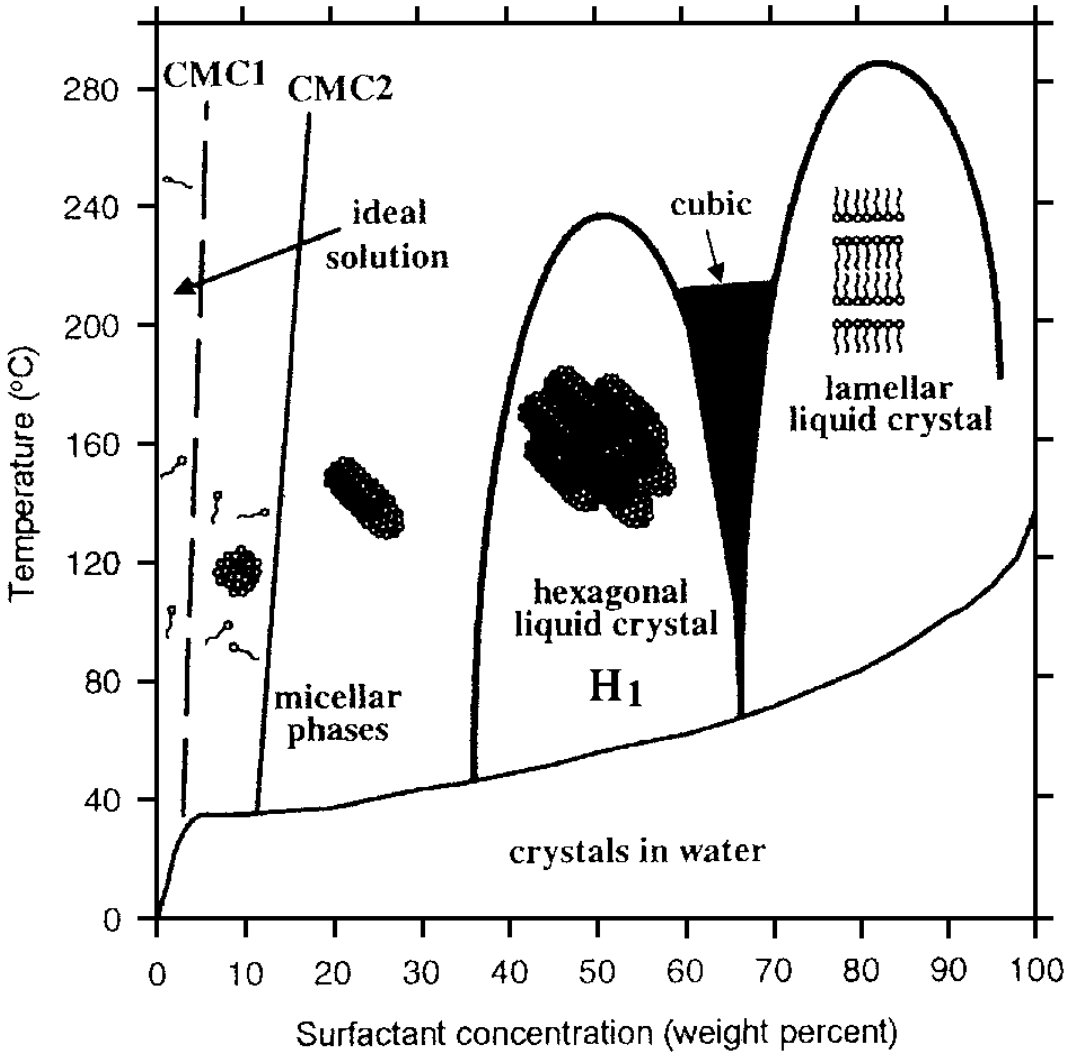

Figure1-3. Schematic phase diagram of C_{16}TMABr in water.

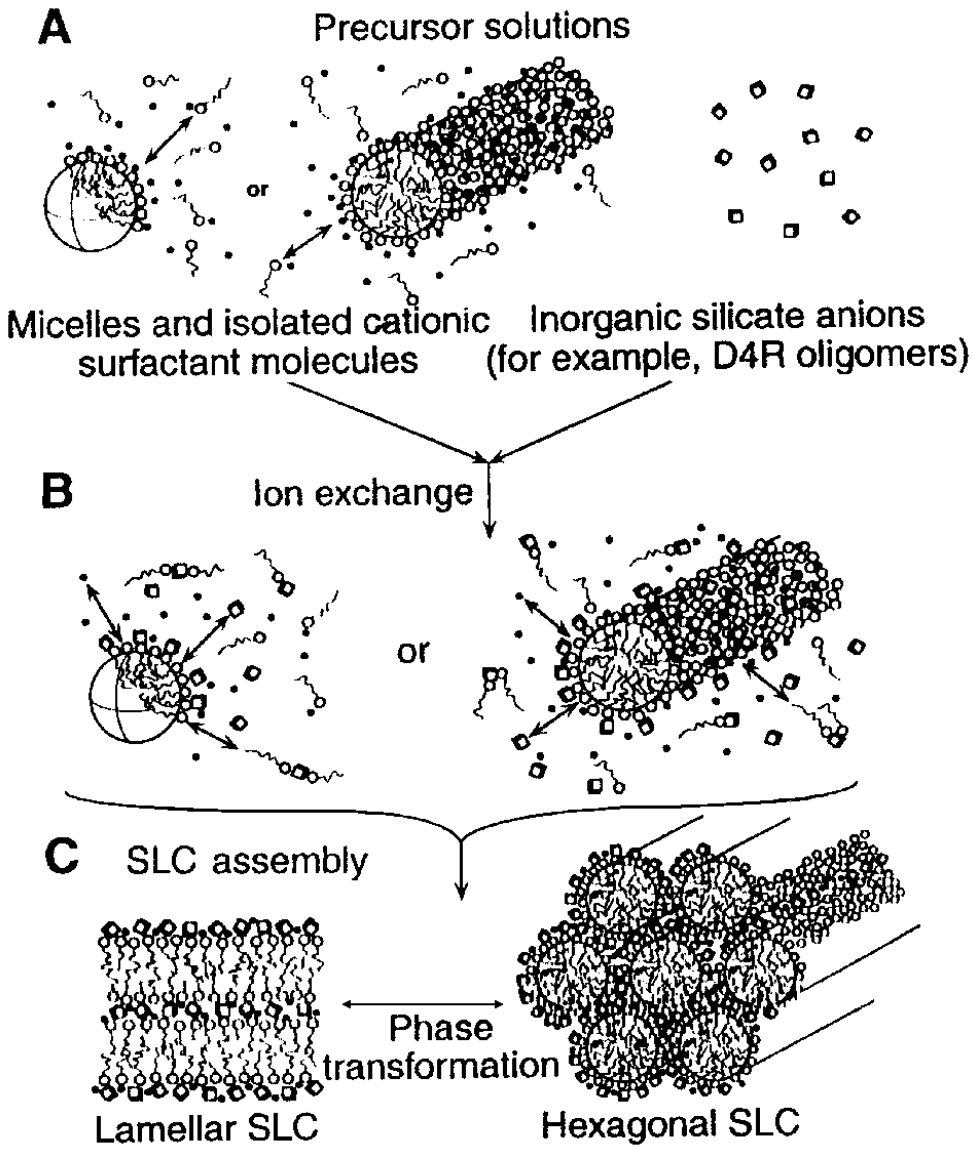

Figure1-4. Schematic diagram of the cooperative organization of silicate-surfactant mesophases. (A) Organic and inorganic precursor solutions. (B) Immediately after the two precursor solutions are mixed. (C) Multidentate interactions of oligomeric silicate units with the surfactant molucules.[32]

1.4 Mesoporous silica derived from layered polysilicate

Before the discovery of mesoporous silica derived from kanemite, there are some porous materials derived from minerals. These materials are so-called pillared-layered sstructures (PLS). However, because of the pore sizes of these materials limited in the region of micropore, the application to relatively large molecule is difficult. Mesoporous silica derived from kanemite, such as FSM-16, KSW-1, and KSW-2, are synthesized by using □–$Na_2Si_2O_5$ as a starting material.[1,24,45] Generally, ordered mesoporous silicas are synthesized with soluble silica source. However, the difference of silica source effects on resulting mesoporous silica. In situ time-resolved energy-dispersive XRD was used by O'Brien et al. to investigate the formation of the mesoporous silicates FSM-16 and MCM-41.[46] Both materials display a similar arrangement of hexagonal mesopores. They differ in the nature of the silica source used for their synthesis, the former being prepared from the layered polysilicate kanemite. The results indicate that the as-synthesized FSM-16 forms from a medium containing a number of intercalated silicate phases; whereas, under the experimental conditions used, no ordered silicate-surfactant phases can be detected during the formation of the MCM-41 phase. This study supports the proposal that the FSM-16 hexagonal phase is derived from the kanemite sheets. The advantage of using kanemite in the synthesis of mesoporous silica is that structural unit of kanemite sheet remains to some extent.[45]

Mesostructures, which are formed through the cooperative organization in the inorganic-surfactant systems, have often been explained by the geometrical packing of surfactant molecules because monomeric and/or oligomeric soluble precursors are mainly used as inorganic sources. The surfactant molecules themselves are uniformly assembled in aqueous solutions depending on the conditions including the geometrical packing of surfactant molecules, while the presence of inorganic species attached to the hydrophilic head groups plays an important role in the mesostructural variation. The geometrical packing of surfactant molecules containing attached inorganic species should

be considered because the charge density of inorganic frameworks is changed by condensation which results in the variation in the amount of accommodated surfactant molecules in the mesostructured materials. However, the mesostructures of ordered mesoporous silicas derived from a layered polysilicate kanemite (FSM-16 and KSW-2) cannot be explained in the same manner because kanemite has two-dimensionally connected silicate networks. The formation of FSM-16 and KSW-2 is much complicated than those of other ordered mesoporous silicas (MCM-41, SBA-15, etc.). Being different from intercalation compounds, kanemite is an attractive layered material applicable for the synthesis of ordered mesoporous silicas. The individual silicate sheets in kanemite are composed of only tetrahedral SiO_4 unit. By the presence of two-dimensionally connected silicate networks, ordered mesoporous silicas with three-dimensionally connected mesopores that are observed for MCM-48, SBA-1, and SBA-2 have never been synthesized in the surfactant-kanemite systems. The formation of disordered (KSW-1) and 2-d hexagonal mesoporous silica (FSM-16) by direct reaction of kanemite with alkyltrimethylammonium (C_nTMA) surfactants has been well recognized. The formation of an orthorhombic mesostructure (KSW-2) is understood on the basis of both the geometrical packing of C_{16}TMA and the interactions of the cationic head groups with the silicate sheets. The assemblies of C_{16}TMA molecules within semi-squared spaces cannot simply be explained by using the geometrical packing. The semi-squared arrangements have never been found among the mesostructured materials reported so far. All the mesostructures are governed by the geometrical packing of surfactant molecules used. The orthorhombic mesostructure is formed through the bending of the individual silicate sheets that are not so flexible as monomeric and/or oligomeric silica species. Thus, the surface curvature of the silicate sheets does not match that of C_{16}TMA assemblies completely and the C_{16}TMA molecules are encapsulated within the semi-squared spaces because of the interactions of the cationic head groups of the C_{16}TMA molecules with the silicate sheets.

1.5 The Aim of the Thesis

There have been a great deal of researches on some kinds of mesostructured and mesoporous silicas since the discovery of ordered mesoporous silicas prepared using organic assemblies. Silica-based mesostructured and mesoporous materials can be fully discussed by using several factors such as formation mechanisms, the interaction of inorganic/surfactant interfaces, the packing parameter of surfactant molecules, the charge balance between inorganic and surfactant phases on the whole, and so on, though

There have been many reports on the uses of ordered mesoporous silicas for catalysts, catalysts supports and adsorbents. However, mesoporous silicas have a few problems against such applications. First, the silicate frameworks are amorphous, and then strong acid sites as well as those in zeolites are not present. Second, pore diameters caused by removal of organic aggregates are too large to handle fine chemicals and their intermediates effectively. It is necessary for resolving these problems to prepare novel mesoporous materials to attempt to synthesize mesoporous silicas with crystalline silicate frameworks by a designed synthetic strategy, such as using crystallinity in starting layered silicate.

In this thesis, the following studies have been conducted from the view point of novel mesostructured and mesoporous materials synthesis using surfactant assemblies based on the above background.

In order to understand the surfactant-kanemite systems to produce mesostructured materials, the reactions of kanemite with various cationic surfactants that are assembled with larger surface curvatures is carried out. In addition, despite the interesting structural and synthetic aspects, studies on the effect of the alkyl chain length of C*n*TMA upon the formation of KSW-2 have not been conducted yet. The length of the alkyl chain should affect the bending of the silicate sheets because of the differences in the packing parameters and the resultant curvature. Therefore, the influence of the alkyl chain length of C*n*TMA on the formation of the precursor to KSW-2 and the possibility

of the pore width control are investigated.

As mentioned in 1.3, as-synthesized FSM-16 is formed through the fragmentation of individual silicate sheets in kanemite, while a mesostructured precursor of KSW-2 is formed through the bending of the individual silicate sheets. In addition, the remaining structural units originated from kanemite in KSW-2 are very interesting in order to improve the functions. Thus, the incorporation of Al into the framework of KSW-2 is carried out to clear how difference in synthetic scheme effects on the physical and catalytic properties.

In contrast to conventional mesoporous silicas composed of amorphous silica walls, the mesostructured precursor of KSW-2 possesses the silicate units originated from kanemite in the wall to some extent. It is interesting that the wall structure of the precursor is composed of partly intralayer-condensed individual silicate sheets in kanemite. Nevertheless, the ordering of the wall structure was reduced during calcination to remove organic fractions. Therefore, a mesostructured precursor of KSW-2 was directly modified with silylating agents on the presumption that the wall might have some regularities after the modification.

Synthesis of mesoporous silicas from layered alkyltrimethylammonium-hydrated sodium disilicate complexes is carried out. This synthetic route is very available for not only mesostructures design but also inorganic framework design because of the differences in the structure of starting material.

1.6 References

(1) Yanagisawa, T.; Shimizu, T.; Kuroda, K.; Kato, C. *Bull.Chem. Soc. Jpn.* 1990, **63**, 988.

(2) Kresge, C. T.; Leonowicz, M. E.; Roth, W. J.; Vartuli, J. C.; Beck, J. S. *Nature* 1992, **359**, 710.

(3) Beck, J. S.; Vartuli, J. C.; Roth, W. J.; Leonowicz, M. E.; Kresge, C. T.; Schmitt, K. D.; Chu, C. T.-W.; Olson, D. H.; Sheppard, E. W.; McCullen, S. B.; Higgins, J. B.; Schlenker, J. L. *J. Am. Chem. Soc.* 1992, **114**, 10834.

(4) Inagaki, S.; Fukushima, Y.; Kuroda, K. *Studies Surf. Sci. Catal.* 1994, **84**, 125.

(5) Vartuli, J. C.; Schmitt, K. D.; Kresge, C. T.; Roth, W. J.; Leonowicz, M. E.; McCullen, S. B.; Hellring, S. D.; Beck, J. S.; Schlenker, J. L.; Olson, D. H.; Sheppard, E. W. *Chem. Mater.* 1994, **6**, 2317.

(6) Vartuli, J. C.; Schmitt, K. D.; Kresge, C. T.; Roth, W. J.; Leonowicz, M. E.; McCullen, S. B.; Hellring, S. D.; Beck, J. S.; Schlenker, J. L.; Olson, D. H.; Sheppard, E. W. *Stud. Surf. Sci. Catal.* 1994, **84**, 53.

(7) Beck, J. S.; Vartuli, J. C.; Kennedy, G. J.; Kresge, C. T.; Roth, W. J.; Schramm, S. E. *Chem. Mater.* 1994, **6**, 1816.

(8) Beck, J. S.; Vartuli, J. C.; Kennedy, G. J.; Kresge, C. T.; Roth, W. J.; Schramm, S. E. *Stud. Surf. Sci. Catal.* 1994, **98**, 15.

(9) Huo, Q.; Leon, R.; Petroff, P. M.; Stucky, F. D. *Science* 1995, **268**, 1324.

(10) Huo, Q.; Margolese, D. I.; Stucky, G. D. *Chem. Mater.* 1996, **8**, 1147.

(11) Tanev, P. T.; Chibwe, M.; Pinnavaia, T. J. *Nature* 1994, **368**, 321.

(12) Tanev, P. T.; Pinnavaia, T. J. *Science* 1995, **267**, 865.

(13) Zhang, W.; Froba, M.; Wang, J.; Tanev, P. T.; Wong, J.; Pinnavaia, T. J. *J. Am. Chem. Soc.* 1996, **118**, 9164.

(14) Tanev, P. T.; Pinnavaia, T. J. *Chem. Mater.* 1996, **8**, 2068.

(15) Zhang, W.; Pauly, T. R.; Pinnavaia, T. J. *Chem. Mater.* 1997, **9**, 2491.

(16) Bagshaw, S. A.; Prouzet, E.; Pinnavaia, T. J. *Science* 1995, **269**, 1242.

(17) Attard, G. S.; Glyde, J. C.; Goeltner, G. *Nature* 1995, **378**, 366.

(18) Zhao, D.; Huo, Q.; Feng, J.; Chmelka, B. F.; Stucky, G. D. *J. Am. Chem. Soc.* 1998, **120**, 6024.

(19) Zhao, D. Y.; Feng, J. L.; Huo, Q. S.; Melosh, N.; Fredrickson, G. H.; Chmelka, B. F.; Stucky, G. D. *Science* 1998, **279**, 548.

(20) Göltner, C. G.; Henke, S.; Weissenberger, M. C.; Antonietti, M. *Angew. Chem. Int. Ed. Engl.* 1998, **37**, 613.

(21) Krämer, E.; Förster, S.; Göltner, C.; Antonietti, M. *Langmuir* 1998, **14**, 2027.

(22) Schacht, S.; Huo, Q.; Voigt-Martin, I. G.; Stucky, G. D.; Schüth, F. *Science* 1996, **273**, 768.

(23) Imhof, A.; Pine, D. J. *Nature* 1997, **389**, 948.

(24) Inagaki, S.; Fukushima, Y.; Kuroda, K. *J. Chem. Soc., Chem. Commun.* 1993, 680.

(25) Inagaki, S.; Koiwai, A.; Suzuki, N.; Fukushima, Y.; Kuroda, K. *Bull. Chem. Soc. Jpn.* 1996, **69**, 1449.

(26) Chen, C.-Y.; Xiao, S.-Q.; Davis, M. E. *Microporous Mater.* 1995, **4**, 1.

(27) O'Brien, S.; Francis, R. J.; Price, S. J.; O'Hare, D.; Clark, S. M.; Okazaki, N.; Kuroda, K. *J. Chem. Soc., Chem. Commun.* 1995, 2423.

(28) Sakamoto, Y.; Inagaki, S.; Ohsuna, T.; Ohnishi, N.; Fukushima, Y.; Nozue, Y.; Terasaki, O. *Micoporous Mesoporous Mater.* 1998, **21**, 589.

(29) Chen, C.-Y.; Li, H.-X.; Davis, M. E. *Microporous Mater.* 1993, **2**, 17.

(30) Cheng, C.-F.; Luan, Z.; Klinowski, J. *Langmuir* 1998, **11**, 2815.

(31) Huo, Q.; Margolese, D. I.; Ciesla, U.; Demuth, D. G.; Feng, P.; Gier, T. E.; Sieger, P.; Firouzi, A.; Chmelka, B. F.; Schüth, F.; Stucky, G. D. *Chem. Mater.* 1994, **6**, 1176.

(32) Firouzi, A.; Kumar, D.; Bull, L. M.; Besier, T.; Sieger, P.; Huo, Q.; Walker, S. A.; Zasadzinski, J. A.; Glinka, C.; Nicol, J.; Margolese, D.; Stucky, G. D.; Chmelka,

B. F. *Science* 1995, **267**, 1138.

(33) Monnier, A.; Schüth, F.; Huo, Q.; Kumar, D.; Margolese, D.; Maxwell, R. S.; Stucky, G. D.; Krishnamurty, M.; Petroff, P.; Firouzi, A.; Janicke, M.; Chmelka, B. F. *Science* 1993, **261**, 1299.

(34) Steel, A.; Carr, S. W.; Anderson, M. W. *J. Chem. Soc., Chem. Commun.* 1994, 1571.

(35) Israelachvili, J. N.; Mitchell, D. J.; Ninham, B. W. *J. Chem. Soc., Faraday Trans*. 1976, **72**, 1525.

(36) Fyfe, C. A.; Fu, G. *J. Am. Chem. Soc.* 1995, **117**, 9709.

(37) Chen, X.; Huang, L.; Li, Q. *J. Phys. Chem. B* 1997, **101**, 8460.

(38) Gallis, K. W.; Landry, C. C. *Chem. Mater.* 1997, **9**, 2035.

(39) Luan, Z.; He, H.; Zhou, W.; Klinowski, J. *J. Chem. Soc., Faraday Trans*. 1998, **94**, 979.

(40) Cheng, C.-F.; Zhou, W.; Park, D. H.; Klinowski, J.; Hargreaves, M.; Gladden, L. F. *J. Chem. Soc, Faraday Trans*. 1997, **93**, 359.

(41) Chen, C.-F.; Zhou, W.; Klinowski, J. *Chem. Phys. Lett.* 1996, **263**, 247.

(42) Sayari, A.; Liu, P.; Kruk, M.; Jaroniec, M. 1997, **9**, 2499.

(43) Kruk, M.; Jaroniec, M.; Sayari, A. *Langmuir* 1997, **13**, 6267.

(44) Corma, A.; Kan, Q.; Navarro, M. T.; Pérez-Pariente, J.; Rey, F. *Chem. Mater.* 1997, **9**, 2123.

(45) Kimura, T.; Kamata, T.; Fuziwara, M.; Takano, Y.; Kaneda, M.; Sakamoto, Y.; Terasaki, O.; Sugahara, Y.; Kuroda, K. *Angew. Chem. Int. Ed.* 2000, **39**, 3855.

(46) O'Brien, S.; Francis, R. J.; Fogg, A.; O'Hare, D.; Okazaki, N.; Kuroda, K. *Chem. Mater.* 1999, **11**, 1822.

Chapter 2

Silica-Based Mesostructured Materials Induced by Surfactant Assemblies within the Two-Dimensionally Limited Space of a Layered Polysilicate Kanemite

2.1. Introduction

Since the discoveries of ordered mesoporous silicas prepared by using surfactant molecules,[1,2] the self-assembling ability of surfactants has attracted much attention in the field of porous materials design.[3,4] Periodic mesoporous materials with various structures, morphologies, and compositions have been developed up to date.[5-9] These materials are useful for catalysts, catalyst supports, and adsorbents for relatively larger molecules, and the potential includes confined reaction vessels and functional materials for electronics and photonics. Mesostructures, which are formed through the cooperative organization in the inorganic-surfactant systems,[10] have often been explained by the geometrical packing of surfactant molecules[11] because monomeric and/or oligomeric soluble precursors are mainly used as inorganic sources. The surfactant molecules themselves are uniformly assembled in aqueous solutions depending on the conditions including the geometrical packing of surfactant molecules,[11] while the presence of inorganic species attached to the hydrophilic head groups plays an important role in the mesostructural variation. The geometrical packing of surfactant molecules containing attached inorganic species should be considered because the charge density of inorganic frameworks is changed by condensation which results in the variation in the amount of accommodated surfactant molecules in the mesostructured materials.[12] However, the mesostructures of ordered mesoporous silicas derived from a layered polysilicate kanemite (FSM-16[13] and KSW-2[14]) cannot be explained in the same manner because kanemite has two-dimensionally connected silicate networks.[15,16] The formation of FSM-16 and KSW-2 is much complicated than those of other ordered mesoporous silicas (MCM-41,[2,10] SBA-15,[17] etc.). In the present study, kanemite was allowed to react with aqueous solutions of various cationic surfactants. The obtained mesostructures, such as lamellar, 2-d hexagonal, and disordered phases, can be explained by combining both the geometrical packing of surfactants and the interactions of the cationic head groups of surfactants with silicate sheets, providing the formation of

surfactant assemblies within the two-dimensionally limited space.

Being different from intercalation compounds,[18] kanemite is an attractive layered material applicable for the synthesis of ordered mesoporous silicas. The individual silicate sheets in kanemite are composed of only tetrahedral SiO_4 unit.[15,16] By the presence of two-dimensionally connected silicate networks, ordered mesoporous silicas with three-dimensionally connected mesopores that are observed for MCM-48, SBA-1, and SBA-2 have never been synthesized in the surfactant-kanemite systems.[19] The formation of disordered (KSW-1) and 2-d hexagonal mesoporous silica (FSM-16) by direct reaction of kanemite with alkyltrimethylammonium (C_nTMA) surfactants has been well recognized.[1,13,20] Through the investigation on the formation of the mesostructured precursor for FSM-16 by TEM and in-situ XRD,[21-23] the formation mechanism has recently been proved by using docosyltrimethylammonium (C_{22}TMA) or docosyltriethylammonium (C_{22}TEA) surfactant that is likely to be assembled as lamellar phases.[24] The 2-d hexagonal phases are formed by the transformation of the lamellar intermediates composed of C_{22}TMA or C_{22}TEA cations and fragmented silicate sheets. Lamellar surfactant-silicate mesostructured materials can also be obtained from kanemite by using C_{16}TMA cations under the appropriate synthetic conditions (C_{16}TMA/Si $\geq$ 0.5).[19] The silicate frameworks are not fragmented, but condensed silicate species are formed through condensation within the individual silicate sheets (intralayer condensation) depending on the reaction temperatures. In addition, a layered C_{16}TMA-kanemite complex retaining the kanemite structure can be converted to a mesostructured precursor for orthorhombic KSW-2 by mild acid treatment.[14] The orthorhombic mesostructure is formed by the bending of the individual silicate sheets in kanemite through the gradual leaching of C_{16}TMA cations with intralayer and interlayer condensation. Thus, the formation of several mesostructures is possible in the C_nTMA-kanemite systems, and the complicacy is due to the two-dimensional nature of kanemite.

The formation of an orthorhombic mesostructure (KSW-2) is understood on the

basis of both the geometrical packing of $C_{16}TMA$ and the interactions of the cationic head groups with the silicate sheets.[14] The assemblies of $C_{16}TMA$ molecules within semi-squared spaces cannot simply be explained by using the geometrical packing. The semi-squared arrangements have never been found among the mesostructured materials reported so far. All the mesostructures are governed by the geometrical packing of surfactant molecules used.[11] The orthorhombic mesostructure is formed through the bending of the individual silicate sheets that are not so flexible as monomeric and/or oligomeric silica species. Thus, the surface curvature of the silicate sheets does not match that of $C_{16}TMA$ assemblies completely and the $C_{16}TMA$ molecules are encapsulated within the semi-squared spaces because of the interactions of the cationic head groups of the $C_{16}TMA$ molecules with the silicate sheets. Therefore, the present study on the reactions of kanemite with various cationic surfactants that are assembled with larger surface curvatures is quite important for further understanding the surfactant-kanemite systems to produce mesostructured materials.

2.2 Experimental

2.2.1 Materials

In order to synthesize a layered polysilicate kanemite, a high quality water glass (SiO_2/Na_2O = 3.32) and sodium hydroxide were obtained from Nissan Kagaku Kogyo Co. and Kokusan Kagaku Kogyo Co., respectively. Kanemite was prepared by the dispersion of □-$Na_2Si_2O_5$ in distilled water. Sodium hydroxide was added to a high quality water glass as to be the Na/Si ratio of 1.0 and the aqueous solution was stirred at room temperature over night. The solution was dried and heated at 750 °C for 1 h in ambient air. After cooling, a calcined solid was obtained and milled, forming □-$Na_2Si_2O_5$ powders. One g of □-$Na_2Si_2O_5$ powder was dispersed in 50 ml of distilled water and the

suspension was stirred at room temperature for 30 min. The resultant product (kanemite, $NaHSi_2O_5 \cdot 3H_2O$) was centrifuged and air-dried. Alkyltrimethylammonium bromides ($C_nH_{2n+1}(CH_3)_3NBr$, C_nTMABr, n = 12-18) were obtained from Tokyo Kasei Kogyo Co. and used without purification. Docosyltrimethylammonium bromide (C_{22}TMABr) was prepared by the reaction of 1-bromodocosane with trimethylamine in ethanol at 80 ℃.[25] The resultant was purified by recrystallization in a mixed solvent of chloroform and methyl acetate and the purity of the bromide was checked by ^1H and ^{13}C NMR and CHN analysis. Alkyltriethylammonium bromides ($C_nH_{2n+1}(C_2H_5)_3NBr$, C_nTEABr, n = 14-22) were synthesized in the similar manner; the reactions of 1-bromoalkanes with triethylamine were conducted.[25] Gemini type diammonium surfactants, such as $C_{16}H_{33}(CH_3)_2NBrC_3H_6NBr(CH_3)_3$, $C_{16}H_{33}(CH_3)_2NBrC_3H_6NBr(CH_3)_2C_{16}H_{33}$ and $C_{16}H_{33}(CH_3)_2NBrC_5H_{10}NBr(CH_3)_2C_{16}H_{33}$ (hereinafter denoted by $C_{16\text{-}3\text{-}1}$, $C_{16\text{-}3\text{-}16}$ and $C_{16\text{-}5\text{-}16}$, respectively) were prepared according to the literature.[26] These surfactants were synthesized by the reactions of 1-bromohexadecane with 3-bromopropyltrimethylammonium bromide, 1,3-dibromopropane and 1,5-dibromopentane, respectively, and then purified by recrystallization in chloroform/methyl acetate.

2.2.2 Reactions of a Layered Polysilicate Kanemite with Various Surfactants

All the reactions were performed at 70 ℃ for 3 h. The reactions of kanemite with monovalent ammonium surfactants (C_nTMABr , C_nTEABr) were conducted according to the previous papers.[13,19] Where the N/Si molar ratio was 0.2,[13] 1 g of kanemite was added to 20 mL of 0.1 M C_nTMABr (n = 12-18, 22) or 0.1 M C_nTEABr (n = 14-22). After the resultants were separated by centrifugation, the products were dispersed in 20 mL of distilled water. The pH values of the suspensions were adjusted to 8.5 by the addition of 2N HCl. After the stirring at 70 ℃ for 3 h, the as-synthesized materials were dried at 60 ℃ and calcined at 550 ℃ for 6 h. Where the N/Si molar ratio was 2.0,[19] 1 g of

kanemite was added to 200 mL of aqueous solutions of the surfactants. After the reactions, the products were centrifuged and air-dried.

The reaction conditions of kanemite with divalent ammonium surfactants ($C_{16\text{-}3\text{-}1}$, $C_{16\text{-}3\text{-}16}$, $C_{16\text{-}5\text{-}16}$), were selected on the basis of the solubility of the divalent ammonium surfactants. The reaction of kanemite with $C_{16\text{-}3\text{-}1}$ was performed by using the same method of the C_nTMABr- and C_nTEABr-kanemite systems. In the $C_{16\text{-}3\text{-}16}$-kanemite system, 1 g of kanemite was added to an aqueous solution of 0.08 M $C_{16\text{-}3\text{-}16}$ (N/Si = 0.32). In the $C_{16\text{-}5\text{-}16}$-kanemite system, 1 g of kanemite was added to an aqueous solution of 0.05 M $C_{16\text{-}5\text{-}16}$ (N/Si = 0.2). In addition, acid-treatment of lamellar phases obtained by the reactions with $C_{16\text{-}3\text{-}16}$ and $C_{16\text{-}5\text{-}16}$ was conducted by the addition of 2N HCl; the pH values of the suspensions were adjusted to 8.5 and the stirring was kept at 70 ℃ for 3 h.

2.2.3 Characterization

Powder XRD patterns were obtained by using a Mac Science M03XHF[22] diffractometer with monochromated Fe K□ radiation. TEM images were taken by using a JEOL JEM-100CX, accelerated at 100 kV. Solid-state ^{29}Si MAS NMR measurements were performed on a JEOL JNM CMX-400 spectrometer at a spinning rate of 3 kHz and a resonance frequency of 79.30 MHz with a 45° pulse length of 4.1 ms and a recycle time of 100 s. The chemical shift was expressed with respect to tetramethylsilane. Intensity ratios of the signals were deconvoluted by using a MacFID software. Conformation of the alkyl chains in surfactant molecules was examined by FT-IR and ^{13}C CP/MAS NMR measurements. FT-IR spectra were recorded by using a Perkin Elmer Spectrum One. Solid-state ^{13}C CP/MAS NMR measurements were performed on a JEOL JNM CMX-400 spectrometer at a spinning rate of 3 kHz and a resonance frequency of 79.30 MHz with a pulse length of 4.1 ms and a recycle time of 5 s. Morphological variation of kanemite was checked by scanning electron microscopy (SEM) (JEOL JSM-T220A). Nitrogen adsorption isotherms of calcined samples were

obtained by using a BELSORP 28 apparatus (Bel Japan, Inc.) at 77 K. The samples were heated at 120 ℃ for 3 h to a residual pressure of 1.3 Pa prior to the measurement. Specific surface areas were determined by BET method using the data before Kelvin condensation and pore size distributions were calculated by BJH method using adsorption branches.

2.3 Results and Discussion

2.3.1 Reactions with Alkyltrimethylammonium Surfactants

The XRD patterns of calcined materials prepared by using C_nTMABr (n = 12-18), where the preparation was followed by the typical synthesis procedure of FSM-16 derived from kanemite[13] (N/Si = 0.2), are shown in Figure 2-1(a)-(d). Four diffraction peaks assignable to 2-d hexagonal phases (space group; *p6mm*) are distinctly observed in low scattering angles. The d_{100}-spacings of the calcined materials are linearly increased with the increase in the alkyl chain lengths of the C_nTMA surfactants used (C_{12}TMA; 2.9 nm, C_{14}TMA; 3.2 nm, C_{16}TMA; 3.5 nm, C_{18}TMA; 3.9 nm). All the N_2 adsorption isotherms of the calcined materials showed type IV behaviors characteristic of ordered mesoporous silicas.[2,13] The BET surface areas, the pore volumes, and the average pore sizes (r) are shown in Table 2-1. The unit cell parameters (a_0) and the wall thicknesses (w) of the mesoporous silicas were calculated by the equations of $a_0 = 2/\sqrt{3} \times d_{100}$ and $w = a_0 - r$, respectively; the wall thickness is almost constant (Table 2-1).

The d_{100}-spacing of the calcined material prepared by using C_{22}TMABr was 4.4 nm, being in agreement with the aforementioned relation between the d_{100}-spacing of the FSM-type mesoporous silicas and the alkyl chain length of the C_nTMA surfactants used.[24] However, the use of C_{22}TMA cations for the synthesis of FSM-16 led to the broadening of the XRD peaks (Figure 2-1(e)). Even in the synthesis of 2-d hexagonal

MCM-41, lamellar MCM-50-type silicas are formed by using C_nTMA surfactants with longer alkyl chains such as C_{20}TMA and C_{22}TMA cations.[12] Although the use of C_{22}TMA cations is not advantageous for the synthesis of MCM-41, MCM-41-type mesoporous materials can be obtained under optimal synthetic conditions.[27,28]

The XRD patterns of the as-synthesized materials prepared by using C_nTMABr (n = 12-18, 22) under the typical synthetic conditions for the synthesis of layered C_{16}TMA-silicate complexes derived from kanemite[19] (N/Si = 2.0) are shown in Figure 2-2(a)-(e). As shown in the figure, the main peaks assignable to (001) and the higher order diffractions are observed for the as-synthesized materials prepared by using C_{16}TMABr, C_{18}TMABr, and C_{22}TMABr (C_{16}TMA; 3.2 nm, C_{18}TMA; 3.4 nm, C_{22}TMA; 3.5 nm). However, in the cases of C_{12}TMABr and C_{14}TMABr, broad peaks were collected in low scattering angles and the d-spacings (C_{14}TMA; 3.4 nm, C_{18}TMA; 3.7 nm) were larger than those observed for the layered C_nTMA-silicates (n = 16, 18, 22) in spite of their shorter alkyl chains. The solubilities of C_{12}TMABr and C_{14}TMABr are higher than those of C_nTMABr (n = 16, 18, 22). In addition, the reactivity of layered materials with surfactant molecules with shorter alkyl chains is lower. Then, the amounts of introduced C_{12}TMA and C_{14}TMA cations between the silicate sheets of kanemite are not enough to be assembled as lamellar phases, meaning that the C_{12}TMA- and C_{14}TMA-silicates are not layered materials.

2.3.2 Reactions with Alkyltriethylammonium Surfactants

The XRD patterns of calcined materials prepared by using C_nTEABr (n = 14-20) where the N/Si molar ratios were 0.2 are shown in Figure 2-3(a)-(d). Being different from the C_nTMA-kanemite system, disordered phases were obtained. However, the XRD pattern of the calcined material prepared by using C_{22}TEABr showed a successful formation of a 2-d hexagonal phase (Figure 2-3(e)), as reported by us recently.[24] The TEM image of the calcined material revealed the presence of ordered hexagonal

arrangements of mesopores (Figure 2-5) and the N_2 adsorption data showed that the material has high surface area, pore volume, and large pore size (Table 2-1).

The formation processes of the 2-d hexagonal mesoporous silica obtained from the C_{22}TEA-kanemite system were investigated by XRD and ^{29}Si MAS NMR. During the synthesis of the mesoporous silica, samples were recovered before and after the pH adjustment at 8.5. The XRD pattern of the sample before the pH adjustment showed that a peak at the d-spacing of 4.3 nm and only the higher order diffractions were observed, suggesting that a layered C_{22}TEA-silicate can be synthesized by the reaction of kanemite with C_{22}TEABr (before pH adjustment).[24] Surfactant molecules with longer alkyl chains are likely to be assembled as lamellar phases because of their geometrical packings.[11] The XRD pattern of the sample after the pH adjustment showed the appearance of four diffraction peaks assignable to a 2-d hexagonal phase accompanied with a slight amount of the remaining layered phase. During the acid treatment (the pH adjustment), the C_{22}TEA cations were partly removed out of the interlayer spaces and the silicate framework of kanemite was condensed further (as described below), meaning that lamellar assemblies of the C_{22}TEA cations are changed into rod-like micelles to induce the 2-d hexagonal phase.

The ^{29}Si MAS NMR spectra of the samples recovered during the synthesis of the mesoporous silica are shown in Figure 2-6. Before the pH adjustment (layered C_{22}TEA-silicate), Q^2 ($(SiO)_2SiO_2$), Q^3 ($(SiO)_3SiO$), and Q^4 ($(SiO)_4Si$) signals were observed at around -90 ppm, -100 ppm, and -110 ppm, respectively. The ^{29}Si MAS NMR measurement of the layered C_{22}TEA-silicate was performed without drying the layered C_{22}TEA-silicate. In addition to those peaks, Q^0 (SiO_4) and Q^1 ($(SiO)SiO_3$) peaks were detected, indicating the presence of soluble silicate species. The presence of both Q^2 and Q^3 silicate species is the direct evidence on the fragmentation of the individual silicate sheets of kanemite in the layered C_{22}TEA-silicate though fragment size has not been clear. The condensed Q^4 silicate species are formed by intralayer condensation and the reaction of the individual silicate sheets with the soluble silicate

species.[19,24] The $Q^4/(Q^3+Q^4)$ ratios were increased by pH adjustment (2-d hexagonal C_{22}TEA-silicate) and the following calcination. Similar results were obtained in the C_{22}TMA-kanemite system. Although the formation mechanism of FSM-16 has been proposed by TEM and in-situ XRD,[21-23] the formation mechanism of FSM-type mesoporous silicas is proved by the results in the present study.

The XRD patterns of as-synthesized materials prepared by using C_nTEABr (n = 14-22), where the N/Si molar ratios were 2.0, are shown in Figure 2-4(a)-(e). The main peaks assignable to (001) and the higher order reflections are observed for the as-synthesized materials prepared by using C_{20}TEABr and C_{22}TEABr (C_{20}TEA; 3.7 nm, C_{22}TEA; 3.9 nm). As in the case of the C_nTMA-kanemite system, the XRD patterns showed that layered C_nTEA-silicates cannot be obtained by using C_nTEABr with shorter alkyl chains (n = 14-18) (C_{14}TEA; 3.7 nm, C_{16}TEA; 3.9 nm, C_{18}TEA; 3.8 nm). The ^{29}Si MAS NMR spectra of the layered C_nTEA-silicates are shown in Figure 2-7. Both Q^3 and Q^4 silicate species are present in the layered C_nTEA-silicates though kanemite is composed of only Q^3 silicate specie.[15,16] The Q^4 silicate species are formed by intralayer condensation depending on the reaction temperatures.[19]

2.3.3 Reactions with Gemini Surfactants

The XRD patterns of the as-synthesized materials prepared by using a gemini type $C_{16\text{-}3\text{-}1}$ surfactant (N/Si = 0.2, 2.0) and the calcined materials are shown in Figure 2-8 and 9, respectively. In both of the cases, the broad peaks at the d-spacings of ca. 4.5 nm were observed for the as-synthesized materials. In addition to the main peaks, the higher order diffractions with very weak intensities are collected as shown in the figure. In spite of the same alkyl chain lengths, the d_{100}-spacings of the $C_{16\text{-}3\text{-}1}$-silicates were ca. 4.5 nm, being larger than that observed for 2-d hexagonal C_{16}TMA-silicate (ca. 4 nm). Although it is possible to index the peaks to 2-d hexagonal phases, the peaks are broadened further after calcination. The $C_{16\text{-}3\text{-}1}$ surfactants are assembled spherically,

being useful for the synthesis of $C_{16\text{-}3\text{-}1}$-silicate with 3-d hexagonal phase (SBA-2, space group; $P6_3/mmm$).[12] The formation of such spherical assemblies are not conceivable within the two-dimensionally limited space of kanemite. Because the surface curvature of the spherical assemblies is higher than that of rod-like micelles composed of C_nTMA molecules, disordered $C_{16\text{-}3\text{-}1}$-silicates are formed in the $C_{16\text{-}3\text{-}1}$-kanemite system.

The XRD patterns of the as-synthesized materials prepared by using other gemini type $C_{16\text{-}3\text{-}16}$ and $C_{16\text{-}5\text{-}16}$ surfactants before and after pH adjustment are shown in Figure 2-10 and 11, respectively. The peaks at the d-spacings of 3.5 nm and the higher order diffractions are observed in the XRD patterns of $C_{16\text{-}3\text{-}16}$-silicates recovered before and after pH adjustment. The $C_{16\text{-}3\text{-}16}$ surfactant has a tendency to be assembled as lamellar phase or rod-like micelles according to the synthetic conditions, being useful for the synthesis of $C_{16\text{-}3\text{-}1}$-silicate with lamellar (MCM-50) and 2-d hexagonal phases (MCM-41, SBA-3).[12] Therefore, the formation of the layered $C_{16\text{-}3\text{-}16}$-silicate is advantageous within the limited interlayer space of kanemite. In contrast, in the $C_{16\text{-}5\text{-}16}$-kanemite system, both lamellar (3.5 nm) and 2-d hexagonal phases (3.9 nm) were obtained as mixed products and the 2-d hexagonal phase (d_{100} = 4.0 nm, d_{110} = 2.3 nm, d_{200} = 2.0 nm) was mainly observed after pH adjustment. The result indicates that the layered $C_{16\text{-}5\text{-}16}$-silicate is also transformed into the 2-d hexagonal phase by acid treatment as well as layered C_{22}TMA- and C_{22}TEA-silicates. The use of $C_{16\text{-}4\text{-}16}$ and $C_{16\text{-}6\text{-}16}$ surfactants is useful for the formation of $C_{16\text{-}4\text{-}16}$- and $C_{16\text{-}6\text{-}16}$-silicates with 2-d hexagonal phases (MCM-41, SBA-3) mainly.[12] By increasing the alkyl chain length between diammonium groups (spacer) in gemini type surfactants, the $C_{16\text{-}5\text{-}16}$ molecules are assembled as rod-like micelles in the present case.

2.3.4 Formation of Mesostructured Materials Derived from Kanemite

In the C_nTMA-kanemite system, the discussion on the formation of FSM-16 has started as one of the research topics why the 2-d hexagonal phase with 3-d silicate

networks is allowed to form from kanemite with 2-d silicate networks. Originally, the folded sheets mechanism has proposed; rod-like micelles of the C_nTMA molecules are formed with the cooperative bending of the individual silicate sheets of kanemite around the micelles.[13] However, the presence of a layered intermediate during the formation of the 2-d hexagonal phase was claimed on the basis of in-situ XRD data.[22] Although both single and double layers of the silicate sheets must be observed by TEM if the 2-d hexagonal phase is formed through the folded sheets mechanism, such parts have never been observed and the wall thickness of FSM-16 is almost constant.[23] Thus, the presence of fragmented silicate sheets during the formation of FSM-16 has been speculated, as was firstly pointed out that the disordered KSW-1 is formed through the fragmentation of the silicate sheets of kanemite.[21] In the present study, a layered intermediate was successfully recovered and then the presence of fragmented silicate sheets was proved on the basis of the NMR data.

The schematic formation routes of ordered mesostructured materials derived from kanemite are shown in Scheme 2-1 on the basis of the present and previous results.[14,19,24] The formation of the 2-d hexagonal phase (FSM-16) is explained above. Layered surfactant-silicates derived from kanemite are unique because the silicate framework contains condensed and ordered silicate species. The formation of the condensed silicate species has already been proved;[19] intralayer condensation occurs within the individual silicate sheets of kanemite and the degree of the condensation is controllable with the reaction temperature. A reaction of kanemite with C_{16}TMA cations at room temperature leads to the formation of a layered C_{16}TMA-silicate composed of mainly Q^3 silicate species. Mild acid treatment of the layered C_{16}TMA-silicate with retaining the kanemite structure induces the mesostructural transformation into an orthorhombic phase (KSW-2, space group; *C2mm*) that is truly formed by the bending of the individual silicate sheets of kanemite.[14] The orthorhombic structure can be formed because of the 2-d connecting silicate framework originated from kanemite. In the MCM-type mesostructured materials, mesostructural transformation is also observed during thermal

and hydrothermal post-treatments.[29,30] However, various chemical reactions occur; silicate species are solubilized and bonded again, surfactant molecules are partly degraded, the derivative organic molecules are solubilized in the remaining surfactant assemblies, and so on. In contrast, in the C_nTMA-kanemite systems, layered C_nTMA-silicate phases are present as key materials during the formation of each mesostructured material. The silicate frameworks of the layered C_nTMA-silicate phases, retaining structural units originated from kanemite through fragmentation of silicate sheets or intralayer condensation within individual silicate sheets of kanemite, have already been investigated in detail[19,24] Consequently, in the present study, the mesostructural transformations can be simply summarized by using the structural change of the silicate frameworks of kanemite such as fragmentation, intralayer condensation and bending.

2.3.5 Surfactant Assemblies in the Two-Dimensionally Limited Space

In the synthesis of MCM-type mesoporous silicas, the mesostructures formed through the cooperative organization have often been explained by the geometrical packing of the surfactant molecules.[11] The presence of inorganic species attached to the hydrophilic head groups induces mesostructural variation depending on the synthetic conditions that reflect the degree of silica condensation. In the surfactant-kanemite systems, 2-d silicate networks originated from kanemite always affect the formation of mesostructured materials because of the interactions of the silicate frameworks with surfactants. The formation of an orthorhombic mesostructure (KSW-2) is a good example proving that surfactant molecules are not freely assembled in accordance with the geometrical packing within the limited space.[14] The C_{16}TMA molecules are allowed to accommodate in the semi-squared spaces because of the interactions of the cationic head groups with the silicate sheets.

Here, the formation of disordered phases is also discussed on the basis of both the geometrical packing of surfactants used and the interactions of the silicate frameworks

with the surfactants. The formation routes of ordered and disordered materials derived from kanemite are summarized in Scheme 2-2. Disordered phases are formed by the reactions of kanemite with C_nTEA (n = 14-18) and C_{16-3-1} surfactants. Although layered materials are very important for the formation of ordered phases in the surfactant-kanemite systems, these surfactant molecules cannot be assembled as lamellar phases.[12] The C_nTEA and C_{16-3-1} surfactants tend to be assembled spherically because of the geometrical packings. One-directional bending of the silicate sheets is possible for the formation of ordered mesostructured precursors (KSW-2).[14] However, two-directional bending of the silicate sheets in order to match the surface curvature between the spherical surfactant assemblies and the bent silicate sheets is not rational because the spherical surfactant assemblies cannot be surrounded by the silicate sheets with long range networks.[15,16] Thus, the disordered phases that afford mesoporous silicas are obtained through the bending of the silicate sheets according to the interactions of the silicate frameworks with those surfactants.

2.4 Conclusions

Silica-based mesostructures are derived from a layered polysilicate kanemite, and the formation is induced by the reactions with various cationic surfactants with different geometrical packings. In the surfactant-kanemite systems, several reactions such as the interactions of cationic surfactants with the silicate sheets, the fragmentation or bending of the silicate sheets, and the geometrical packing of surfactant molecules are complicated. However, the formation of ordered (lamellar, 2-d hexagonal, and 2-d orthorhombic) and disordered mesostructured materials can be simply summarized on the basis of the presence of layered surfactant-silicate intermediates. The obtained insights are potentially applicable for simultaneous control of short (framework) and long range orderings (mesostructure) in mesostructured materials obtained from layered

polysilicates. Several research groups have challenged the transformation of silicate frameworks of MCM-41 into crystallized frameworks.[30-34] However, the mesostructural orderings of MCM-41 was lost by crystallization though catalytic performance and hydrothermal stability of MCM-41 were enhanced by post-treatment. In contrast, silicate frameworks of lamellar mesophase silicates can be successfully transformed into molecularly ordered inorganic frameworks by hydrothermal post-treatment.[35] The molecularly ordered inorganic frameworks are formed depending on the shapes of head groups in cationic surfactants. Therefore, the sheet-like silicate framework in KSW-2 constructing semi-squared mesopores is especially attractive to realize the preparation of mesostructured and mesoporous materials with truly crystallized silicate frameworks.

2.5 References

(1) Yanagisawa, T.; Shimizu, T.; Kuroda, K.; Kato, *C. Bull. Chem. Soc. Jpn*. 1990, **63**, 988.

(2) (a) Kresge, C. T.; Leonowicz, M. E.; Roth, W. J.; Vartuli, J. C.; Beck, J. S. *Nature* (London) 1992, **359**, 710. (b) Beck, J. S.; Vartuli, J. C.; Roth, W. J.; Leonowicz, M. E.; Kresge, C. T.; Schmitt, K. D.; Chu, C. T.-W.; Olson, D. H.; Sheppard, E. W.; McCullen, S. B.; Higgins, J. B.; Schlenker, J. L. *J. Am. Chem. Soc*. 1992, **114**, 10834.

(3) (a) Huo, Q.; Margolese, D. I.; Ciesla, U.; Feng, P.; Gler, T. E.; Sieger, P.; Leon, R.; Petroff, P. M.; Schüth, F.; Stucky, G. D. *Nature* (London) 1994, **368**, 317. (b) Huo, Q.; Margolese, D. I.; Ciesla, U.; Demuth, D. G.; Feng, P.; Gler, T. E.; Sieger, P.; Firouzi, A.; Chmelka, B. F.; Schüth, F.; Stucky, G. D. *Chem. Mater*. 1994, **6**, 1176.

(4) Behrens, P. *Angew. Chem., Int. Ed*. 1996, **35**, 515.

(5) Corma, A. *Chem. Rev*. 1997, **97**, 2373.

(6) Moller, K.; Bein, T. *Chem. Mater*. 1998, **10**, 2950.

(7) Lindén, M.; Schacht, S.; Schüth, F.; Steel, A.; Unger, K. K. *J. Porous Mater*. 1998, **5**, 177.

(8) Ying, J. Y.; Mehnert, C. P.; Wong, M. S. *Angew. Chem., Int. Ed*. 1999, **38**, 56.

(9) Stein, A.; Melde, B. J.; Schroden, R. C. *Adv. Mater*. 2000, **12**, 1403.

(10) (a) Monnier, A.; Schüth, F.; Huo, Q.; Kumar, D.; Margolese, D.; Maxwell, R. S.; Stucky, G. D.; Krishnamurty, M.; Petroff, P.; Firouzi, A.; Janicke, M.; Chmelka, B. F. *Science* 1993, **261**, 1299. (b) Firouzi, A.; Kumar, D.; Bull, L. M.; Besier, T.; Sieger, P.; Huo, Q.; Walker, S. A.; Zasadzinski, J. A.; Glinka, C.; Nicol, J.; Margolese, D.; Stucky, G. D.; Chmelka, B. F. *Science* 1995, **267**, 1138.

(11) Israelachvili, J. N.; Mitchell, D. J.; Ninham, B. W. *J. Chem. Soc., Faraday Trans*. 2 1976, **72**, 1525.

(12) (a) Huo, Q.; Leon, R.; Petroff, P. M.; Stucky, G. D. *Science* 1995, **268**, 1324. (b)

Huo, Q.; Margolese, D. I.; Stucky, G. D. *Chem. Mater*. 1996, **8**, 1147.

(13) (a) Inagaki, S.; Fukushima, Y.; Kuroda, K. J. Chem. Soc., *Chem. Commun*. 1993, 680. (b) Inagaki, S.; Koiwai, A.; Suzuki, N.; Fukushima, Y.; Kuroda, K. *Bull. Chem. Soc. Jpn*. 1996, **69**, 1449.

(14) Kimura, T.; Kamata, T.; Fuziwara, M.; Takano, Y.; Kaneda, M.; Sakamoto, Y.; Terasaki, O.; Sugahara, Y.; Kuroda, K. *Angew. Chem. Int. Ed*. 2000, **39**, 3855.

(15) (a) Gies, H.; Marler, B.; Vortmann, S.; Oberhagemann, U.; Bayat, P.; Krink, K.; Rius, J.; Wolf, I.; Fyfe, C. *Microporous Mesoporous Mater*. 1998, **21**, 183. (b) Vortmann, S.; Rius, J.; Marler, B.; Gies, H. *Eur. J. Mineral*. 1999, **11**, 125.

(16) Garvie, L. A. J.; Devouard, B.; Groy, T. L.; Camara, F.; Buseck, P. R. *Am. Mineral*. 1999, **84**, 1170.

(17) (a) Zhao, D.; Feng, J.; Huo, Q.; Melosh, N.; Fredrickson, G. H.; Chmelka, B. F.; Stucky, G. D. *Science* 1998, **279**, 548. (b) Zhao, D.; Huo, Q.; Feng, J.; Chmelka, B. F.; Stucky, G. D. *J. Am. Chem. Soc*., 1998, **120**, 6024.

(18) (a) Ogawa, M.; Kuroda, K. *Chem. Rev*. 1995, **95**, 399. (b) Ogawa, M.; Kuroda, K. *Bull. Chem. Soc. Jpn*. 1997, **70**, 2593.

(19) Kimura, T.; Itoh, D.; Okazaki, N.; Kaneda, M.; Sakamoto, Y.; Terasaki, O.; Sugahara, Y.; Kuroda, K. *Langmuir* 2000, **16**, 7624.

(20) Kuroda, K. *J. Porous Mater*. 1996, **3**, 107.

(21) Chen, C.-Y.; Xiao, S.-Q.; Davis, M. E. *Microporous Mater*. 1995, **4**, 1.

(22) (a) O'Brien, S.; Francis, R. J.; Price, S. J.; O'Hare, D.; Clark, S. M.; Okazaki, N.; Kuroda, K. *J. Chem. Soc., Chem. Commun*. 1995, 2423. (b) O'Brien, S.; Francis, R. J.; Fogg, A.; O'Hare, D.; Okazaki, N.; Kuroda, K. *Chem. Mater*. 1999, **11**, 1822.

(23) Sakamoto, Y.; Inagaki, S.; Ohsuna, T.; Fukushima, Y.; Nozue, Y.; Terasaki, O. *Microporous Mesoporous Mater*. 1998, **21**, 589.

(24) Kimura, T.; Itoh, D.; Shigeno, T.; Kuroda, K. *Langmuir* 2002, **18**, 9574.

(25) Bacaloglu, R.; Bunton, C. A.; Ortega, F. *J. Phys. Chem*. 1989, **93**, 1497.

(26) Zana, R.; Benrraou, M.; Rueff, R. *Langmuir* 1991, **7**, 1072.

(27) Namba, S.; Mochizuki, A.; Kito, M. *Stud. Surf. Sci. Catal*. 1998, **117**, 257.

(28) (a) Kimura, T.; Sugahara, Y.; Kuroda, K. *Chem. Commun*. 1998, 559. (b) Kimura, T.; Sugahara, Y.; Kuroda, K. *Microporous Mesoporous Mater*. 1998, **22**, 115.

(29) Fyfe, C. A.; Fu, G. *J. Am. Chem. Soc*. 1995, **117**, 9709.

(30) Luan, Z.; He, H.; Zhou, W.; Klinowski, J. *J. Chem. Soc., Faraday Trans*. 1998, **94**, 979.

(31) Mokaya, R.; Jones, W. *Chem. Commun*., 1997, 2185.

(32) (a) Kloetstra, K. R.; van Bekkum, H.; Jansen, J. C. *Chem. Commun*., 1997, 2281. (b) Kloetstra, K. R.; Zandbergen, H. W.; Jansen, J. C.; van Bekkum, H. *Microporous Mater*., 1996, **6**, 287. (c) Kloetstra, K. R.; van Bekkum, H.; Jansen, J. C. *Chem. Commun*., 1997, 2281.

(33) Karlsson, A.; Stocker, M.; Schmidt, R. *Microporous Mesoporous Mater*., 1999, **27**, 181.

(34) Huang, L.; Guo, W.; Deng, P.; Xue, Z.; Li, Q. *J. Phys. Chem. B*, 2000, **104**, 2817.

(35) Christiansen, S. C.; Zhao, D.; Janicke, M. T.; Landry, C. C.; Stucky, G. D.; Chmelka, B. F. *J. Am. Chem. Soc*. 2001, **123**, 4519.

Table 2-1. Characteristics of FSM-type mesoporous silicas by using C_nTMABr (n =12-18) and C_{22}TEABr.

Surfactant	BET surface area /m^2 g^{-1}	Pore volume /mL g^{-1}	Average pore size (r) / nm	Unit cell parameter (a_0) / nm	Wall thickness (w) / nm
C_{12}TMA	650	0.34	2.1	3.3	1.3
C_{14}TMA	882	0.51	2.3	3.7	1.4
C_{16}TMA	843	0.68	2.8	4.0	1.3
C_{18}TMA	921	0.72	3.2	4.5	1.3
C_{22}TEA	823	0.64	3.7	5.1	1.5

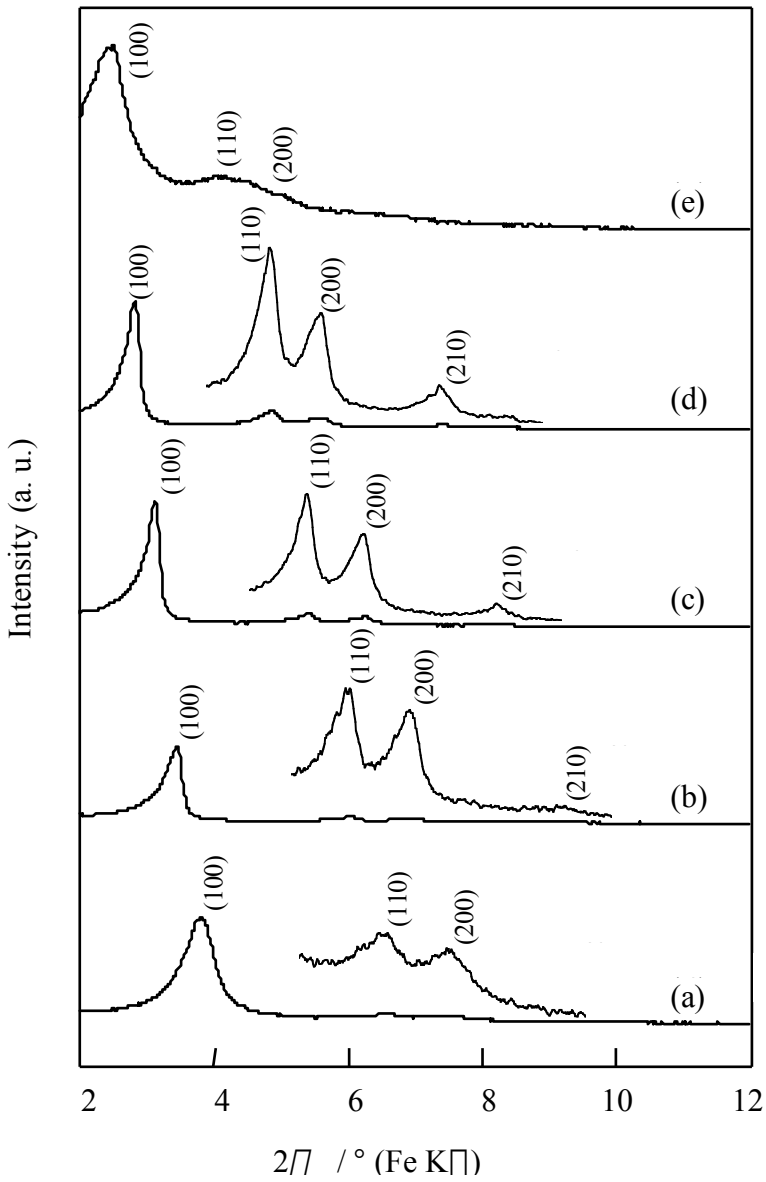

Figure 2-1. XRD patterns of calcined materials prepared by using (a) C_{12}TMABr, (b) C_{14}TMABr, (c) C_{16}TMABr, (d) C_{18}TMABr, and (e) C_{22}TMABr where the N/Si molar ratios were 0.2.

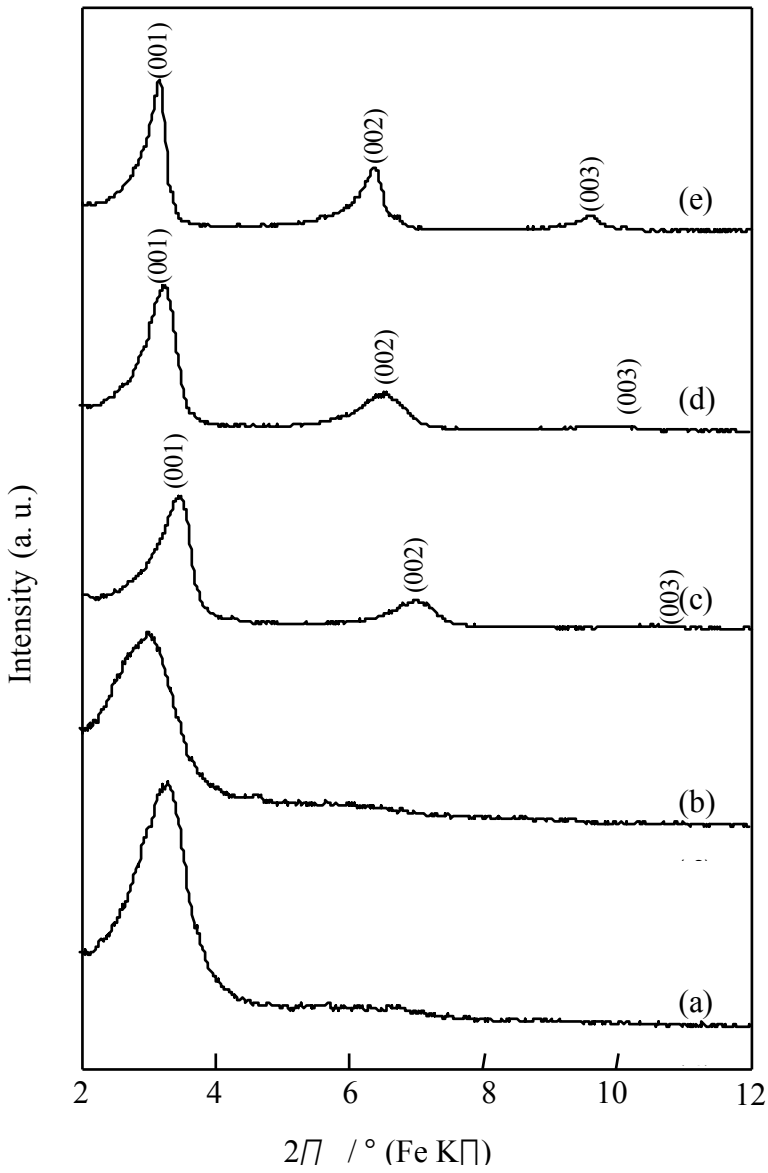

Figure 2-2. XRD patterns of as-synthesized materials prepared by using (a) C_{12}TMABr, (b) C_{14}TMABr, (c) C_{16}TMABr, (d) C_{18}TMABr, and (e) C_{22}TMABr where the N/Si molar ratios were 2.0.

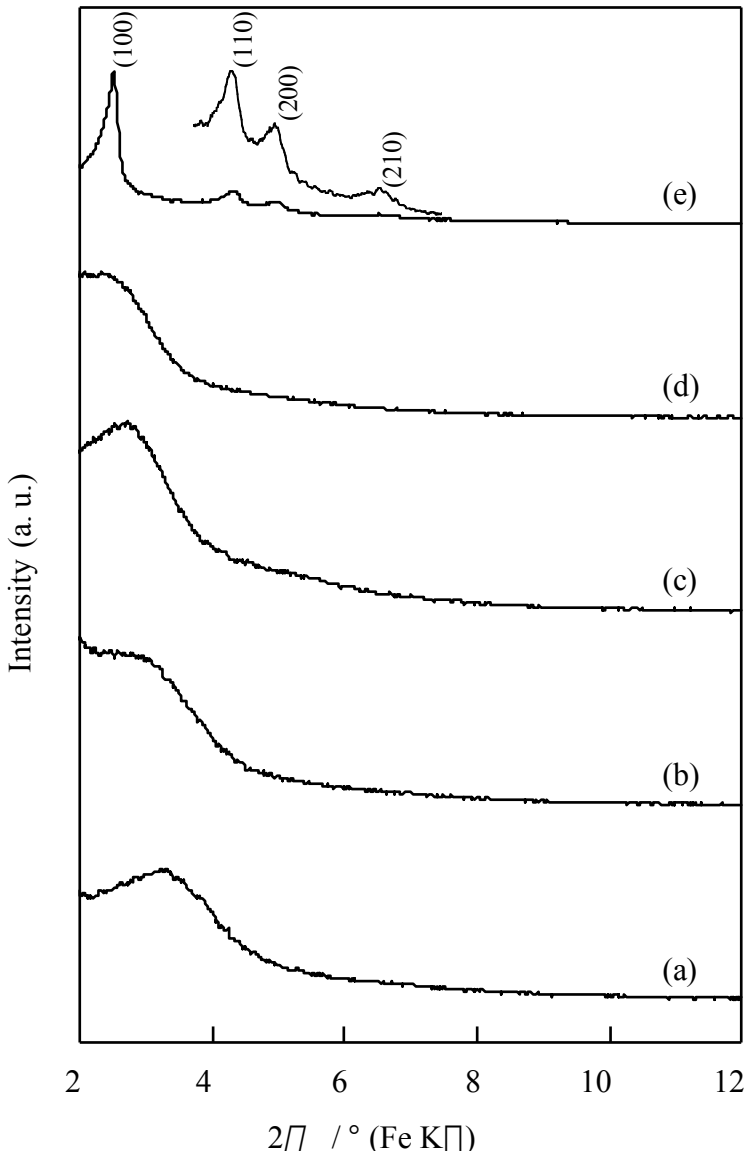

Figure 2-3. XRD patterns of calcined materials prepared by using (a) C_{14}TEABr, (b) C_{16}TEABr, (c) C_{18}TEABr, (d) C_{20}TEABr, and (e) C_{22}TEABr where the N/Si molar ratios were 0.2.

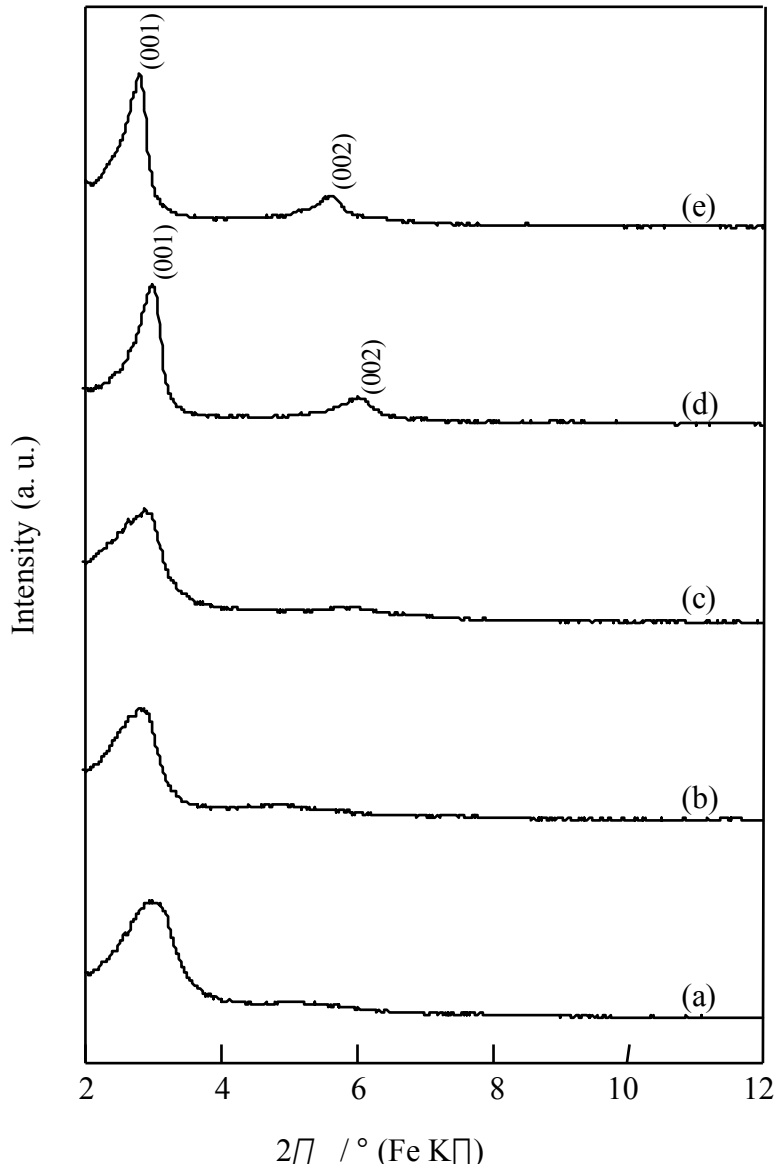

Figure 2-4. XRD patterns of as-synthesized materials prepared by using (a) C_{14}TEABr, (b) C_{16}TEABr, (c) C_{18}TEABr, (d) C_{20}TEABr, and (e) C_{22}TEABr where the N/Si molar ratios were 2.0.

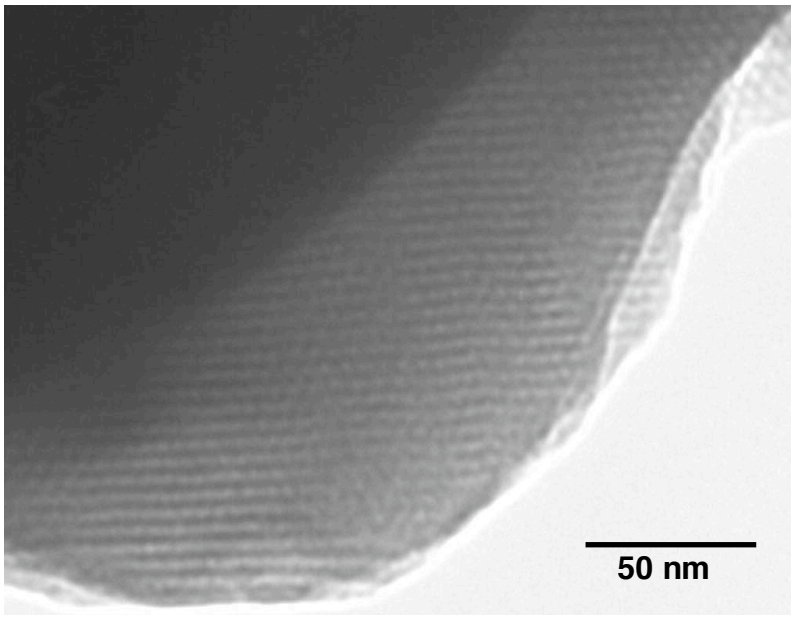

Figure 2-5. TEM image of the calcined material prepared by using C_{22}TEABr where the N/Si molar ratio was 0.2.

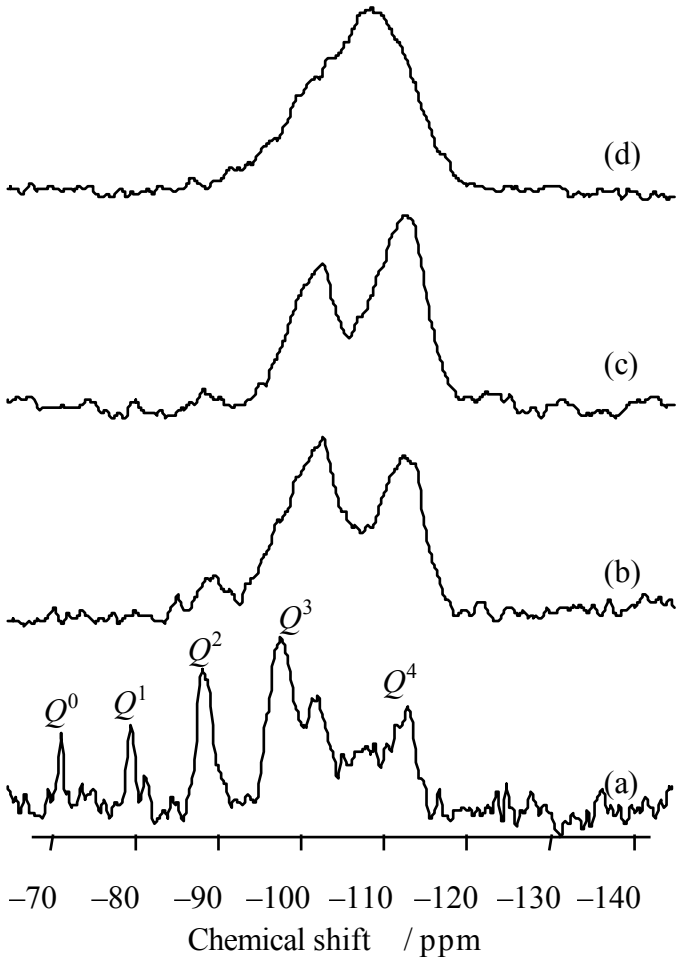

Figure 2-6. ^{29}Si MAS NMR spectra of the samples obtained during the synthesis of a 2-d hexagonal mesoporous silica by using C_{22}TEABr; before pH adjustment (a) without and (b) with drying, (c) after pH adjustment and (d) the calcined material.

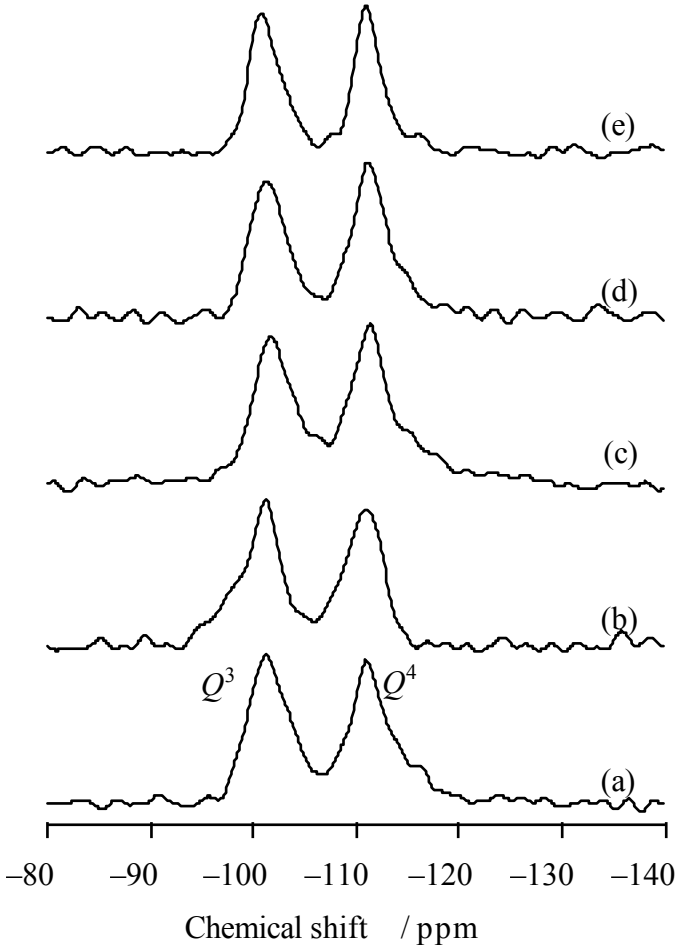

Figure 2-7. ^{29}Si MAS NMR spectra of the as-synthesized materials prepared by using (a) C_{14}TEABr, (b) C_{16}TEABr, (c) C_{18}TEABr, (d) C_{20}TEABr, and (e) C_{22}TEABr where the N/Si molar ratios were 2.0.

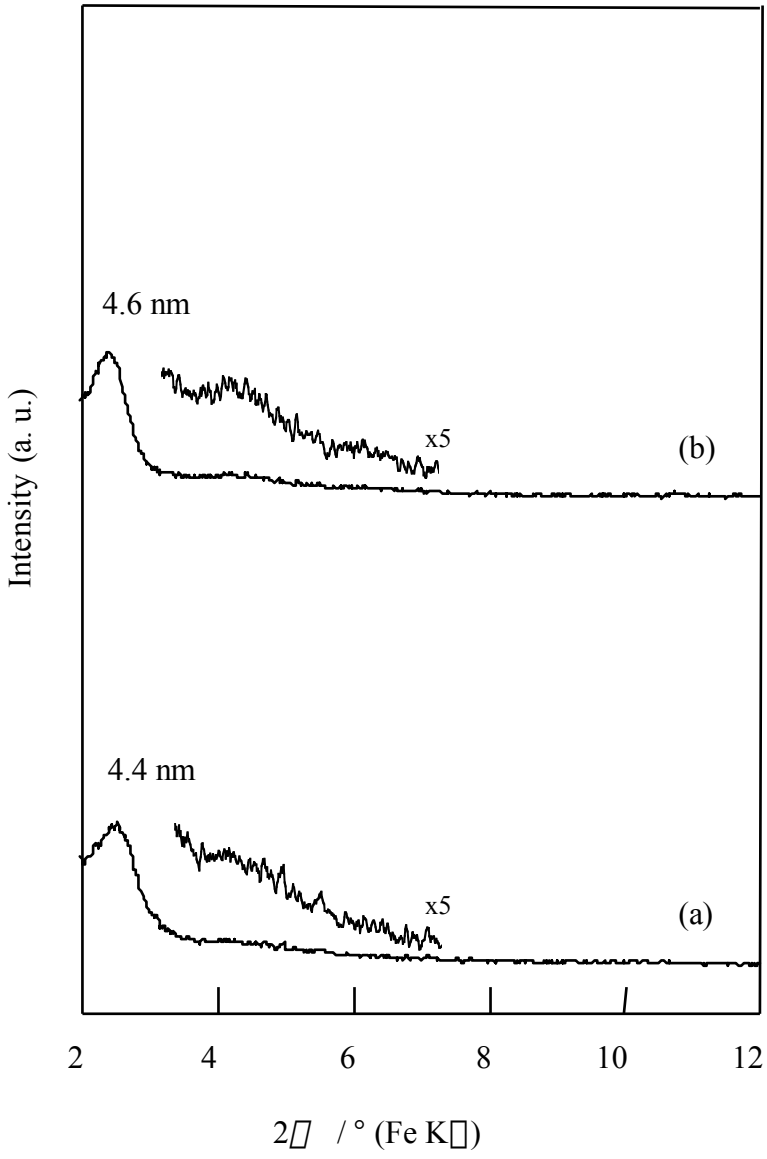

Figure 2-8. XRD patterns of the products obtained during the synthesis of C_{16-3-1}–silicates where the N/Si molar ratios were (a) 0.2 and (b) 2.0 after pH.

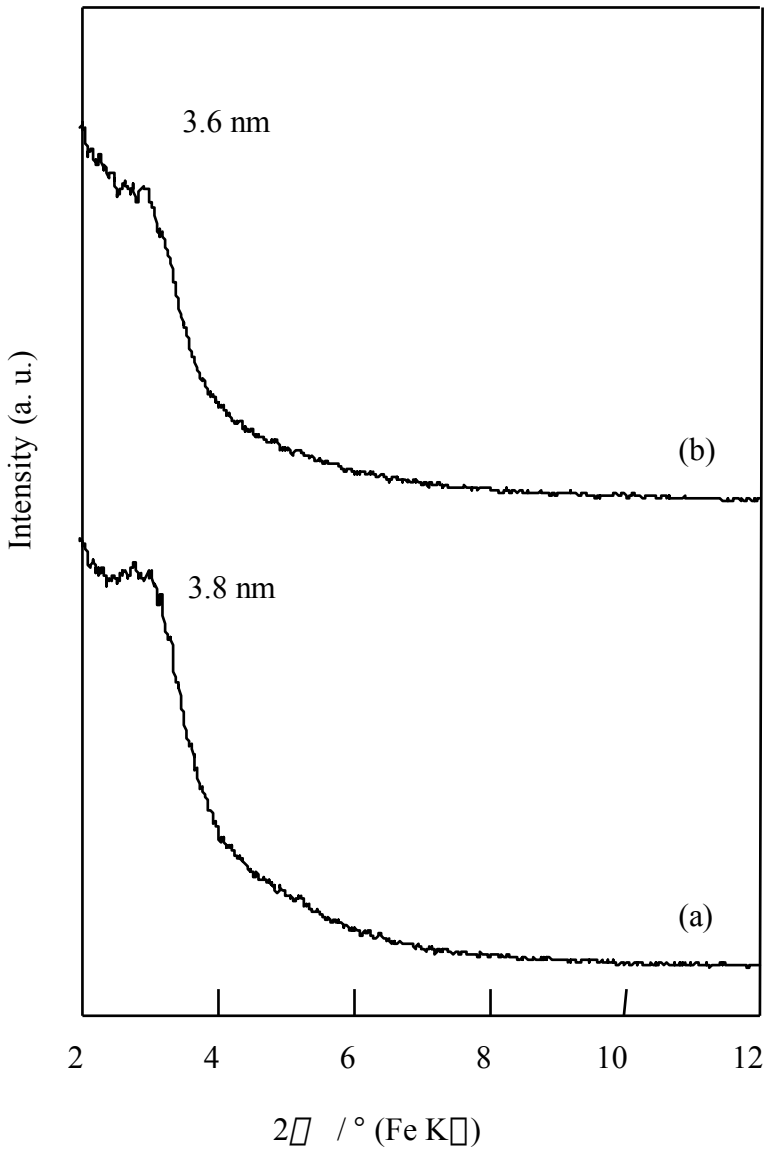

Figure 2-9. XRD patterns of the calcined products obtained during the synthesis of C_{16-3-1}–silicates where the N/Si molar ratios were (a) 0.2 and (b) 2.0.

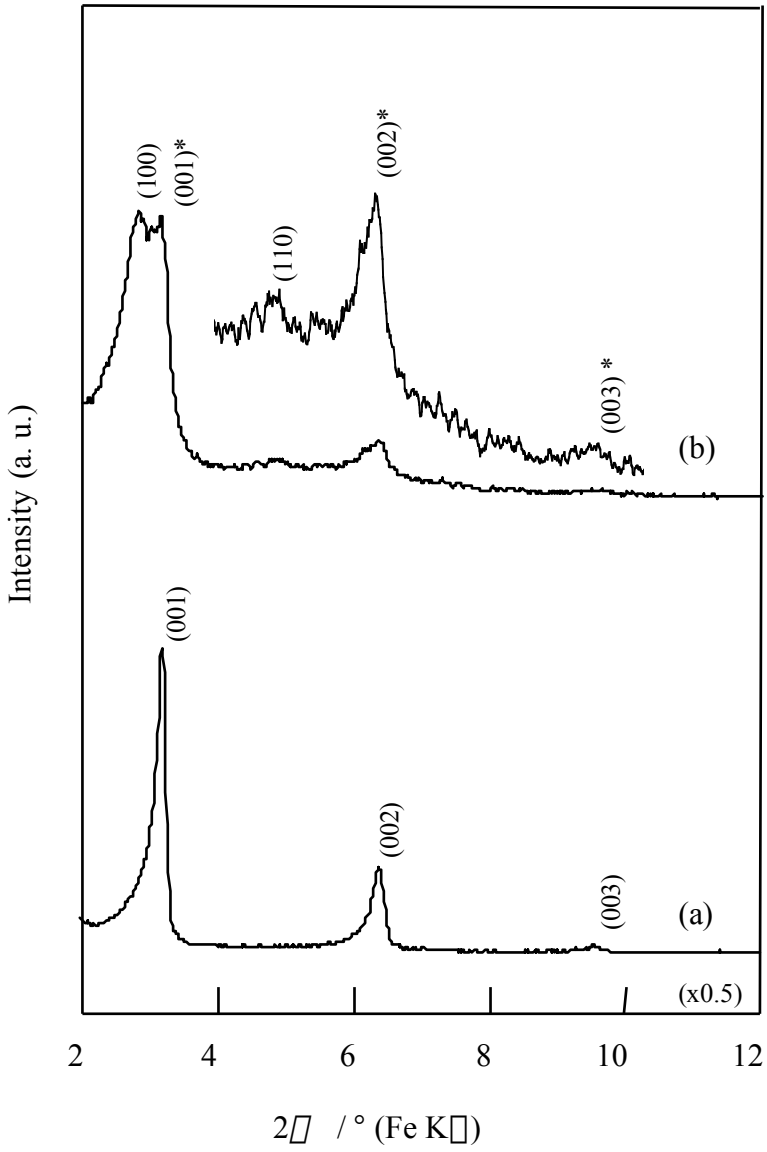

Figure 2-10. XRD patterns of the products obtained during the synthesis of (a), $C_{16-3-16}$–(N/Si = 0.32) and (b) $C_{16-5-16}$–silicates (N/Si 0.2) before pH adjustment.

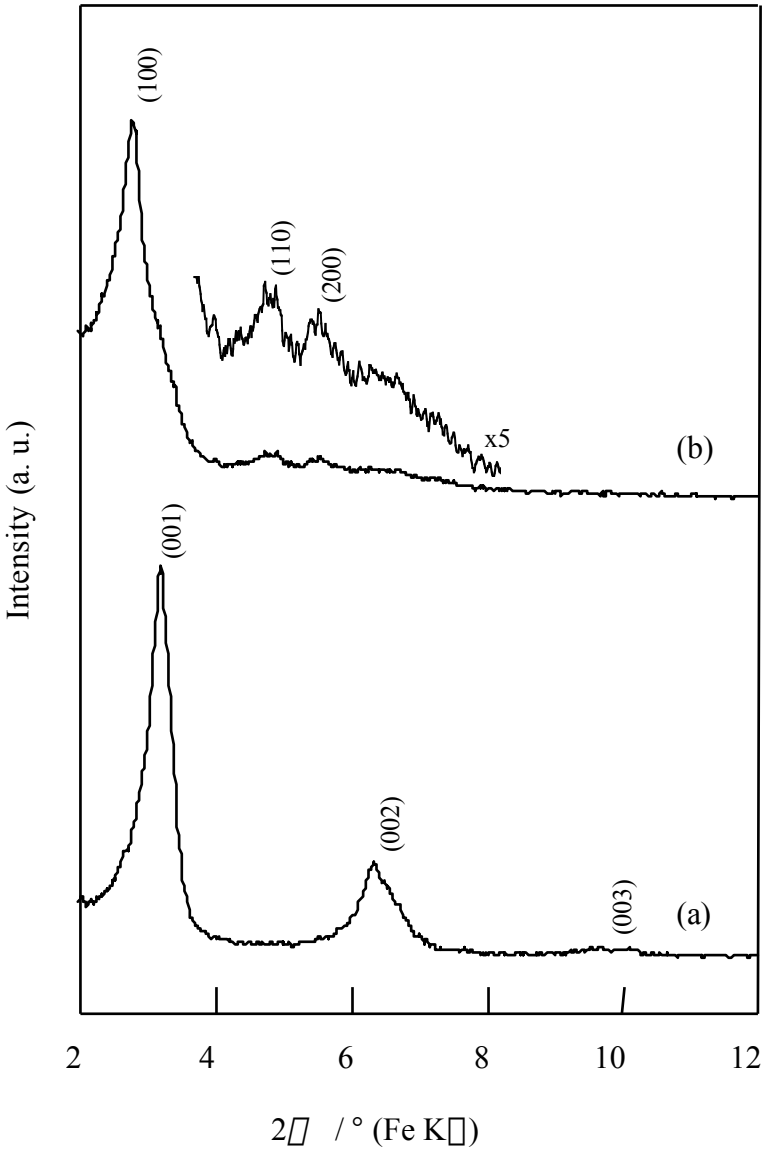

Figure 2-11. XRD patterns of the products obtained during the synthesis of (a) $C_{16-3-16}$–(N/Si = 0.32) and (b) $C_{16-5-16}$–silicates (N/Si 0.2) after pH adjustment.

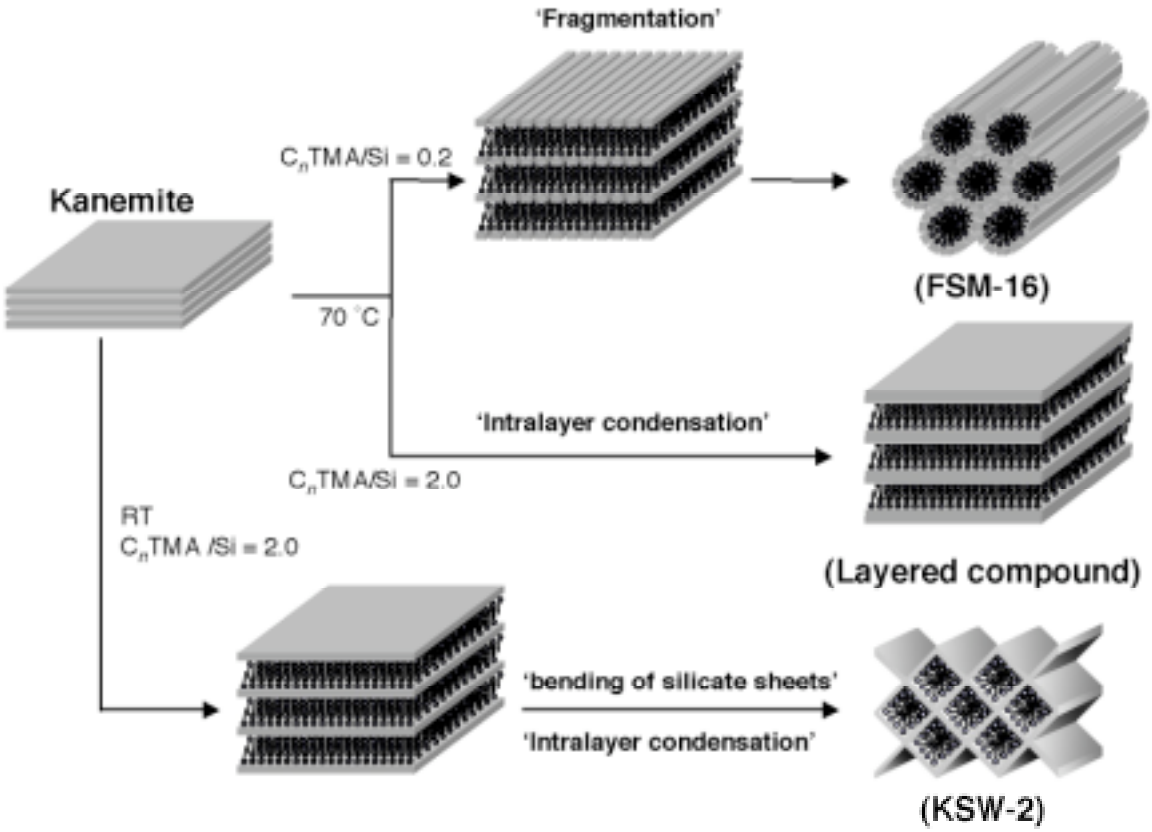

Scheme 2-1. Schematic formation routes of ordered mesostructured and mesoporous materials derived from kanemite.

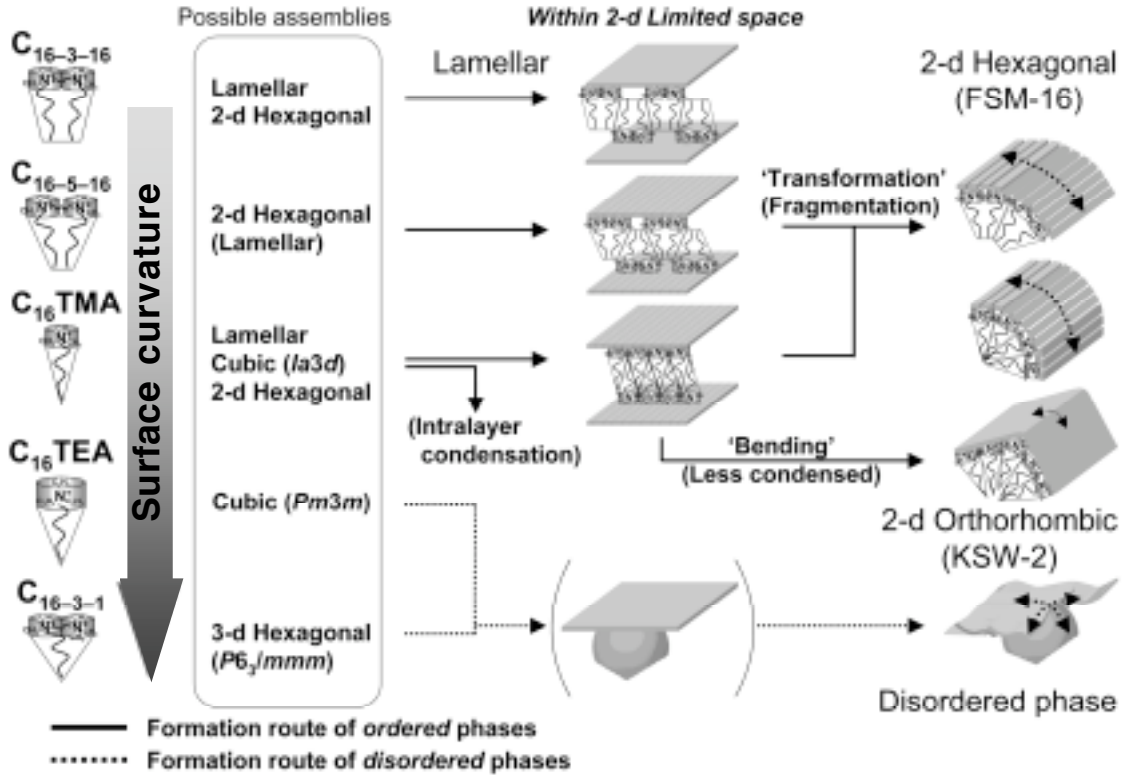

Scheme 2-2. Schematic formation routes of ordered and disordered materials derived from kanemite.

Chapter 3

Synthesis of mesoporous silica KSW-2 from kanemite and alkyltrimethylammonium ions with various alkyl chain lengths

3.1 Introduction

Mesoporous materials have attracted keen interests because they exhibit large surface areas, narrow pore size distributions in mesoporous region, and high pore volumes.[1-5] They are very useful to the fields, such as catalysts, catalyst supports, adsorbents, inclusion vessels, optical and electronic devices, and so on, because these characteristics can not be realized by using zeolites.

Until now there have been many reports on mesoporous materials with very wide range of compositions and structures.[6,7] Morphological control to films and fibers has also been reported.[8-12] However, the structures reported hitherto have been limited by the geometrical packing of surfactants because the formation of mesostructured precursors depends on the cooperative organization of inorganic species and surfactants.[13,14]

Recently, Kimura *et al.* reported the formation of novel mesoporous silica KSW-2.[15] Mesoporous silica KSW-2 is synthesized by mild acid treatment of a layered hexadecyltrimethylammonium (C_{16}TMA)-kanemite complex.[16] Being different from hexagonal mesoporous silicas, such as FSM-16[17,18] and MCM-41[2,3], KSW-2 has a rectangular arrangement of square or lozenge one-dimensional channels. The formation of KSW-2 is totally different from those for silica-based mesostructured materials reported so far. Layered silicate-surfactant intercalation compounds are formed from kanemite and the individual silicate sheets of the compounds bend by intra- and inter-layer condensation upon gradual acid treatment of the intercalation compounds. Because the square or lozenge shape of mesochannels has not previously been found, KSW-2 and the mesostructured precursor are very unique and they stimulate the development of mesoporous materials.

Kanemite, a starting material of KSW-2, is a layered silicate composed of single sheets which are made up with SiO_4 tetrahedral units.[19] The ^{29}Si MAS NMR spectrum of kanemite shows only one peak attributed to Q^3 environment (O-<u>Si</u>(-O-Si≡)$_3$). Though a part of tetrahedral SiO_4 units in kanemite sheets are somewhat varied to Q^4 environment (<u>Si</u>(-O-Si≡)$_4$) by the formation of a three-dimensional silicate network, a substantial amount of Q^3 species remains unreacted even after the formation of the

mesostructured precursor. Therefore, the silicate framework has abundant silanol groups which can be modified by organic groups. Recently I have succeeded in the silylation of KSW-2 and the precursor by the reaction with alkylchlorosilane.[20] The grafted number of silyl groups varied depending on the size of silylating agent. The hydrophobic and the stability against water vapor significantly increase. The pore wall thickness and the width of the pore can be tunable.

More importantly, the mesostructures after acid treatment retain some ordering or regularities of the polysilicate structure. This should reflect the structure of the calcined mesoporous silica, which would be related to the structural control of pore walls of mesoporous silica. Recently there have been some reports on the preparation of mesoporous silicas with crystalline walls derived from zeolite nanocrystallites.[21] However, KSW-2 is unique mesoporous silica with retaining the structural units of layered silicates to some extent. This would provide regular arrangement of silanol groups as well as the homogeneous wall, which is useful for future mesoporous materials design.

Despite the interesting structural and synthetic aspects, studies on the effect of the alkyl chain length of C*n*TMA upon the formation of KSW-2 have not been conducted yet. Based on the formation mechanism, the length of the alkyl chain should affect the bending of the silicate sheets because of the differences in the packing parameters and the resultant curvature. In the present study, therefore, the influence of the alkyl chain length of C*n*TMA on the formation of the precursor to KSW-2 and the possibility of the pore width control were investigated.

3.2 Experimental

3.2.1. Materials

High purity water glass was obtained from Nissan Chemical Co. Dodecyltrimethylammonium chloride, tetradecyltrimethylammonium chloride, hexadecyltrimethylammonium chloride, and octadecyltrimethylammonium chloride were purchased from Tokyo Kasei Co., and used without further purification. Acetic

acid (Kanto Chemical Co., GP Grade) was used. Sodium hydroxide was obtained from Kokusan Chemical Co.

3.2.2. Preparation of a Layered Polysilicate Kanemite

An aqueous solution of sodium hydroxide was added to high-quality water glass to prepare a precursor solution with the Na/Si ratio of 1.0, and the aqueous solution was stirred at room temperature. The solution was dried and heated at 750 °C for 1 h in air, which results in the formation of □-$Na_2Si_2O_5$ after cooling. Resulting □- $Na_2Si_2O_5$ (1 g) was pulverized and dispersed in 50 mL of distilled water, and the suspension was stirred at room temperature for 30 min. The product (kanemite, $NaHSi_2O_5 \cdot 3H_2O$) was centrifuged and air-dried.

3.2.3. Synthesis of Layered Mesostructured Complexes

Layered C*n*TMA-kanemite complexes (*n* = 12, 14, 16, 18) were prepared by stirring 10 g of kanemite and an aqueous solution of C*n*TMACl (0.1 M, 2 L) at room temperature for 3 d, where the C*n*TMA/Si molar ratio was 2.0. Each reaction mixture was centrifuged and dispersed in distilled water. A part of the suspension was centrifuged again and a wet product was air-dried.

3.2.4. Synthesis of Mesoporous Silica KSW-2 Precursor

The resulting layered C*n*TMA-kanemite complexes dispersed in water, as described above, were acid-treated. The pH values of the suspension were adjusted to the desired values (9.0 – 4.0) by the addition of 1 M acetic acid. The as-synthesized mesostructured precursors were air-dried and calcined at 550 ˚C at a heating rate of 5 ˚C min^{-1} in ambient air for 6 h to remove organic fractions.

3.2.5. Characterization

Powder X-ray diffraction (XRD) patterns were obtained by using a Mac Science M03XHF[22] diffractometer with monochromated Fe K□ radiation. IR spectra were

recorded on a Perkin-Elmer FT-IR Spectrum One spectrometer by KBr and Nujol techniques after a sample was dehydrated at 120 ˚C. Nitrogen adsorption isotherms were obtained by using a BELSORP 28 (Bel Japan, Inc.) at 77 K. Samples were heated at 120 ˚C for 3 h to a residual pressure of 1.3 Pa (10^{-2} Torr) prior to these adsorption measurements. Specific surface areas were determined by a BET method using the data before Kelvin condensation. Because the shape of the mesopores is almost rectangular (semi-squared), the width of the pore was determined by the equation of 4V/S, where V is pore volume and S is inner surface area, which is the most reliable estimation of the pore size in this case. Inner surface area was calculated by the subtraction of outer surface area by *t*-plot method from total BET surface area. Solid-state ^{29}Si MAS NMR measurements were performed on a JEOL CMX-400 spectrometer at a spinning rate of 5 kHz and a resonance frequency of 79.30 MHz with a 45 ° pulse length of 4.1 ms and a recycle time of 100 s. This recycle time has been proven to be long enough to permit complete relaxation of the Si nucleus. Consequently, the intensities of the signals are reliable and valid. The chemical shift was expressed with respect to tetramethylsilane. Integration of the signals in the ^{29}Si spectra was achieved by deconvoluting the peaks using a MacFID simulation program.

3.3 Results and Discussion

3.3.1 Products in the system of C_{18}TMA

The XRD patterns of C_{18}TMA-kanemite and the acid-treated products are shown in Figure 3-1a. The peak at the basal spacing of 3.1 nm and the peaks of higher order diffractions were observed for the sample before the acid treatment, indicating that C_{18}TMA-kanemite has a layered structure. The arrangements of the alkyl chains in C_{18}TMA-kanemite were examined by IR spectroscopy. The IR spectra are shown in Figure 3-2. The absorption bands due to methylene modes (ν_{as} and ν_{s} CH_2) appeared at 2919 and 2850 cm^{-1}. This result indicates that the arrangement of the alkyl chains in the layered complex almost takes a *all-trans* conformation.[22]

When the pH value of the suspension was lowered, the peak intensities in the XRD patterns of the acid-treated products decreased a little and the peaks were gradually shifted to lower angles with the acid treatment. However, the patterns were almost similar to that of starting C_{18}TMA-kanemite, though the basal spacing was increased to 3.4 nm when the pH value was lowered to 5.0. After calcination of the product acid-treated at pH 5.0 showed no characteristic peaks in the XRD pattern, showing the collapse of the structure. These results suggest that the change to a three dimensional structure did not occur during the acid treatment. Very interestingly, the peak (*d*-spacing = 0.37 nm) attributed to the diffraction due to (002) plane of the original silicate framework of kanemite was observed for the acid treated samples as well as C_{18}TMA-kanemite, and the higher order peaks at 0.18 nm and 0.12 nm were also detected.

After the acid treatment, the IR absorption bands due to methylene modes were shifted slightly to higher frequencies, indicating that the arrangements of the alkyl chains changed into a little disordered states. The variations in the amount of C_{18}TMA over Si and the $Q^4/(Q^3+Q^4)$ ratios during the acid treatment are shown in Figures 3-3 and 4, respectively. The molar ratio of C_{18}TMA/Si was 0.31 before the acid treatment and lowered down to 0.25 at pH 5.0. The $Q^4 / (Q^3+Q^4)$ ratio was 0.03 before the acid treatment and it was almost constant until pH 7.0. The ratio increased to 0.10 at pH 6.0 and 0.23 at pH 5.0. This increase seems to be attributed to intralayer condensation of silicate sheets in C_{18}TMA-kanemite complex because the layered structure was retained after the acid treatment.

3.3.2. Products in the systems of C_{16}TMA and C_{14}TMA

The XRD pattern of C_{16}TMA-kanemite was similar to that of C_{18}TMA-kanemite (Figure 3-1b), suggesting that C_{16}TMA-kanemite has a layered structure before the acid treatment. The basal spacing of 2.9 nm and the peaks of higher order diffractions were also observed. The intensities of the peak due to the layered structure were lowered and the new peak at the *d*-spacing of 4.2 nm appeared when the pH value was decreased. The peaks due to the layered structure totally disappeared at pH 6.0 and the other peaks were assigned to an orthorhombic structure, indicating that the mesostructured KSW-2

precursor was formed, as reported previously.

C_{14}TMA-kanemite has also a layered structure where the basal spacing was 2.6 nm (Figure 3-1c). Being similar to C_{16}TMA-kanemite, a new peak at the *d*-spacing of 3.6 nm appeared as the pH value was decreased and the mesostructured KSW-2 derived from C_{14}TMA was formed at pH 7.0. The peaks at the *d*-spacings of 0.37 nm, 0.18 nm, and 0.12 nm were also observed for these samples as well as C_{16}TMA- and C_{14}TMA-kanemites.

The IR absorption bands due to methylene modes appeared at 2919 and 2850 cm^{-1} for both for C_{16}TMA- and C_{14}TMA-kanemites before the acid treatment, indicating that the arrangements of the alkyl chains in the layered complexes take rather *all-trans* conformation, as was found for C_{18}TMA-kanemite. These two bands in the mesostructured precursors after the acid treatment were shifted toward higher frequencies; 2922 and 2852 cm^{-1} for n =16 and 2923 and 2853 cm^{-1} for n =14. This result is related with the increase of gauche conformers and the disordered state.

With the acid treatment the molar ratio of C_{16}TMA/Si decreased slightly and the $Q^4/(Q^3+Q^4)$ ratio increased until pH 7.0. Because the structural change was hardly observed by XRD at pH 8.0, these results suggest that intralayer condensation occurred, as reported previously. In the range of pH 7.0 - 6.0, the Q^4 / (Q^3+Q^4) ratio increased further and the ratio of C_{16}TMA/Si decreased swiftly, indicating that transformation of the layered complex into a mesostructured precursor by the interlayer condensation as well as the progressive intralayer condensation and the partial removal of C_{16}TMA ions.

Though the structural change occurred at a higher pH value for C_{14}TMA than for C_{16}TMA, C_{14}TMA-kanemite showed similar tendencies of the variation of the ratios of C_{14}TMA/Si and Q^4 / (Q^3+Q^4).

Contraction of the mesostructures occurred during calcination, because all the diffraction peaks found for the C_{16}TMA-kanemite acid-treated at pH = 6.0 were shifted to higher diffraction angles and spacing of 4.2 nm changed to 3.6 nm. The spacing found for the case of C_{14}TMA decreased from 3.6 nm to 3.2 nm. These decreases are attributed to the loss of the organic surfactants located within the pores and further condensation of the silicate walls. The degree of the contraction found for C_{16}TMA (the difference of the spacing before and after the calcination) was larger (0.6 nm) than that for C_{14}TMA (0.4 nm). As Figure 3-4 shows, the Q^4 / (Q^3+Q^4) ratios of both of

the acid-treated products before calcination are almost same (ca. 0.5). Therefore, the differences between these two systems can not be explained at present. The N_2 adsorption isotherms are shown in Figure 3-5. The isotherms showed type IV behavior typical of mesoporous materials. The BET surface areas, pore volumes, and the widths of the pore of calcined products are summarized in Table 3-1. All these values for KSW-2 derived from C_{14}TMA are smaller than those for KSW-2 derived from C_{16}TMA, proving the effect of the alkyl chain length.

3.3.3. Products in the system of C_{12}TMA

As for C_{12}TMA-kanemite, a broad peak at d = 3.0 nm appeared (Figure 3-1d). However, no characteristic peaks due to a layered structure were observed. The Q^4 / (Q^3+Q^4) ratio for C_{12}TMA-kanemite was much larger than those for C_{14}, C_{16}, and C_{18}TMA-kanemite. These results suggest that the condensation of silicate sheets to a mesostructure occurred even before the acid treatment. The IR bands for C_{12}TMA-kanemite appeared at 2924 and 2854 cm^{-1}. These bands suggest that the arrangement of the alkyl chains in C_{12}TMA-kanemite is similar to those of the acid-treated samples of C_{16}TMA at pH 6.0 and C_{14}TMA at pH 7.0.

The intensity of the peak at d = 3.0 nm was gradually decreased and broadened upon acid treatment. The decrease in the ratio of C_{12}TMA/Si and the increase in the Q^4 / (Q^3+Q^4) ratio were less profound than those of the acid-treated C_{14}TMA, C_{16}TMA samples. Even though the patterns were not well resolved, the peaks at the *d*-spacing of 0.37 nm, 0.18 nm, and 0.12 nm were also observed for C_{12}TMA-kanemite and the acid-treated samples. This indicates that the original silicate framework of kanemite was still retained to some extent.

After calcination of C_{12}TMA-kanemite before acid treatment, the peak at *d* = 3.0 nm did not disappear completely and became very broad. The intensity was substantially decreased, indicating the substantial disordering of the mesostructure. The N_2 adsorption isotherm showed type I behavior typical of microporous materials and the BET surface area, pore volume, and the width of the pore were much smaller than those for KSW-2 derived from C_{16}TMA and C_{14}TMA (Table 3-1).

3.3.4. Effects of alkyl chain lengths

The relation between the alkyl chain lengths and d-spacings is shown in Figure 3-6. Before acid treatment, the alkyl chain length and the d-value exhibited a good linear correlation from C_{14}TMA to C_{18}TMA and the slope gave an average increment of ca. 0.14 nm per one methylene carbon (CH_2). Because the length of one methylene unit in alkyl chain is 0.127 nm, this value seems to be nearly consistent with a monolayer arrangement with the chains in an *all-trans* conformation. On the other hand, another linear correlation was found among acid treated C_nTMA-kanemite samples (n = 14 at pH 7.0, n = 16 at pH 6.0) and original C_{12}TMA-kanemite complex before acid treatment and the average increment of ca. 0.28 nm per one methylene carbon. Because the value exceeds the length of a bilayer arrangement of the surfactants,

In contrast to conventional mesoporous silicas, the present results show that the formation mechanism of KSW-2 is totally different from those obtained by cooperative organization with dissolved silica species and organic surfactants. Based on the mechanism proposed previously, the bending of the silicate sheets is essential for the formation of the precursor. In fact the use of C_{18}TMA ions tend to form a lamellar mesophase because of the curvature of the surfactant assembly, while C_{16}TMA and C_{14}TAM ions forms mesostructured precursors. These tendency is due to the two-dimensionally limited spaces of kanemite.

3.4. Conclusions

KSW-2 is a novel mesoporous silica with semi-squared mesopores and is obtained by mild acid treatment of layered alkyltrimethylammonium silicate mesostructured materials in which the silicate is derived from kanemite, a single layered sodium polysilicate. The effect of the carbon chain length of the alkyltrimethylammonium cations on the mesostructures was investigated. Hexadecyl- and tetradecyl-trimethylammonium exchanged silicate mesophases are successfully converted to the precursors with higher ordering, whereas the mesophase with

octadecyltrimethylammonium cations exhibit a strong tendency to hold the layered nature. On the other hand, the mesophase containing dodecyltrimethylammonium cations tends to be converted to less ordered three dimensional structure at relatively higher pH region. The width of the semi-squared pore of KSW-2 derived from hexadecyltrimethylammonium cations is larger than that from tetradecyltrimethyl-ammonium cations. The structure of the mesophase containing C_{18}TMA cations collapsed after the heat treatment at 550 °C for 6 h. The mesophase derived from C_{12}TMA cations was calcined under the same conditions and the product was porous with a very disordered structure.

3.5 References

(1) Yanagisawa, T.; Shimizu, T.; Kuroda, K.; Kato, C. *Bull.Chem. Soc. Jpn.* 1990, **63**, 988-992.

(2) Kresge, C. T.; Leonowicz, M. E.; Roth, W. J.; Vartuli, J. C.; Beck, J. S. *Nature* 1992, **359**, 710-712.

(3) Beck, J. S.; Vartuli, J. C.; Roth, W. J.; Leonowicz, M. E.; Kresge, C. T.; Schmitt, K. D.; Chu, C. T.-W.; Olson, D. H.; Sheppard, E. W.; McCullen, S. B.; Higgins, J. B.; Schlenker, J. L. *J. Am. Chem. Soc.* 1992, **114**, 10834-10843.

(4) Huo, Q.; Margolese, D. I.; Ciesla, U.; Demuth, D. G.; Feng, P.; Gier, T. E.; Sieger, P.; Firouzi, A.; Chmelka, B. F.; Schüth, F.; Stucky, G. D. *Chem. Mater.* 1994, **6**, 1176-1191.

(5) Huo, Q.; Margolese, D. I.; Ciesla, U.; Feng, P.; Gier, T. E.; Sieger, P.; Leon, R.; Petroff, P. M.; Schüth, F.; Stucky, G. D. *Nature* 1994, **368**, 317-321.

(6) Corma, A. *Chem. Rev.* 1997, **97**, 2373-2419.

(7) Stein, A.; Melde, B. J.; Schroden, R. C. *Adv. Mater.* 2000, **12**, 1403-1419.

(8) Ogawa, M.; Kikuchi, T. *Adv. Mater.* 1998, **10**, 1077-1080.

(9) Ogawa, M.; Yamamoto, N. *Langmuir* 1999, **15**, 2227-2229.

(10) Huo, Q.; Zhao, D.; Feng, J.; Weston, K.; Buratto, S. K.; Stucky, G. D.; Schacht, S.; Schüth, F. *Adv. Mater.* 1997, **9**, 974-979.

(11) Marlow, F.; McGehee, M. D.; Zhao, D.; Chelka, B. F.; Stucky, G. D. *Adv. Mater.* 1999, **11**, 632-636.

(12) Yang, H.; Ozin, G. A.; Kresge, C. T. *Adv. Mater.* 1998, **10**, 883-887.

(13) Monnier, A.; Schüth, F.; Huo, Q.; Kumar, D.; Margolese, D.; Maxwell, R. S.; Stucky, G. D.; Krishnamurty, M.; Petroff, P.; Firouzi, A.; Janicke, M.; Chmelka, B. F. *Science* 1993, **261**, 1299-1303.

(14) Firouzi, A.; Kumar, D.; Bull, L. M.; Besier, T.; Sieger, P.; Huo, Q.; Walker, S. A.; Zasadzinski, J. A.; Glinka, C.; Nicol, J.; Margolese, D.; Stucky, G. D.; Chmelka, B. F. *Science* 1995, **267**, 1138-1143.

(15) Kimura, T.; Kamata, T.; Fuziwara, M.; Takano, Y.; Kaneda, M.; Sakamoto, Y.; Terasaki, O.; Sugahara, Y.; Kuroda, K. *Angew. Chem. Int. Ed.* 2000, **39**, 3855-3859.

(16) Kimura, T.; Itoh, D.; Okazaki, N.; Kaneda, M.; Sakamoto, Y.; Terasaki, O.; Sugahara, Y.; Kuroda, K. *Langmuir* 2000, **16**, 7624-7628.

(17) Inagaki, S.; Fukushima, Y.; Kuroda, K. *J. Chem. Soc., Chem. Commun.* 1993, 680-682.

(18) Inagaki, S.; Koiwai, A.; Suzuki, N.; Fukushima, Y.; Kuroda, K. *Bull. Chem. Soc. Jpn.* 1996, **69**, 1449-1457.

(19) Vortmann, S.; Rius, J.; Marler, B.; Gies, H. *Eur. J. Mineral.* 1999, **11**, 125-134.

(20) Shigeno, T.; Nagao, M.; Kimura, T.; Kuroda, K. *Langmuir* 2002, **18**, 8102-8107.

(21) Khushalani, D.; Hasenzahl, S.; Mann, S. *J. Nanosci. Nanotechnol.,* 2001, **1**, 129-132.

(22) Shimojima, A.; Sugahara, Y.; Kuroda, K. *Bull. Chem. Soc. Jpn.* 1997, **70**, 2847-2853.

Table 3-**1.** The BET surface area, pore volume, and pore width of calcined acid-treated C_nTMA-kanemite.

	BET surface area m^2g^{-1}	Pore volume cm^3g^{-1}	Pore width nm
C_{16}TMA	1210	0.65	2.7
C_{14}TMA	1050	0.42	1.9
C_{12}TMA	690	0.35	1.0 *

* Calculated by *t* - plot method

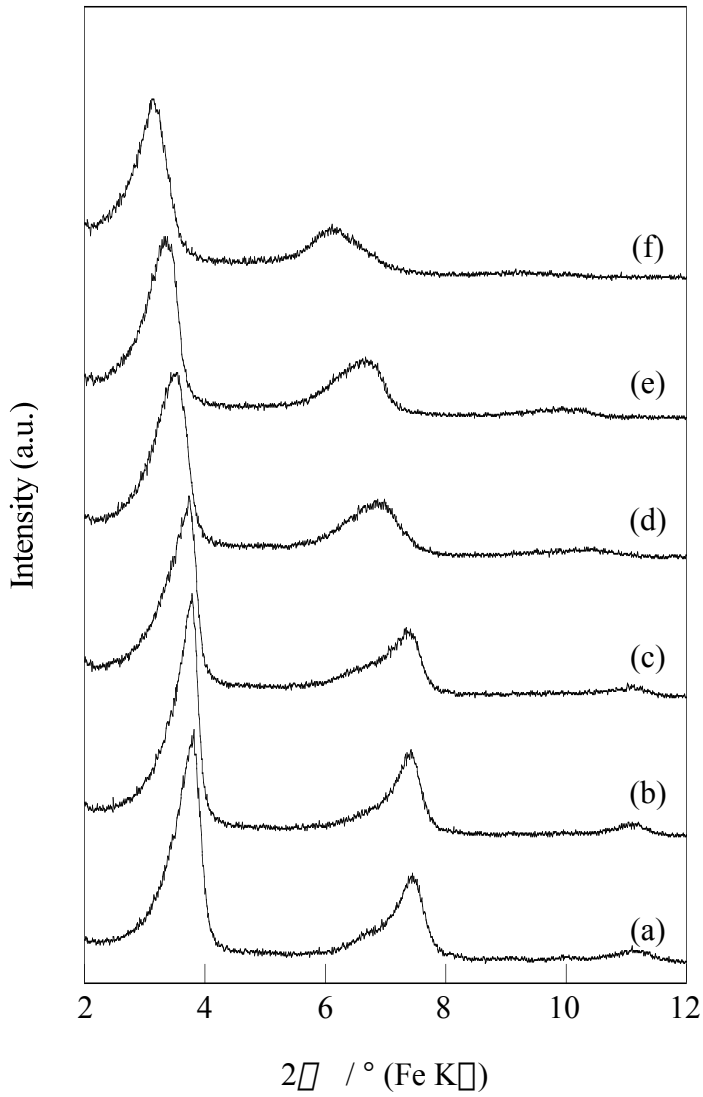

Figure 3-**1a.** XRD patterns of (a) C_{18}TMA-kanemite, the acid-treated products at (b) pH 9.0, (c) pH 8.0, (d) pH 7.0, (e) pH 6.0, and (f) pH 5.0.

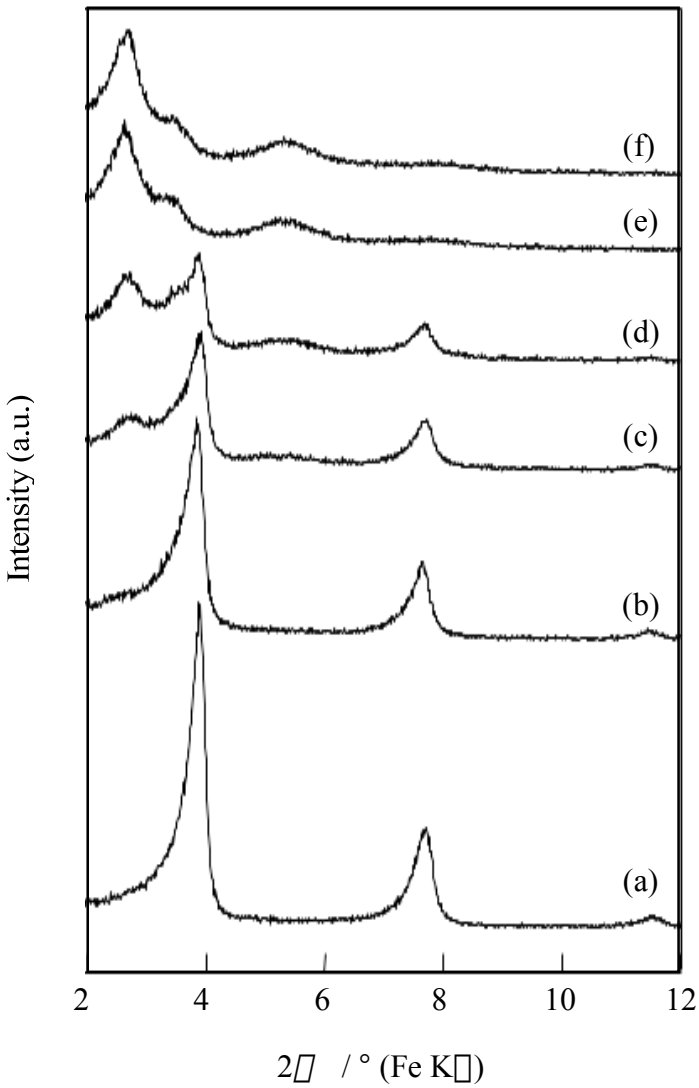

Figure 3-**1b.** XRD patterns of (a) C_{16}TMA-kanemite, the acid-treated products at (b) pH 7.0, (c) pH 6.6, (d) pH 6.4, (e) pH 6.2, and (f) pH 6.0.

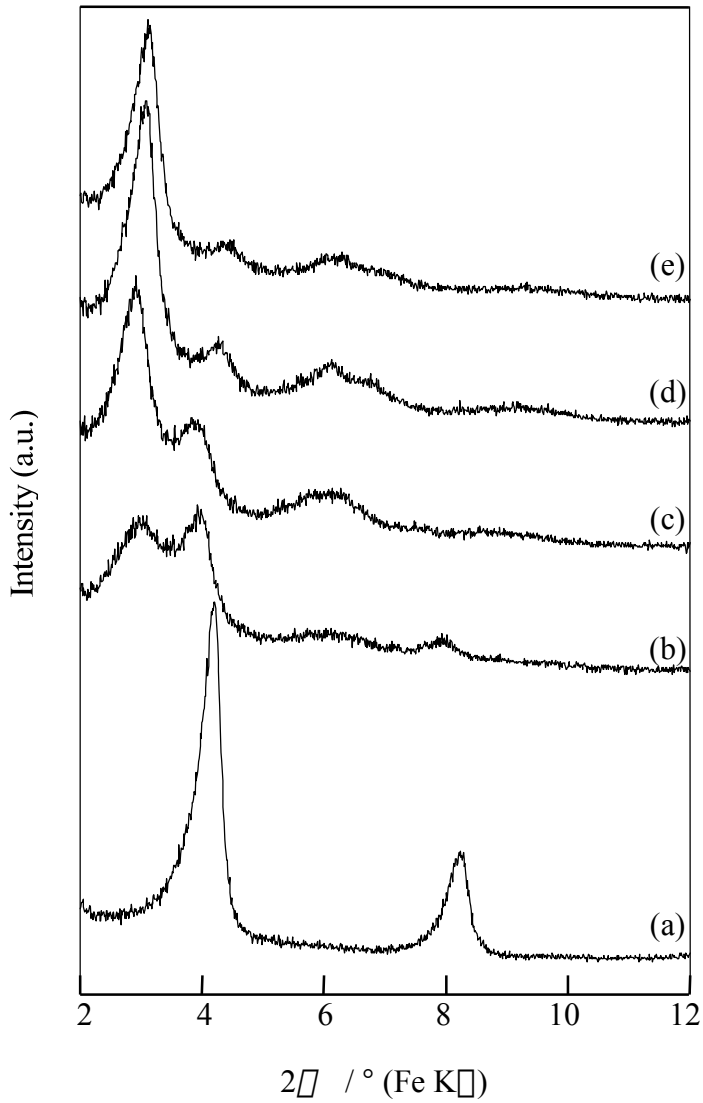

Figure 3-**1c.** XRD patterns of (a) C_{14}TMA-kanemite, the acid-treated products at (b) pH 8.0, (c) pH 7.7, (d) pH 7.0, and (e) pH 6.0.

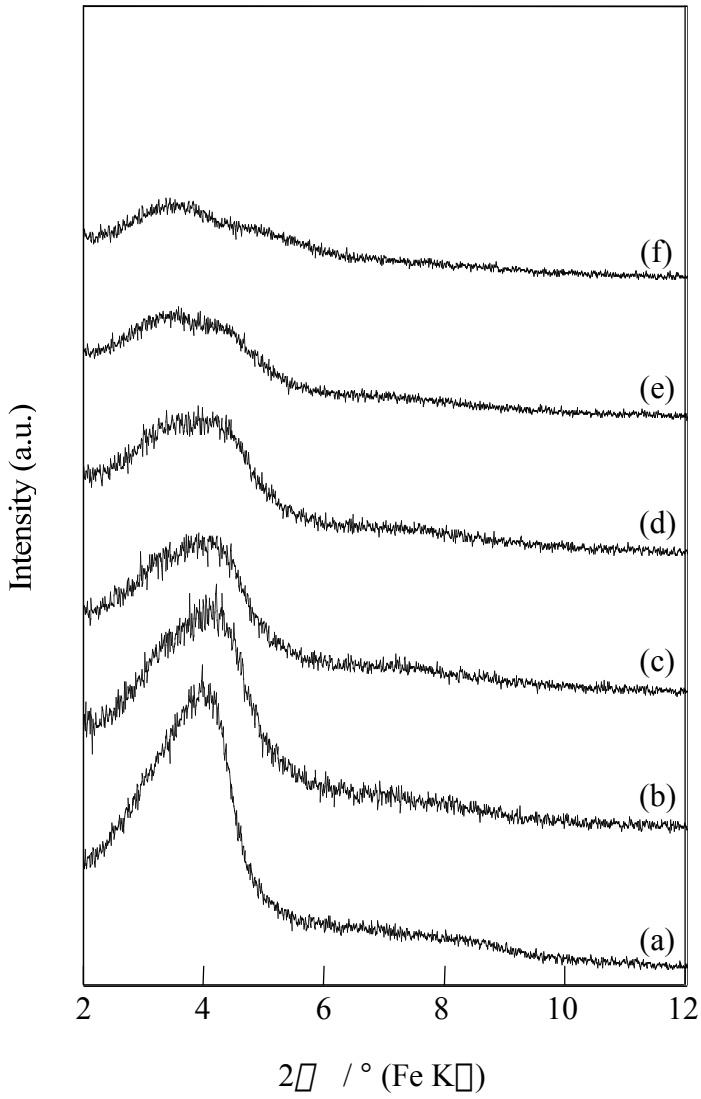

Figure 3-**1d.** XRD patterns of (a) C_{12}TMA-kanemite, the acid-treated products at (b) pH 9.0, (c) pH 8.6, (d) pH 8.0, (e) pH 7.0, and (f) pH 5.0.

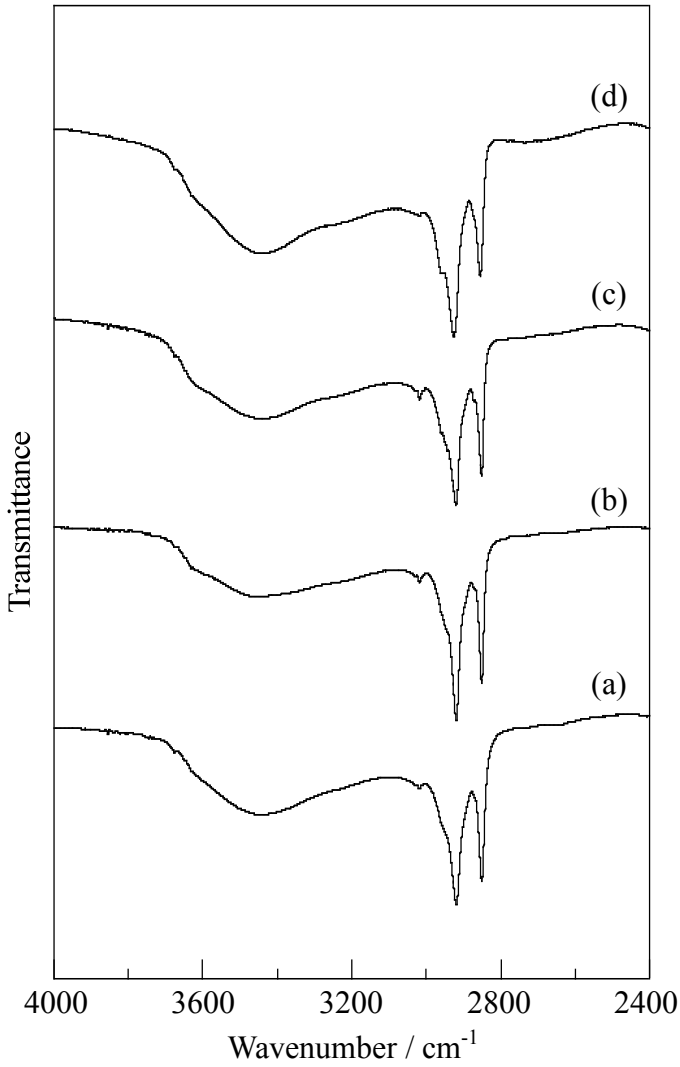

Figure 3-**2.** IR spectra of (a) C_{18}TMA-kanemite, (b) C_{16}TMA-kanemite, (c) C_{14}TMA-kanemite, and (d) C_{12}TMA-kanemite.

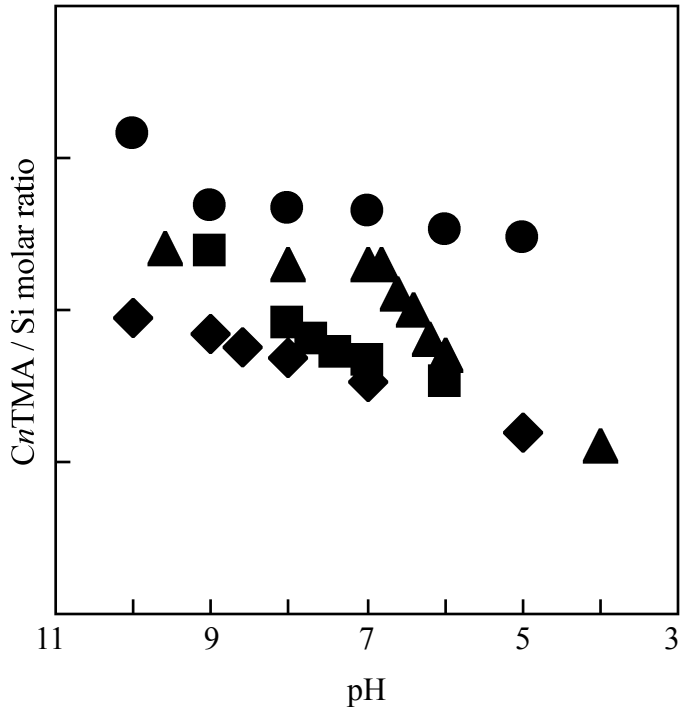

Figure 3-**3.** The variations in the amount of C*n*TMA during acid-treatment; (a) *n* = 12 (◆), (b) *n* = 14 (■), (c) *n* = 16 (▲), and (d) *n* = 18 (●).

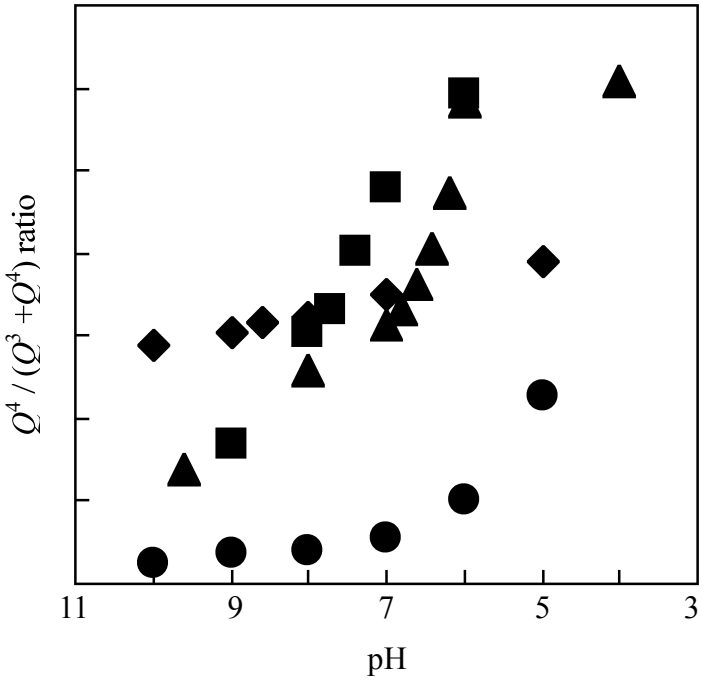

Figure 3-**4.** The variations in the Q^4 / (Q^3 +Q^4) ratio during acid-treatment; (a) n = 12 (◆), (b) n = 14 (■), (c) n = 16 (▲), and (d) n = 18 (●).

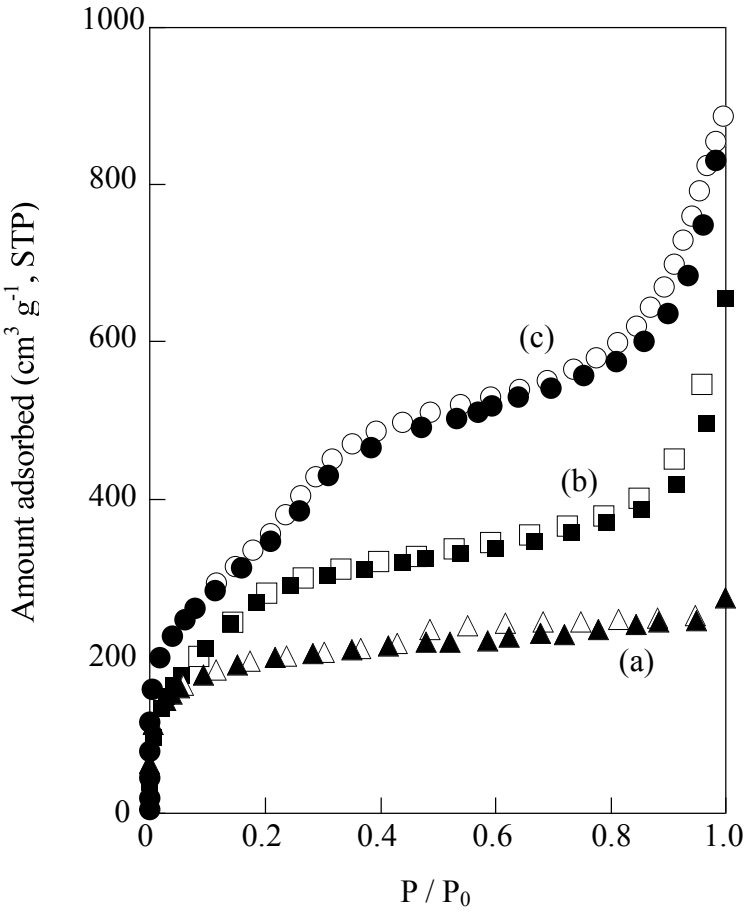

Figure 3-5. N_2 adsorption-desorption isotherms of (a) calcined acid-treated C_{12}TMA-kanemite, (b) calcined acid-treated C_{14}TMA-kanemite, and (c) calcined acid-treated C_{16}TMA-kanemite.

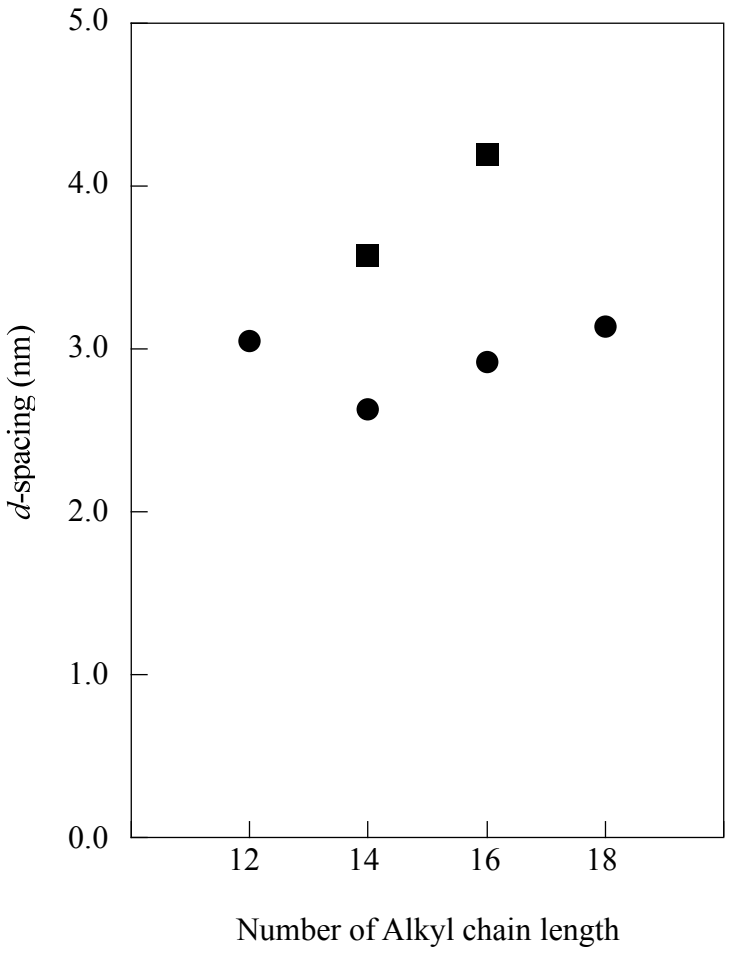

Figure 3-6. The variations between *d*-spacings and the number of alkyl chain length. Filled circles are C*n*TMA-kanemite before acid-treatment.

Chapter 4

Synthesis of Al Containing Mesoporous Silica (KSW-2) with Semi-Squared Channels by Incorporation of Al into the Framework of Kanemite

4.1. Introduction

The synthesis of periodic mesoporous silicas by using organic assemblies has attracted much attention because of their characteristics such as uniform mesopores, high surface areas, large pore volumes, as well as their potential applications to catalysts, catalyst supports, adsorbents, inclusion vessels, optical and electronic devices, and so on.[1-5] Very many researches on long-range (mesostructure) and short-range (framework) structural control as well as morphological and compositional control of mesoporous silicas have been conducted to expand their functions. Recently, Kimure *et al.* reported the synthesis of novel mesoporous silica (denoted as KSW-2) by mild acid treatment of a layered C_{16}TMA–kanemite complex.[6,7] Being different from FSM-16,[2,3] MCM-41,[4,5] SBA-3 and SBA-15[8-10] with one-dimensional (1-d) ordered mesopores (2-d hexagonal, *p6mm*), KSW-2 has an orthorhombic structure (*C2mm*) with rectangular arrangements of semi-squared 1-d channels. Depending on the formation mechanism of KSW-2, the structural units originated from kanemite are retained to some extent in the silicate framework of KSW-2. Therefore, KSW-2 is quite unique and the synthetic method shows the simultaneous control of the mesostructure and framework.

Ordered mesoporous silicas are generally not highly acidic because of their amorphous walls. Nevertheless, the isomorphous substitution of Si with Al and transition metals is of much interest because it affects the catalytic and adsorptive properties.[11,12] In fact, there are many reports on Al incorporation into mesoporous silica like MCM-41.[13-16] In the systems of mesoporous silica derived from kanemite, however, there have been only a few reports on this material though striking differences in the catalytic properties have been clarified between FSM-16 and MCM-41.[17] Inagaki *et al.* reported the syntheses of mesoporous aluminosilicates (Al-FSM-16) from Al-kanemite with tetrahedral Al.[18] Kan *et al.* reported the transformation of layered aluminosilicates and gallosilicates with the kanemite structure into mesoporous materials.[19] Both Al and Ga were four-coordinated in the final forms (Al- and Ga-

FSM-16). However, there have been few characterization data concerning Al-kanemite. In this paper, I report the incorporation of Al into the framework of KSW-2. The present system is totally different from those of the aforementioned Al- and Ga-FSM-16. As-synthesized FSM-16 is formed through the fragmentation of individual silicate sheets in kanemite,[20-24] while a mesostructured precursor of KSW-2 is formed through the bending of the individual silicate sheets.[6] In addition, the remaining structural units originated from kanemite in KSW-2 is very interesting in order to improve the functions.

4.2 Experimental

4.2.1 Materials

An aqueous solution of NaOH was added to high-quality water glass (Nissan Chemical Co.) to adjust the Na/Si ratio (Na_2O/SiO_2 = 1:2). Then, an aqueous solution of $NaAlO_2$ was added to the solution with stirring for 1 h, where the Al/Si ratios were 0.01, 0.03 and 0.05. The starting aqueous solutions were dried and heated for 1 h in air, which results in the formation of Al containing δ-$Na_2Si_2O_5$ powders after cooling. The heating temperature was varied from 750 °C up to 810 °C in order to clarify the effect. Al containing δ-$Na_2Si_2O_5$ (1 g) was dispersed in distilled water (50 mL) and stirred for 30 min at room temperature. The products (Al-kanemite) were centrifuged and air-dried at room temperature.

4.2.2 Synthesis of Al-KSW-2

A layered precursor for Al-KSW-2 was prepared by mixing Al-kanemite and an aqueous solution of C_{16}TMACl (0.1 M) at room temperature for 3 days, where the C_{16}TMA/Si molar ratio was 2.0. The resulting layered precursor was dispersed in 150 ml of distilled water. The pH value of this suspension was decreased down to 5.5 by

the addition of 1 M acetic acid for 30 min and the pH value was kept for 1 h. The mesostructured precursor was air-dried and calcined in ambient air at a heating rate of 5 °C min^{-1} and kept at 550 °C for 6 h to remove organic fractions.

4.2.3 Adsorption of dye molecules on Al-KSW-2

Monovalent cationic dye molecules (methylene blue = MB) were adsorbed on Al-KSW-2 and siliceous KSW-2. Dried KSW-2 (0.02 g) was dispersed in an acetonitrile solution (10 ml) containing MB (0.1 mmol). The suspension was stirred for 1 day and was washed with acetonitrile 5 times. By centrifuging the resultant suspension, solid samples were separated and air-dried. The adsorbed amounts of MB were calculated by subtracting the contents in the supernatants from the initial amounts in the solutions.

4.2.4 Characterization

Powder X-ray diffraction (XRD) patterns were collected by using a Mac Science M03XHF[22] diffractometer with monochromated Fe Kα radiation and a Mac Science MXP[3] diffractometer with monochromated Cu Kα radiation. Nitrogen adsorption and desorption isotherms were obtained by using a BELSORP 28 apparatus (Bel Japan, Inc.) at 77 K. Samples were heated at 120 °C for 3 h to a residual pressure of 1.3 Pa prior to the measurements. Specific surface areas were calculated by the BET method using the data before Kelvin condensation. Because the shape of the mesopores is almost squared, the width of the pore was determined by the equation of $4V/S$, where V is pore volume and S is inner surface area, which is the most reliable estimation of the pore size in this case. Inner surface areas were calculated by the subtraction of outer surface areas by the *t*–plot method from total BET surface areas. Solid-state ^{27}Al and ^{29}Si MAS NMR measurements were performed on a JEOL JNM CMX-400 spectrometer at resonance frequencies of 104.17 MHz (^{27}Al) and 79.30 MHz (^{29}Si) with 45° pulse lengths of 4.0 μs

(^{27}Al) and 4.1 μs (^{29}Si) and recycle times of 5 s (^{27}Al) and 100 s (^{29}Si). The contents of Si, Al, and Na were analysed by inductively coupled plasma arc emission spectrometry (ICP) with a SPS7000A spectrometer (Seiko Instruments Ltd.). Visible absorption spectra were recorded on a Shimadzu UV-2500PC spectrophotometer. To investigate the acidic properties, NH_3-TPD was measured using a Japan Bel Inc., TPD-AT-1 equipment. After evacuation of the sample at 500 °C for 1h, ammonia was adsorbed at 100 °C, and a water vapor treatment was carried out at 100°C in order to remove ammonia adsorbed on non-acidic sites (e.g., hydrogen-bonded one). Then the bed was heated at a rate of 10 °C min^{-1} from 100 °C until all ammonia was desorbed. Desorbed ammonia was detected by a mass spectrometer (Anelva M-QA 100F).[25]

4.3 Results and Discussion

4.3.1 Synthesis of Al containing α-$Na_2Si_2O_5$ and Al-kanemite

The XRD patterns of Al containing α-$Na_2Si_2O_5$ with various Al/Si ratios, obtained by heating in ambient air at 750 °C, are shown in Figure 4-1. Almost all peaks in each pattern were attributed to α-$Na_2Si_2O_5$ phase,[26] suggesting that the main product is α-$Na_2Si_2O_5$. However, in addition to those peaks, several peaks assignable to β-$Na_2Si_2O_5$ appeared at 14.9, 20.8, 21.5 and 30.1°[27] and the peak intensity gradually increased with the Al/Si ratios. Figure 4-2 shows the variation of the XRD patterns of Al containing α-$Na_2Si_2O_5$ prepared at various heating temperatures, where the Al/Si ratio was 0.03. All the patterns were mainly assigned to α-$Na_2Si_2O_5$ though several peaks assigned to β-$Na_2Si_2O_5$ were observed for the samples calcined below 790 °C. The samples calcined above 800 °C showed no peaks assigned to β-$Na_2Si_2O_5$ and a few peaks due to the presence of β-$Na_2Si_2O_5$ at 23.1 and 27.0°.[28,29] Therefore, the most appropriate heating temperature to obtain Al containing α-$Na_2Si_2O_5$ is around 800 °C. Also, the

temperature was varied in accordance with the increase of the Al/Si ratio (Al/Si = 0.01; 785 °C, Al/Si = 0.05; 810 °C).

The ^{27}Al MAS NMR spectrum of Al containing □-$Na_2Si_2O_5$ with the Al/Si ratio of 0.03 is shown in Figure 4-3a. A broad signal was observed at 55 ppm without peaks at around 0 ppm, showing that all Al atoms were four-coordinated and bonded to Si atoms bridged by oxygen atoms ($Al(OSi)_3(ONa)$).

These results about the heating temperature to produce the Al-containing □-$Na_2Si_2O_5$ phase including the presence and absence of □- and □-$Na_2Si_2O_5$ phases give the new information on the synthetic conditions of layered sodium disilicates. Higher heating temperatures are needed to prepare Al containing layered sodium disilicates.

Al-kanemites were easily prepared from the above Al containing □-$Na_2Si_2O_5$ with different Al/Si ratios by the dispersion in distilled water. The powder XRD pattern of Al-kanemite (Al/Si = 0.03) (Figure 4-4) shows a profile characteristic to kanemite. Other products (Al/Si = 0.01, 0.05) showed similar patterns. The ^{27}Al MAS NMR spectrum of Al-kanemite (Al/Si = 0.03) (Figure 4-3b) exhibits a profile very similar to that for Al-containing □-$Na_2Si_2O_5$. The ^{29}Si MAS NMR spectrum of Al-kanemite (Al/Si = 0.03) shows a signal at around –97 ppm, showing the presence of characteristic Q^3 unit of kanemite. (Figure 4-5)

4.3.2 Conversion of Al-kanemite to Al-KSW-2

The XRD patterns of the products during the synthesis of Al-KSW-2 (Al/Si = 0.03) are shown in Figure 4-6. In the product obtained by the reaction of Al-kanemite and an aqueous solution of C_{16}TMACl (C_{16}TMA/Si = 2.0), a peak at the *d*-spacing of 2.9 nm and the higher order diffractions were observed, indicating the formation of a layered material. The ^{29}Si MAS NMR spectrum of the layered material mainly showed a Q^3 peak ($OSi(OSi)_3$), meaning that the framework structure of Al-kanemite was retained in the layered material.

The XRD pattern was drastically changed by the mild acid treatment of the layered material, as reported for the siliceous KSW-2 synthesis,[6] though the peaks became slightly broader in this case. This broadening of the peaks is attributable to the decrease in the regularity of the silicate network because of the incorporation of Al. Similar observations have been reported previously for Al-containing mesoporous silica. [13-16,30]

The retention of the environment of tetrahedral Al during the synthesis of Al-KSW-2 was confirmed by ^{27}Al MAS NMR (Figure 4-3c). Being different from the profiles due to AlO_4 units incorporated into the frameworks of crystalline □-$Na_2Si_2O_5$ and kanemite, the peak due to tetrahedral Al in KSW-2 was broadened. This variation is caused by the structural change during the formation of the three-dimensional silicate network. The ^{29}Si MAS NMR spectrum of Al-KSW-2 (Figure 4-7) showed broader signals assigned to Q^3 and Q^4 ($Si(OSi)_4$) units. According to the incorporation Al into the silicate framework of KSW-2, the Q^4 signal was shifted to lower magnetic fields than that of siliceous KSW-2.

The N_2 adsorption isotherm of Al-KSW-2 (0.03) showed a type IV behavior characteristic of mesoporous materials. (Figure 4-8) The BET surface area, the pore volume and the pore width of Al-KSW-2 (0.03) were 830 m^2g^{-1}, 0.38 cm^3g^{-1} and 2.7 nm, respectively. Those values of siliceous KSW-2 were 890 m^2g^{-1}, 0.43 cm^3g^{-1} and 2.8 nm, respectively. The TEM images of Al-KSW-2 (0.03) showed that semi-squared mesopores are observed clearly (Figure 4-9) and that the periodic distance of adjacent pores corresponds to the value from the XRD data (ca. 3.3 nm). These data are in good agreement with those for siliceous KSW-2. These findings clearly demonstrate the successful formation of Al-KSW-2.

The Al contents of Al-kanemites were 0.43 and 0.59 mol kg^{-1} for the samples of the Al/Si ratios of 0.03 and 0.05, respectively. The Al content of siliceous KSW-2 was also checked to be 0.0097 mol kg^{-1}, which is possibly due to impurities in starting water glass. The ratio of Al/Si for Al-KSW-2 (0.03) was proved to be 0.032, indicating the retention of the Al content during the synthesis of Al-KSW-2.

4.3.3 TPD of ammonia

In order to estimate the acidity of the products, NH_3-TPD was conducted. The NH_3-TPD profiles of Al-KSW-2 (0.03) and siliceous KSW-2 are shown in Figure 4-10. The amounts of acid sites in Al-KSW-2 and KSW-2 are 0.062 and 0.008 mol kg^{-1}, respectively. Because the amount of acid sites of KSW-2 is almost identical to the Al content (0.0097 mol kg^{-1}), the acid sites are attributable to the impurities of KSW-2. Al-KSW-2 exhibits a broad pattern with two peaks at around 250 °C and 400 °C, suggesting a wide distribution of the acid strength.[31] The profile also suggests the presence of a variety of acid sites with different strengths, though further studies should be required. The amount of ammonia for Al-KSW-2 is about 7 times larger than that for KSW-2, indicating that the total amount of acid sites of Al-KSW-2 was increased by the incorporation of Al, though the amount of acid sites corresponded to only 15 % of the Al content, meaning that the incorporated Al was not so efficiently utilized. The ICP data showed that the Na/Si ratio for Al-KSW-2 (0.03) was 0.023 and that the Na/Al ratio was calculated to be 0.72. Consequently, the reason for the small amount of the acid sites of the sample can be explained by the presence of sodium cations which counteract the acid sites. Future work should be necessary to clarify the nature of the acidity of Al-KSW-2 if sodium cations are appropriately removed without probable degradation of the mesostructure.

4.3.4 Adsorption property of dye molecules on Al-KSW-2

MB molecules were adsorbed onto both Al-KSW-2 (Al/Si = 0.03) and siliceous KSW-2. After the adsorption experiments, the N_2 adsorption data indicated the decrease of the pore volumes, meaning that the dye molecules were adsorbed on both the outer and inner surfaces.

In both of the cases, the visible absorption spectra of MB (Figure 4-11) showed the peak at 660 nm, indicating that the dye molecules were adsorbed in a monomeric state.[30,32,33] Even for siliceous KSW-2, MB molecules were adsorbed because of the presence of both surface silanol groups which can weakly interact with MB and a small amount of acid sites due to the impurities. The absorbance of MB for Al-KSW-2 increased with the incorporation of Al compared to that for KSW-2. The adsorbed amount of MB on Al-KSW-2 (25.9 mmol g^{-1}) was larger than that on siliceous KSW-2 (6.8 mmol g^{-1}). Though the ratio of MB/Al-KSW-2 to MB/KSW-2 was smaller than that of acid sites/Al-KSW-2 to acid sites/KSW-2, the incorporation of Al surely contributes to the formation of negatively charged sites on KSW-2.

4.4 Conclusions

Layered sodium disilicate δ-$Na_2Si_2O_5$ containing four-coordinated Al was successfully prepared by heating treatment at appropriate temperatures, depending on the Al contents. Al-containing δ-$Na_2Si_2O_5$ were transformed into Al-kanemite without the variation of Al coordination. By the reaction of Al-kanemite with C_{16}TMA, 2-d orthorhombic mesoporous silica (KSW-2) containing AlO_4 units can be obtained. This synthetic route was useful for the isomorphous substitution of Al atoms within the silicate framework of KSW-2. The incorporation of Al affords the acid sites that are more effective for the adsorption of cationic dyes than siliceous KSW-2. This study reveals that the incorporation of other metal oxides into starting layered silicates is feasible for realizing the compositional variation of ordered mesoporous silicas derived from layered silicates, which would be applicable to various catalytic and adsorptive reactions.

4.5 References

(1) Yanagisawa, T.; Shimizu, T.; Kuroda, K.; Kato, C. *Bull.Chem. Soc. Jpn.* 1990, **63**, 988.

(2) Inagaki, S.; Fukushima, Y.; Kuroda, K. *J. Chem. Soc., Chem. Commun.* 1993, 680.

(3) Inagaki, S.; Koiwai, A.; Suzuki, N.; Fukushima, Y.; Kuroda, K. *Bull. Chem. Soc. Jpn.* 1996, **69**, 1449.

(4) Kresge, C. T.; Leonowicz, M. E.; Roth, W. J.; Vartuli, J. C.; Beck, J. S. *Nature* 1992, **359**, 710.

(5) Beck, J. S.; Vartuli, J. C.; Roth, W. J.; Leonowicz, M. E.; Kresge, C. T.; Schmitt, K. D.; Chu, C. T.-W.; Olson, D. H.; Sheppard, E. W.; McCullen, S. B.; Higgins, J. B.; Schlenker, J. L. *J. Am. Chem. Soc.* 1992, **114**, 10834.

(6) Kimura, T.; Kamata, T.; Fuziwara, M.; Takano, Y.; Kaneda, M.; Sakamoto, Y.; Terasaki, O.; Sugahara, Y.; Kuroda, K. *Angew. Chem. Int. Ed.* 2000, **39**, 3855.

(7) Kimura, T.; Itoh, D.; Okazaki, N.; Kaneda, M.; Sakamoto, Y.; Terasaki, O.; Sugahara, Y.; Kuroda, K. *Langmuir* 2000, **16**, 7624.

(8) Huo, Q.; Margolese, D. I.; Stucky, G. D. *Chem. Mater.* 1996, **8**, 1147.

(9) Zhao, D.; Huo, Q.; Feng, J.; Chmelka, B. F.; Stucky, G. D. *J. Am. Chem. Soc.* 1998, **120**, 6024.

(10) Zhao, D. Y.; Feng, J. L.; Huo, Q. S.; Melosh, N.; Fredrickson, G. H.; Chmelka, B. F.; Stucky, G. D. *Science* 1998, **279**, 548.

(11) Corma, A. *Chem. Rev.* 1997, **97**, 2373.

(12) Liu, Y.; Pinnavaia, T. J. *J. Mater. Chem.* 2002, **12**, 3179.

(13) Janicke, M. T.; Landry, C. C.; Christiansen, S. C.; Kumar, D.; Stucky, G. D.; Chmelka, B. F. *J. Am. Chem. Soc.* 1998, **120**, 6940.

(14) Luan, Z. H.; Cheng, C. F.; He, H. Y.; Klinowski, J. *J. Phys. Chem.* 1995, **99**, 10590.

(15) Ryoo, R.; Ko, C. H.; Howe, R. F. *Chem. Mater.* 1997, **9**, 1607.

(16) Weglarski, J.; Datka, J.; He, H.; Klinowski, J. *J. Chem. Soc, Faraday Trans.* 1996, **92**, 5161.

(17) Inaki, Y.; Yoshida, H.; Kimura, K.; Inagaki, S.; Fukushima, Y.; Hattori, T. *Phys. Chem. Chem. Phys.* 2000, **2**, 5293.

(18) Inagaki, S.; Yamada, Y.; Fukushima, Y. *Stud. Surf. Sci. Catal.* 1997, **105**, 109.

(19) Kan, Q.; Fornés, V.; Rey, F.; Corma, A. *J. Mater. Chem.* 2000, **10**, 993.

(20) Chen, C.-Y.; Xiao, S.-Q.; Davis, M. E. *Microporous Mater.* 1995, **4**, 1.

(21) O'Brien, S.; Francis, R. J.; Price, S. J.; O'Hare, D.; Clark, S. M.; Okazaki, N.; Kuroda, K. *J. Chem. Soc., Chem. Commun.* 1995, 2423.

(22) O'Brien, S.; Francis, R. J.; Fogg, A.; O'Hare, D.; Okazaki, N.; Kuroda, K. *Chem. Mater.* 1999, **11**, 1822.

(23) Sakamoto, Y.; Inagaki, S.; Ohsuna, T.; Ohnishi, N.; Fukushima, Y.; Nozue, Y.; Terasaki, O. *Micoporous Mesoporous Mater.* 1998, **21**, 589.

(24) Kimura, T.; Itoh, D.; Shigeno, T.; Kuroda, K. *Langmuir* 2002, **18**, 9574.

(25) Niwa, M.; N. Katada, C. *Catal. Surveys Jpn.* 1997, **1**, 215.

(26) Kahlenberg, V.; Wendschuh-Josties, M.; Fischer, R. X.; Bauer, H.; Holz, J.; Schimmel, G.; Tapper, A. *Powder Diffraction* 2000, **15**, 139.

(27) Pant, A. K. *Acta Crystallogr.* 1968, **B24**, 1077.

(28) Pant, A. K.; Cruickshank, D. W. J. *Acta Crystallogr.* 1968, **B24**, 13.

(29) Williamson, J.; Glasser, F. P. *Phys. Chem. Glasses* 1966, **7**, 127.

(30) Yoshikawa, T.; Nakamura, T.; Kuroda, K.; Ogawa, M. *Bull. Chem. Soc. Jpn.* 2002, **75**, 2589.

(31) Katada, N.; Fujinaga, H.; Nakamura, Y.; Okumura, K.; Nishigaki, K.; Niwa, M. *Cata. Let.* 2002, **80**, 47.

(32) Otsuki, S.; Adachi, K. *Polym. J.* 1993, **25**, 1107.

(33) Jacobs, K. Y.; Schoonheydt, R. A. *Langmuir* 2001, **17**, 5150.

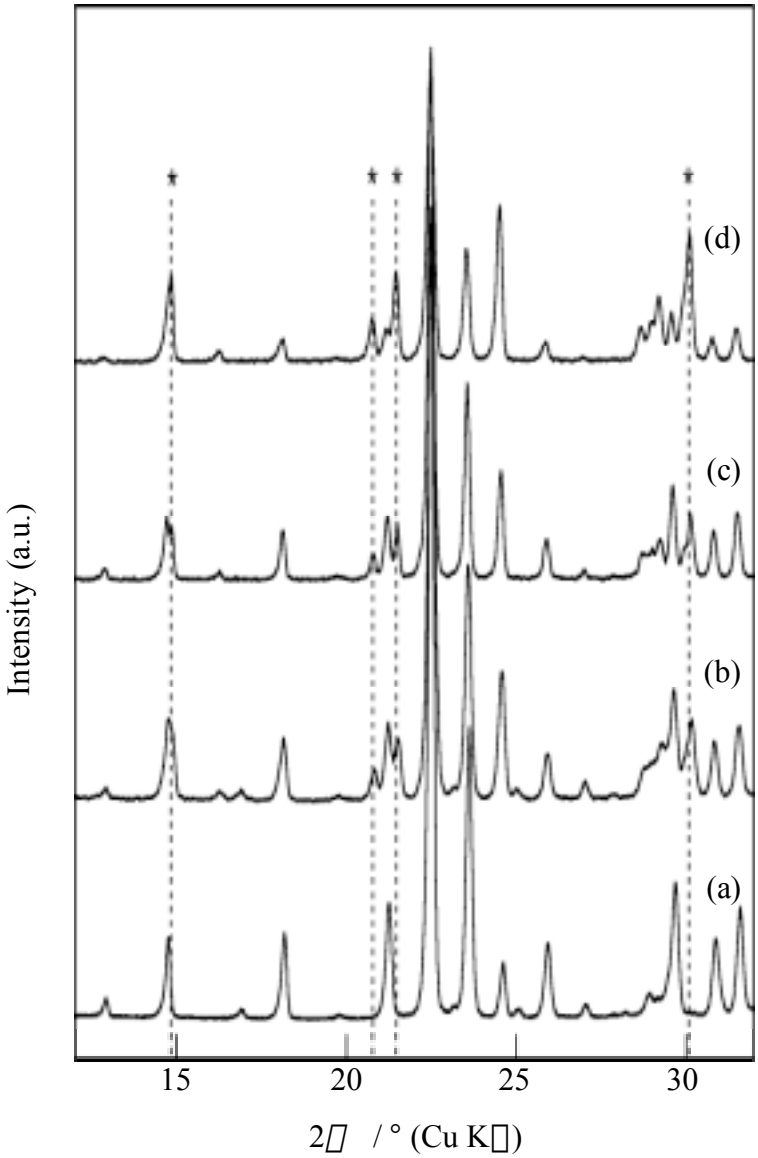

Figure 4-1. XRD patterns of (a) α-$Na_2Si_2O_5$ and Al containing α-$Na_2Si_2O_5$ with various Al/Si ratios: (b) Al/Si = 0.01, (c) Al/Si = 0.03, and (d) Al/Si = 0.05. The peaks with asterisks are assigned to α-$Na_2Si_2O_5$.

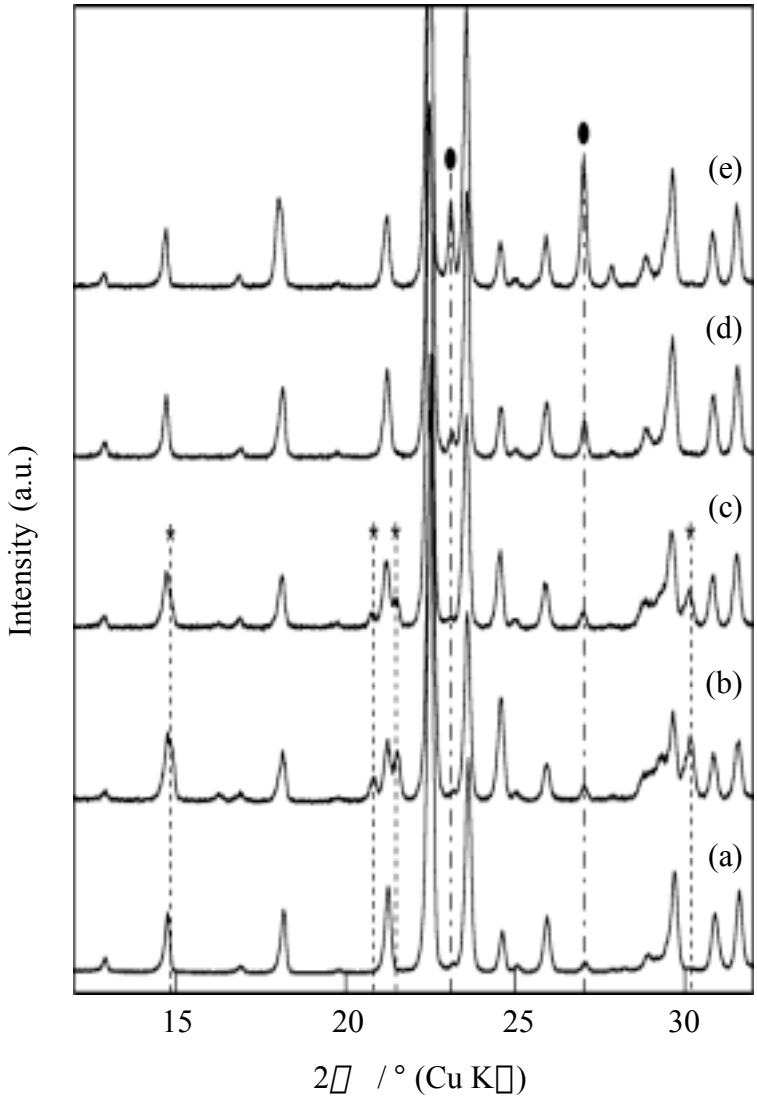

Figure 4-2. XRD patterns of (a) δ-$Na_2Si_2O_5$ and Al containing δ-$Na_2Si_2O_5$ with the Al/Si ratio of 0.03 at various calcination temperature: (b) 780 °C, (c) 790 °C, (d) 800 °C and (e) 810 °C. The peaks with asterisks and filled circles are assigned to δ-$Na_2Si_2O_5$ and α-$Na_2Si_2O_5$, respectively.

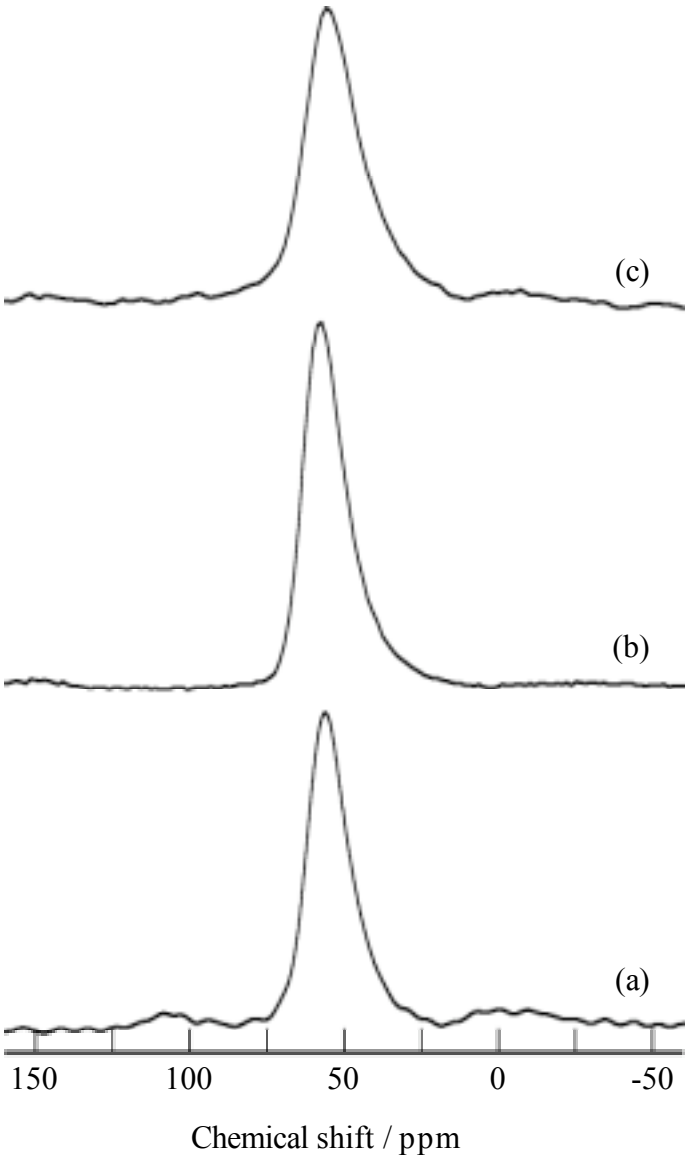

Figure 4-3. ^{27}Al MAS NMR spectra of (a) Al containing □-$Na_2Si_2O_5$, (b) Al–kanemite with the Al/Si ratio of 0.03, and (c) Al–KSW-2.

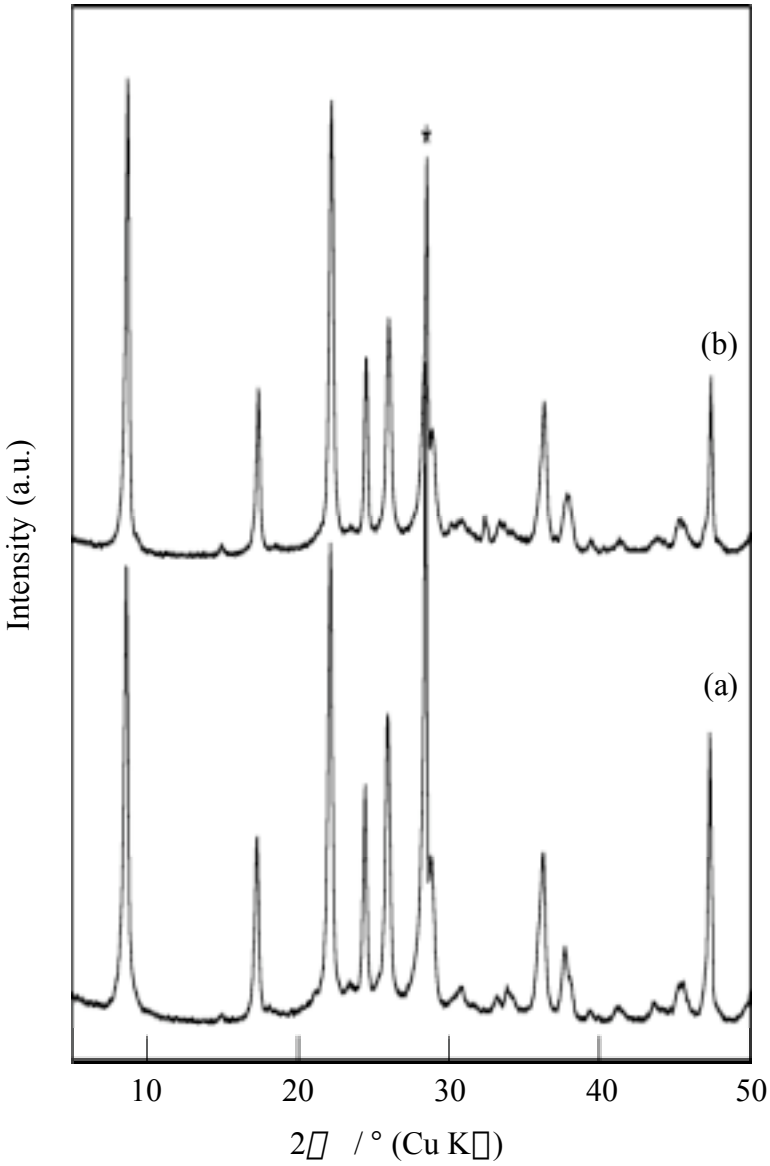

Figure 4-4. XRD patterns of (a) kanemite and (b) Al-kanemite (Al/Si = 0.03). The peaks with asterisks are assigned to Si standard.

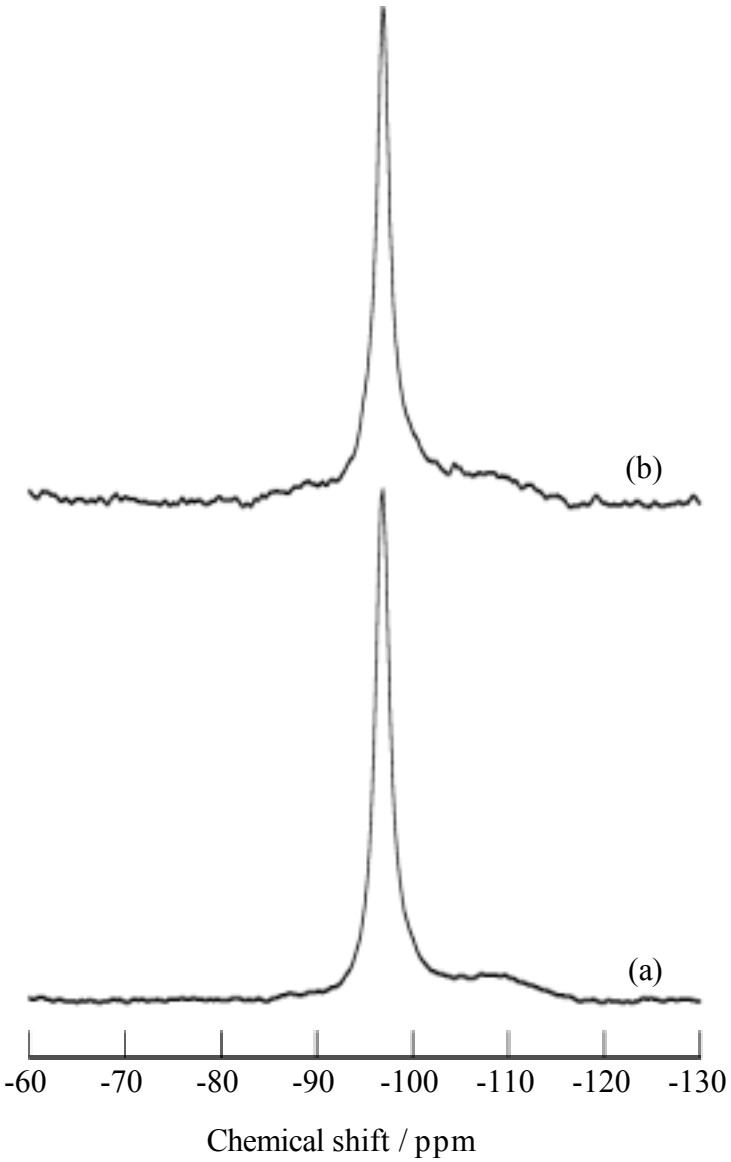

Figure 4-5. ^{29}Si MAS NMR spectra of (a) kanemite and (b) Al-kanemite (Al/Si = 0.03).

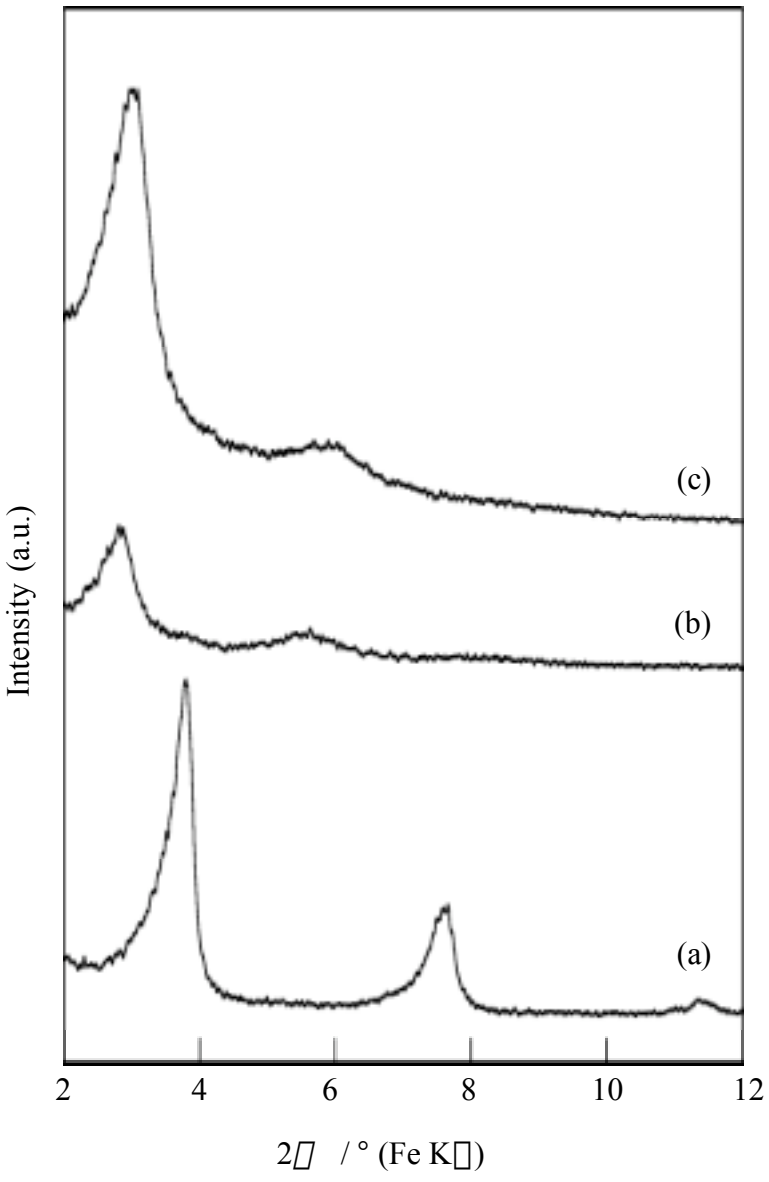

Figure 4-6. XRD patterns of (a) Al containing layered precursor, (b) mesostructured Al–KSW-2 precursor, and (c) Al–KSW-2.

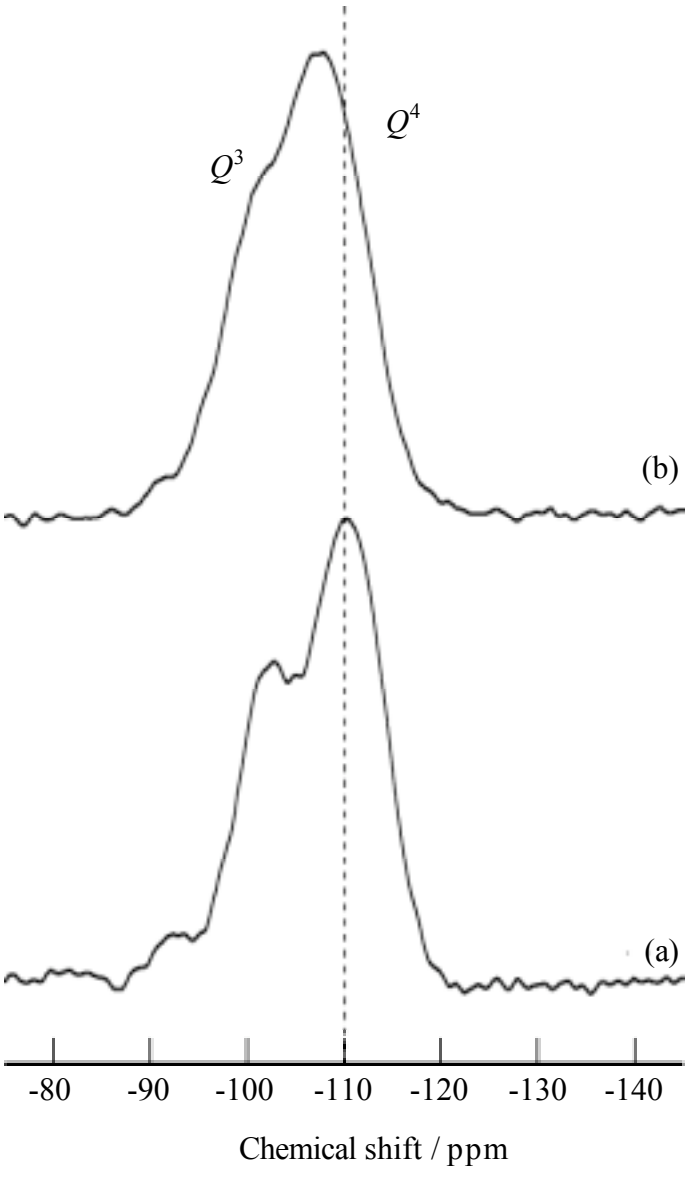

Figure 4-7. ^{29}Si MAS NMR spectra of (a) KSW-2 and (b) Al–KSW-2.

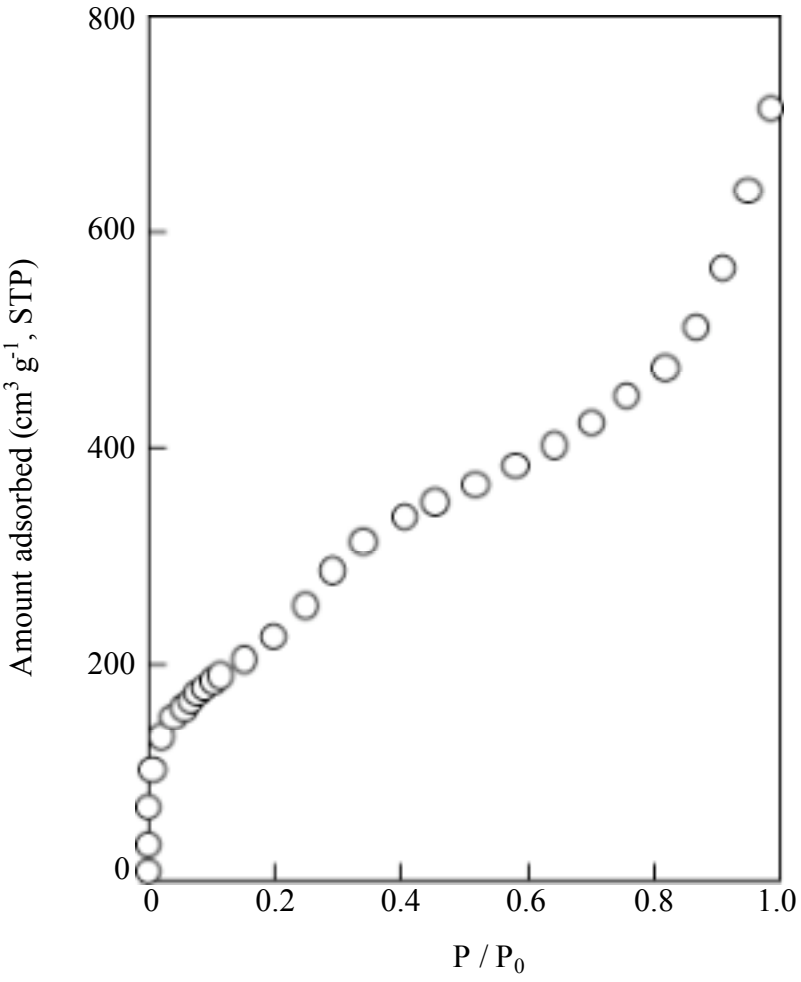

Figure 4-8. N_2 adsorption isotherm of Al-KSW-2 (0.03).

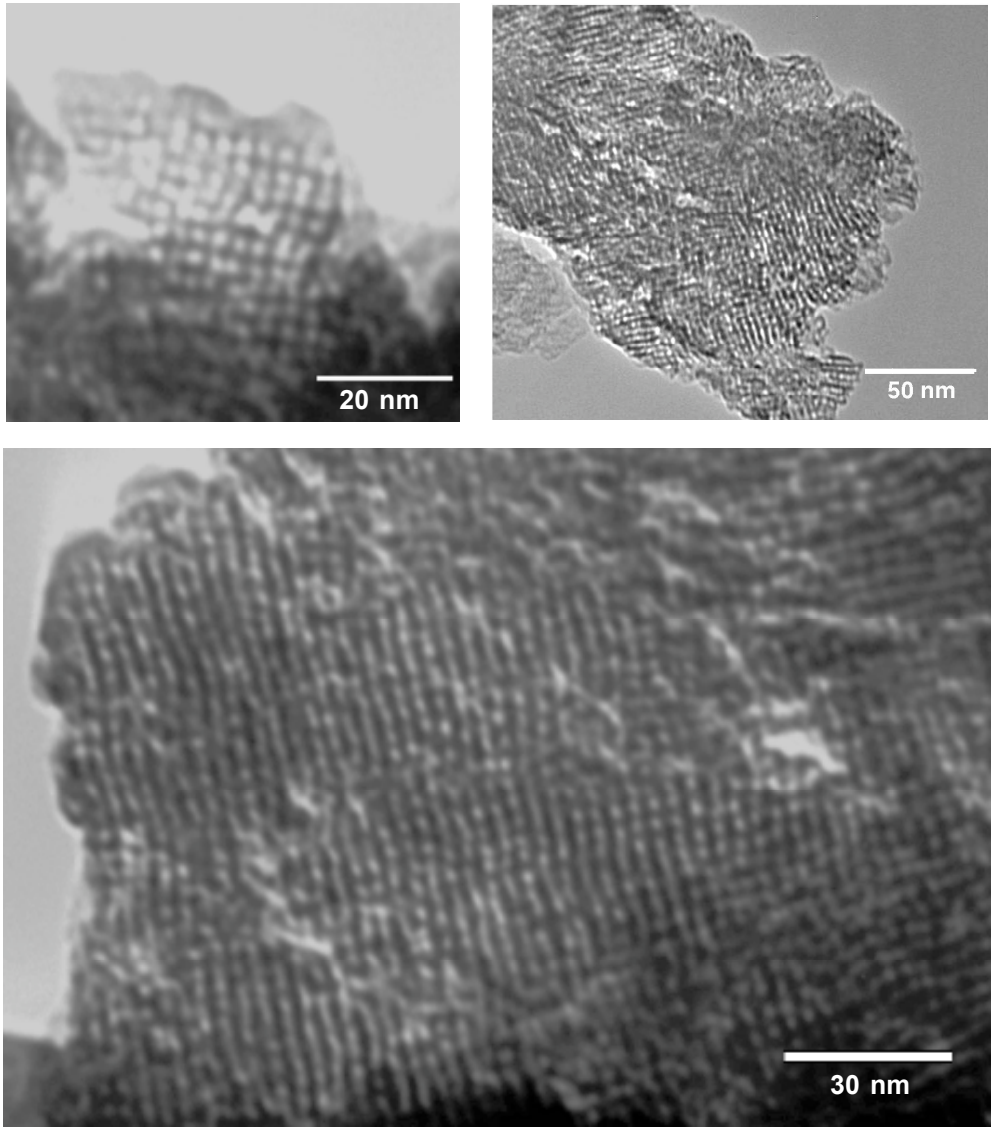

Figure 4-9. TEM images of Al-KSW-2 (0.03).

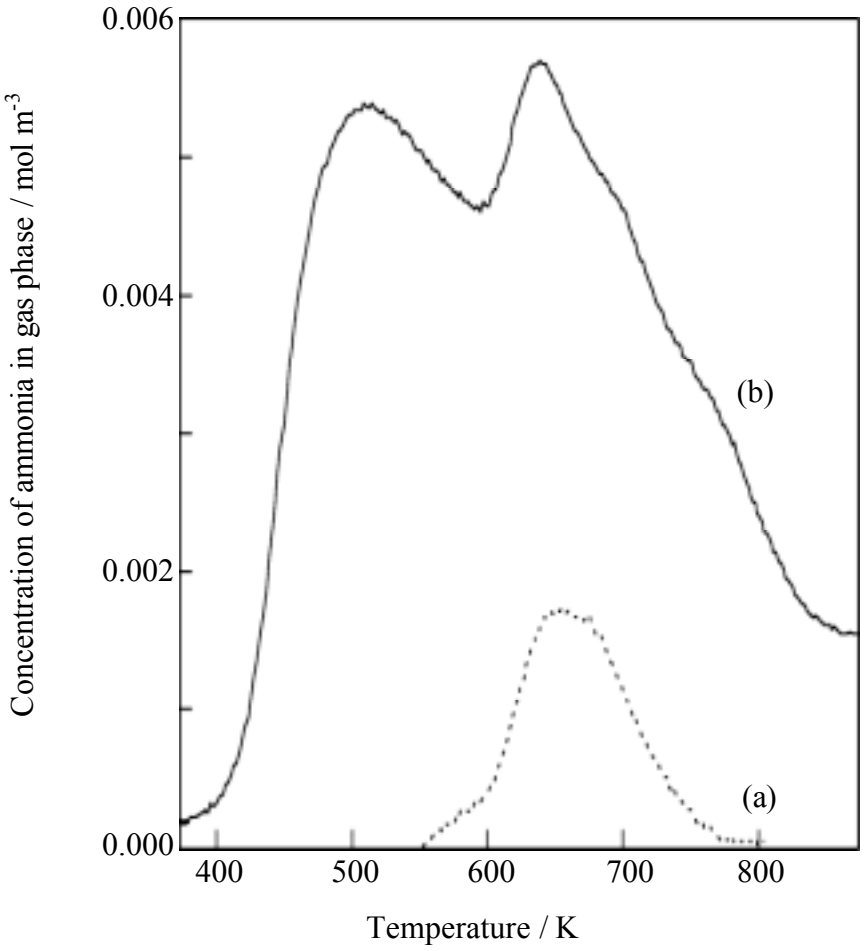

Figure 4-10. Variation of the NH_3-TPD profiles of (a) KSW-2 and (b) Al-KSW-2 (Al/Si = 0.03).

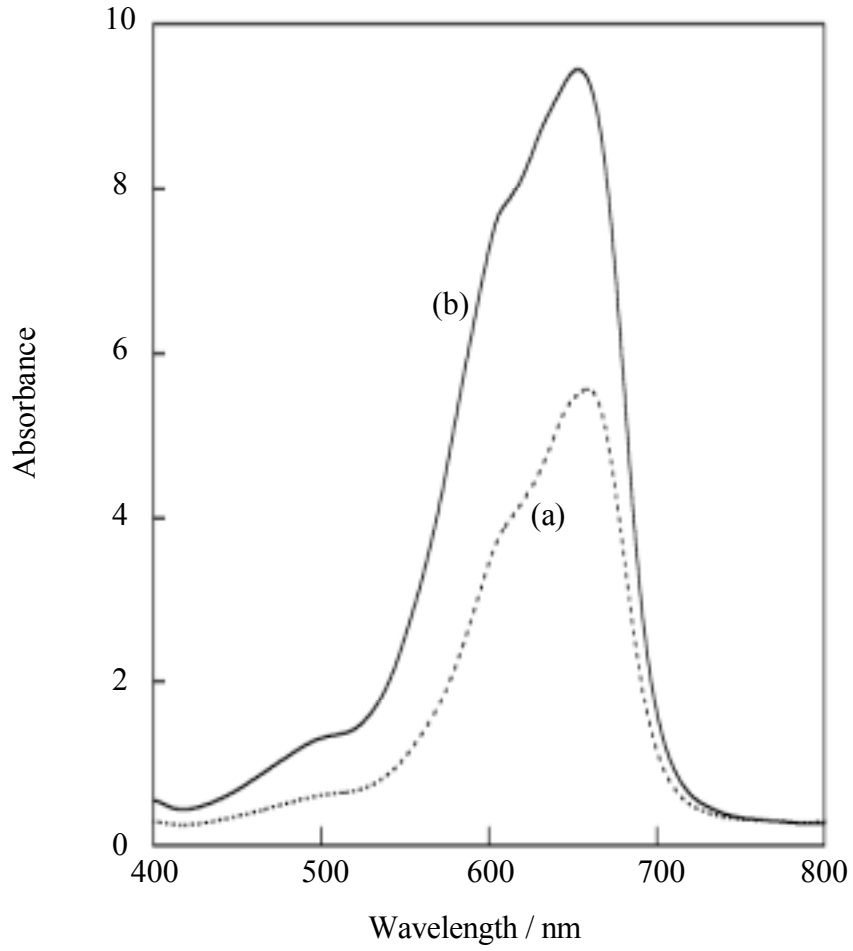

Figure 4-11. Visible absorption spectra of MB on (a) KSW-2 and (b) Al–KSW-2.

Chapter 5

Direct Silylation of a Mesostructured Precursor for Novel Mesoporous Silica KSW-2

5.1. Introduction

Much attention has been paid for the synthesis of ordered mesoporous silicas with high surface areas as well as their applications to catalysts, catalyst supports, adsorbents, inclusion vessels, optical and electronic devices, and so on.[1–5] Various morphologies of mesoporous silica, such as fibers, films, and spheres, have been extensively studied because of their scientific and technological importance.

Recently, Kimure *et al.* reported the formation of novel mesoporous silica (denoted as KSW-2) by mild acid treatment of a layered aklyltrimethylammonium (C_nTMA)–kanemite complex.[6,7] Being different from hexagonal mesoporous silica (FSM-16) derived from kanemite,[2,3] KSW-2 has an orthorhombic structure with rectangular arrangements of semi-squared one–dimensional channels which have not been found previously because the shapes of all the other ordered mesopores have been governed by those of organic assemblies as structure directing agents.[8,9] Therefore, KSW-2 is quite unique and has stimulated the development of ordered mesoporous materials. The mesostructured precursor of KSW-2 is formed through the bending of individual silicate sheets of kanemite.[6] Kanemite is a layered silicate composed of single sheets which are made up with SiO_4 tetrahedral units.[10] Consequently, the structural unit of the silicate sheet in kanemite is retained in the precursor to some extent though the regularity is reduced after calcination.[6]

One of the most important features of mesoporous silica is the presence of silanol groups (Si–OH) on the inner surfaces and the Si–OH groups can be modified in various ways. Ordered mesoporous silica has been organically modified by grafting, coating, and co-condensation methods.[11] Among them, grafting by post treatment with reactive reagents is used most frequently. Typical reactions include silylation[12,13] (Eq. (1)), esterification[14] with alcohols (Eq. (2)), and functionalization with Grignard reagents[15] (Eq. (3)):

$$\equiv Si–OH + R_3Si–Cl \rightarrow \equiv Si–O–SiR_3 + HCl \qquad (1)$$

$$\equiv Si–OH + R–OH \rightarrow \equiv Si–O–R + H_2O \quad (2)$$

$$\equiv Si–OH + R–OH \rightarrow \equiv Si–O–R, \quad \equiv Si–O–R + RMgX \rightarrow \equiv Si–R \quad (3)$$

Consequently, the material systems can be extended to a wide variety of organic-silicate mesostructured materials.[16] Organic modification of ordered mesoporous silica is very effective to control pore size, and it improves the mechanical strength and tailors the surface functionality.[5,12,13,17–23] Trimethylsilylation of ordered mesoporous silica has been reported since the beginning of the researches on ordered mesoporous materials.[5,12] Recent advances include the removal of toxic heavy metal ions, polymer syntheses in a confined space, optical resolution of racemic mixtures, and immobilization of biological molecules.[11,24]

In contrast to conventional mesoporous silicas composed of amorphous silica walls, the mesostructured precursor of KSW-2 possesses the silicate units originated from kanemite in the wall to some extent.[6] It is interesting that the wall structure of the precursor is composed of partly intralayer-condensed individual silicate sheets in kanemite.[6] Nevertheless, the ordering of the wall structure was reduced during calcination to remove organic fractions. Therefore, in this study, a mesostructured precursor of KSW-2 was directly modified with silylating agents on the presumption that the wall might have some regularities after the modification. KSW-2 was also silylated for comparison and the adsorption characteristics of these materials are presented.

5.2 Experimental

5.2.1 Materials

An aqueous solution of NaOH was added to high-quality water glass to prepare a solution with the Na/Si ratio of 1.0.[6] The solution was dried and heated at 750 °C for 1 h in air, which results in the formation of δ-$Na_2Si_2O_5$ after cooling. One gram of δ-$Na_2Si_2O_5$ was pulverized and dispersed in 50 mL of distilled water, and the suspension

was stirred at room temperature for 30 min. The product (kanemite, $NaHSi_2O_5 \cdot 3H_2O$) was centrifuged and used for further reactions without air-drying. The purity of air-dried kanemite was checked by powder XRD and the ^{29}Si MAS NMR spectrum of kanemite showed only one peak attributed to Q^3 environment (O–Si(–O-Si≡)$_3$).[10] A layered C_{16}TMA-kanemite complex was prepared by mixing kanemite and an aqueous solution of C_{16}TMACl (0.1 M) at room temperature for 3 d, where the C_{16}TMA/Si molar ratio was 2.0. The resulting layered C_{16}TMA-kanemite complex was dispersed in distilled water. The pH value of this suspension was decreased down to 5.5 by the addition of 1 M acetic acid for 30 min. Mesoporous silica KSW-2 was also prepared for comparison. The mesostructured precursor was air-dried and calcined at 550 °C at a heating rate of 5 °C min^{-1} in ambient air for 6 h to remove organic fractions.

5.2.2 Silylation of the precursor

Chlorotrimethylsilane (TMS–Cl) and octyldimethylchlorosilane (ODMS–Cl), both of which were purchased from Tokyo Kasei Co., were used without further purification. The mesostructured precursor was preheated at 150 °C for 3 h under vacuum. After 1 g of the precursor was dispersed in 50 mL of toluene, 10 mL of the silylating agent (TMS–Cl or ODMS–Cl) was added to the mixture. The suspension was refluxed for 24 h in the presence of 5 mL of pyridine under N_2 atmosphere. Pyridine was used as an agent both to promote the direct reaction of the chlorosilyl groups with the surface hydroxyl groups as a catalyst[25] and to trap excess hydrogen chloride generated during the reaction. The degree of silylation was slightly decreased when pyridine was not added. The products were air-dried after washing with toluene and ethanol. Silylation of KSW-2 was also carried out in a similar manner. In order to examine whether the silyl groups can be used to cover the surface of the mesopores of KSW-2, trimethylsilylated KSW-2 (TMS-KSW-2) and trimethylsilylated precursor (TMS-precursor) were calcined at 550 °C at a heating rate of 5 °C min^{-1} in ambient air for 6 h to remove the methyl groups.

5.2.3 Characterization

Powder X-ray diffraction (XRD) patterns were obtained by using a Mac Science M03XHF[22] diffractometer with monochromated Fe K radiation for the measurement of low angle regions and a Mac Science MXP[3] diffractometer with monochromated Cu K radiation for higher angles. IR spectra were recorded on a Perkin-Elmer FT-IR Spectrum One spectrometer by KBr disc technique after samples were dehydrated at 120 °C. Nitrogen adsorption and desorption isotherms were obtained by using a BELSORP 28 apparatus (Bel Japan, Inc.) at 77 K. Samples were heated at 120 °C for 3 h to a residual pressure of 1.3 Pa (10^{-2} Torr) prior to the measurements. Specific surface areas were determined by BET method using the data before Kelvin condensation. Because the shape of the mesopores is almost squared, the width of the pore was determined by the equation of $4V/S$, where V is pore volume and S is inner surface area, which is the most reliable estimation of the pore size in this case. Inner surface area was calculated by the subtraction of outer surface area by a *t*–plot method from total BET surface area. The hydrophobic nature of the silylated derivatives was examined by water vapor adsorption measurement. Water adsorption isotherms were obtained by using a BELSORP 18 apparatus (Bel Japan, Inc.) at 298 K. Thermogravimetry and differential thermal analysis (TG-DTA) were performed by a Mac Science 2000S apparatus with a heating rate of 10 °C/min in an air flow. CHN analysis was conducted with a Perkin-Elmer PE2400II instrument. Solid-state ^{29}Si MAS NMR measurements were performed on a JEOL JNM CMX-400 spectrometer at a spinning rate of 5 kHz and a resonance frequency of 79.30 MHz with a 45° pulse length of 4.1 s and a recycle time of 100 s. This recycle time has been proven to be long enough to permit complete relaxation of the Si nucleus, based on our previous measurements. The chemical shift was expressed with respect to tetramethylsilane. Intensity ratios of the signals in the ^{29}Si spectra were calculated after deconvolution of the peaks by the use of a MacFID simulation program.

5.3 Results and Discussion

5.3.1 Characterization of a mesostructured precursor and the calcined product (KSW-2)

A mesostructured precursor of KSW-2 was prepared by mild acid treatment of a layered C_{16}TMA-kanemite complex.[6] The XRD pattern of the mesostructured precursor is shown in Figure 5-1. All the XRD peaks in low angles are assignable to an orthorhombic structure (d_{110} = 4.1 nm). In addition, broad peaks containing a peak at the *d*-spacing of 0.37 nm were observed in the range of 15–30°. This observation indicates that the structural units in kanemite were retained in the mesostructured precursor to some extent, as reported previously.[6] This is one of the most interesting characters of novel mesoporous silica KSW-2 derived from kanemite. The broad XRD peaks were further broadened after calcination, indicating the transformation to a less ordered local structure. Nevertheless, the mesostructure did not change (d_{110} = 3.8 nm) and the peak intensities increased because of no scattering due to the surfactants (Figure 5-1).

The density of silanol (Si–OH) groups at the surface of KSW-2 was calculated by using the data of N_2 adsorption and ^{29}Si MAS NMR measurements. The BET surface area of KSW-2 was 1190 $m^2\ g^{-1}$. The ^{29}Si MAS NMR spectra of the precursor and KSW-2 are shown in Figure 5-2. The peaks due to Q^3 (O<u>Si</u>(O–Si≡)$_3$) and Q^4 (<u>Si</u>(O–Si≡)$_4$) environments were observed at around –101 and –110 ppm, respectively. The Q^3 and Q^4 intensity ratios are also shown in the figure. The ratio decreased during calcination, meaning the condensation of the Q^3 sites in the precursor and a shrinkage of the network. Because the Si atoms of KSW-2 are consisted of only Q^3 and Q^4 environments, the density of Si–OH groups can be calculated on the basis of the Q^3 and Q^4 intensity ratio of KSW-2 (Fig. 2b bottom) and the specific surface area, supposing that all Q^3 sites are due to Si–OH groups. The density was estimated to be 2.8 groups

nm^{-2}. It is quite difficult to estimate the density of the Si–OH groups in the precursor by the same manner because the specific surface area cannot be determined. In addition, Si-O^- sites, associated with the surfactants, are present in the precursor. Therefore, the total density of both the Si–OH groups and Si-O^- sites was roughly estimated on the basis of the Q^3 and Q^4 intensity ratio of the precursor (86:100), being about 1.8 times larger than that of KSW-2. Consequently, the total density of both Si–OH groups and Si-O^- sites in the precursor is calculated to be approximately 5 groups nm^{-2}.

The unique character of the precursor is that it retains the original silicate framework to some extent. In addition, the precursor has a larger amount of Si–OH groups than KSW-2, indicating less condensation of the network. Therefore, silylation of the precursor can be a way to synthesize organically modified mesoporous silica retaining the original silicate units at least partly.

5.3.2 Silylation of the precursor.

The XRD patterns of the silylated products (Figure 5-1) showed the retention of the mesostructure of the precursor. There were basically no significant changes in the 2θ range between 2° and 12° in the XRD patterns of the precursor after the reactions with TMS–Cl and ODMS–Cl. The main peaks due to d_{110} were unchanged (TMS-precursor; 4.1 nm to 4.1 nm, ODMS-precursor; 4.1 nm to 4.0 nm). The TEM image of TMS-precursor showed that semi-squared mesopores are observed clearly and their periodic distance of adjacent pores is in good agreement with the value from the XRD data (ca. 3.9 nm). These results indicate that the original mesostructure was retained.

In the IR spectra of the precursor and the silylated products (Figure 5-3), the spectrum of the TMS-precursor showed the absorption bands attributed to TMS groups at 1257 (δ_s $SiCH_3$), 848 (ρ $Si(CH_3)_3$), and 758 cm^{-1} (ρ $Si(CH_3)_3$). As to the ODMS-precursor, the absorption bands attributed to ODMS groups were observed at 2959 (δ_{as} CH_3), 2926 (δ_{as} CH_2), 2857 (δ_s CH_2), 1255 (δ_s $SiCH_3$), and 846 cm^{-1} (ρ $Si(CH_3)_2$). The ^{29}Si MAS NMR spectra of the TMS- and ODMS-precursors are shown in Figure 5-2a.

The intense Q^4 peaks (–110 ppm) with shoulder Q^3 signals (–101 ppm) were detected and the M^1 peaks due to the silyl groups ($R_3\underline{Si}$–O–Si≡) newly appeared at 14 ppm. The presence of the M^1 peaks and the substantial decrease in the Q^3 signals in the spectra indicate the successful silylation. All of these results strongly support that TMS and ODMS groups have attached to the precursor.

On the other hand, the characteristic bands due to C_{16}TMA cations at 1408 (δNH_4^+), which is observed for the precursor, disappeared after silylation. This result indicates that the surfactants were virtually removed during trimethylsilylation. The almost complete removal of C_{16}TMA cations during silylation was also proved by CHN analysis (Table 5-1). Nitrogen contents due to C_{16}TMA cations were negligibly small in both of the derivatives (< 0.1 mass %). The removal of surfactants can be explained by ion-exchange reaction of C_{16}TMA cations with protons formed by silylation.[26]

The degree of grafting for the precursor is estimated by using the number of silyl groups per SiO_2 (Table 1) because the surface area of the precursor cannot be determined. The numbers of the silyl groups per 1 mol SiO_2 for the silylated precursors were calculated to be 0.25 for TMS and 0.17 for ODMS by using both CHN and TG data. The higher grafting ratio of TMS groups is possibly due to the lower occupying area and lower steric hindrance.

5.3.3 Silylation of calcined KSW-2

KSW-2 was also silylated with TMS–Cl and ODMS–Cl. As was found for the silylated precursors, the XRD patterns of the silylated KSW-2 (Figure 5-1) also showed the retention of the mesostructure. The main peaks due to d_{110} were 3.7 nm for TMS-KSW-2 (d_{110} = 3.8 nm before silylation) and 3.7 nm for ODMS-KSW-2 (d_{110} = 3.7 nm before silylation).

The ^{29}Si MAS NMR spectra of TMS- and ODMS-KSW-2 are shown in Figure 5-2b. In addition to the intense Q^4 peaks (–110 ppm) with shoulder Q^3 peaks (–101 ppm), the M^1 peaks due to the silyl groups were observed at 14 ppm. The result indicates that the

successful silylation of KSW-2 was also achieved by the same procedure. On the basis of the carbon contents, the grafted numbers of TMS and ODMS groups on the surface of KSW-2 were 1.6 and 1.3 groups nm^{-2}, respectively. These values are equivalent to 0.17 TMS groups/SiO_2 and 0.14 ODMS/SiO_2, being smaller than those for the silylated precursors (0.25 for TMS and 0.17 for ODMS). This is quite reasonable because KSW-2 has less Si-OH groups than the precursor.

Compared to the TMS system, a larger amount of silanol groups remained in the ODMS system, as was discussed for the silylated precursors. The amounts of TMS and ODMS groups grafted on FSM-type mesoporous silica are 1.7 and 1.3 groups nm^{-2}, respectively.[13] Therefore, the packing densities of the silyl groups on the surfaces are almost similar in these two mesoporous silicas derived from kanemite.

5.3.4 Local structures of the precursor and KSW-2 after silylation.

The mesostructures of the precursor and KSW-2 did not change during the silylation as described above and organically modified mesoporous silica with a novel mesostructure (semi-square mesopores) was obtained by direct silylation. All the N_2 adsorption isotherms of KSW-2 and the TMS derivatives from both the precursor and KSW-2 showed a type IV behavior characteristic of mesoporous materials, while type I-like isotherms were observed for the ODMS derivatives (Figure 5-4). The BET surface areas, the pore volumes, and the widths of the square mesopores are listed in Table 1. The BET surface area and the pore volume as well as the width of the pore were decreased for all the silylated samples. These changes correlate with the size of the silyl groups. Because ODMS group is bulkier than TMS group, these parameters for the ODMS derivatives are lower than those for TMS derivatives. Silylated precursors show slightly larger values on the mesoporosity than silylated KSW-2 both in the TMS and ODMS derivatives, which should be attributable to the less condensed structure of the precursor. This is consistent with the larger lattice constants of the precursor and suggests that the derivatives should have the structural units of the original framework of

the starting material.

However, the peak at the *d*-spacing of 0.37 nm, found in the pattern of the precursor, became very broad through silylation, suggesting that the capping induced the variation of the local arrangement of the silicate framework. Shimojima *et al.* have recently succeeded in synthesizing organic derivatives of a layered C_{16}TMA-kanemite by monochloroalkyldimethyl-, dichloroalklymethl-, and trichloroalkylsilanes and found that the structural variations are diverse, depending on the kind of the silylating reagent and the alkyl chain length.[27] Therefore, silylation of the mesostructured precursor of KSW-2 under milder conditions and by using bi-functional and tri-functional silylating reagents would also be interesting for further silylation.

5.3.5 Properties of the silylated derivatives

The water vapor adsorption isotherms of KSW-2 and the silylated derivatives from both the precursor and KSW-2 are shown in Figure 5-5. The isotherm of KSW-2 showed a type V behavior, indicating weak interactions between the surface of KSW-2 and water molecules. The amounts of adsorbed water for the silylated derivatives were much smaller than that observed for KSW-2. The silylated derivatives equally displayed their hydrophobic behavior. Though the grafted number of the silyl groups on TMS-KSW-2 was larger than that on ODMS-KSW-2, there were no appreciable differences between them. All the data indicate that the hydrophobicity of KSW-2 was drastically increased by silylation.

The XRD patterns of KSW-2 and the TMS derivatives from both the precursor and KSW-2 before and after the adsorption of water vapor are shown in Figure 5-6. The XRD pattern of KSW-2 after the adsorption did not exhibit any distinct peaks, indicating a structural collapse. On the other hand, the XRD patterns of the silylated derivatives did not change after the adsorption. The increased hydrophobicity of the silylated derivatives improved the stability against water vapor. It has been reported that the stability of MCM-41 materials against the treatment with water depends on the nature of

pore walls. The instability in the presence of water is explained by the hydrolysis of Si–O–Si bonds.[19,28] Accordingly, the increased stability presented here is attributed to the formation of Si–$OSiR_3$ linkage on the inner surfaces.

The TG-DTA curve of TMS-KSW-2 (Figure 5-7) showed a sharp exothermic peak at 475 °C and a weak and broad exothermic peak at around 595 °C. The sharp peak is ascribed to the oxidative decomposition of TMS groups, while the weak peak may be assigned to the combustion of remaining carbon species. On the other hand, ODMS-KSW-2 showed a sharp peak at 228 °C with a shoulder centered at 252 °C and a weak broad peak at around 592 °C. The peak at relatively lower temperature is due to the combustion of octyl groups. The presence of the exothermic peaks strongly supports the silylation and it should also be noted that the peaks appeared at relatively high temperature for the TMS derivatives

Trimethylsilylated products of the precursor and KSW-2 were calcined to find the possibility of tuning the pore size. After calcination of TMS-precursor and TMS-KSW-2, the main peaks due to d_{110} were very slightly shifted to higher angles in the XRD patterns. As shown in Table 1, the BET surface areas and pore volumes were larger than those of the corresponding silylated derivatives and lower than that of KSW-2, while the width of the pores was reduced from 2.7 nm (KSW-2) to 2.3 and 2.1 nm for the calcined TMS-precursor and TMS-KSW-2, respectively. These results indicate the pores of the calcined TMS derivatives were partly covered with silica which was formed by oxidation of attached TMS groups. Because the lattice constants of *a* and *b* axes of KSW-2 are very similar, the average value can be calculated from the d_{110} value of KSW-2 by assuming the lattice is square. Based on the d_{110} (Figure 5-1), the *a* parameter was estimated to be 3.8 nm. From the N_2 adsorption data of KSW-2, the width of the square mesopore was estimated to be 2.7 nm. Consequently, the wall thickness of KSW-2 was evaluated to be ca. 1.1 nm. On the other hand, both of the wall thicknesses of calcined TMS-KSW-2 and calcined TMS-precursor were ca. 1.6 nm by assuming the retention of the structure. Therefore, the wall was thickened by calcining silylated derivatives,

confirming an additional role of silyl groups to control the structure of the pore wall of mesoporous silica derived from the single layered polysilicate.

5.4 Conclusions

Mesoporous silica KSW-2 and the precursor are silylated by the reaction with chlorotrimethylsilane and octyldimethlchlorosilane without the collapse of the mesostructures. The semi-squared mesopores found only for KSW-2 and the precursor are retained after silylation. The grafted numbers for the silylated derivatives derived from the precursor are larger than those from KSW-2. All the silylated derivatives show the lower values of BET surface area, pore volume, and width of the mesopore than those for KSW-2 and the values for ODMS derivatives are lower than those for TMS derivatives because of the steric hindrance. The hydrophobicity and the stability against water vapor significantly increase by silylation. The calcined products of the silylated derivatives have shorter widths of the mesopores than KSW-2. The wall thickness and the width of the pore of KSW-2 can be tunable if silylating agents are properly chosen. Therefore, the present results suggest possible molecular design based on this mesoporous silica. Novel silica-organic hybrids are obtained by silylation of mesoporous silica KSW-2 and the precursor. Because KSW-2 has a very unique shape of mesopores, the organic derivatives should afford distinctive characteristics, such as specific reaction media and adsorption sites, which other mesoporous silicas cannot provide. Although the regularity of the silicate framework retained in the precursor was not found for the silylated derivatives by powder XRD, there should be some ordering in the framework because restructuring of the skeleton cannot occur during the silylation. Further researches are required toward the construction of organically modified mesoporous silicas with retaining a higher ordered silica network close to the original structure, which would be realized under milder reaction conditions by using well designed reagents.

5.5 References

(1) Yanagisawa, T.; Shimizu, T.; Kuroda, K.; Kato, C. *Bull.Chem. Soc. Jpn*. 1990, **63**, 988.

(2) Inagaki, S.; Fukushima, Y.; Kuroda, K. *J. Chem. Soc., Chem. Commun*. 1993, 680.

(3) Inagaki, S.; Koiwai, A.; Suzuki, N.; Fukushima, Y.; Kuroda, K. *Bull. Chem. Soc. Jpn*. 1996, **69**, 1449.

(4) Kresge, C. T.; Leonowicz, M. E.; Roth, W. J.; Vartuli, J. C.; Beck, J. S. *Nature* 1992, **359**, 710.

(5) Beck, J. S.; Vartuli, J. C.; Roth, W. J.; Leonowicz, M. E.; Kresge, C. T.; Schmitt, K. D.; Chu, C. T.-W.; Olson, D. H.; Sheppard, E. W.; McCullen, S. B.; Higgins, J. B.; Schlenker, J. L. *J. Am. Chem. Soc*. 1992, **114**, 10834.

(6) Kimura, T.; Kamata, T.; Fuziwara, M.; Takano, Y.; Kaneda, M.; Sakamoto, Y.; Terasaki, O.; Sugahara, Y.; Kuroda, K. *Angew. Chem. Int. Ed*. 2000, **39**, 3855.

(7) Kimura, T.; Itoh, D.; Okazaki, N.; Kaneda, M.; Sakamoto, Y.; Terasaki, O.; Sugahara, Y.; Kuroda, K. *Langmuir* 2000, **16**, 7624.

(8) Monnier, A.; Schüth, F.; Huo, Q.; Kumar, D.; Margolese, D.; Maxwell, R. S.; Stucky, G. D.; Krishnamurty, M.; Petroff, P.; Firouzi, A.; Janicke, M.; Chmelka, B. F. *Science* 1993, **261**, 1299.

(9) Huo, Q.; Margolese, D. I.; Ciesla, U.; Demuth, D. G.; Feng, P.; Gier, T. E.; Sieger, P.; Firouzi, A.; Chmelka, B. F.; Schüth, F.; Stucky, G. D. C*hem. Mater.* 1994, **6**, 1176.

(10) Vortmann, S.; Rius, J.; Marler, B.; Gies, H. *Eur. J. Mineral.* 1999, **11**, 125.

(11) Stein, A.; Melde, B. J.; Schroden, R. C. *Adv. Mater.* 2000, **12**, 1403.

(12) Yanagisawa, T.; Shimizu, T.; Kuroda, K.; Kato, C. *Bull. Chem. Soc. Jpn.* 1990, **63**, 1535.

(13) Kimura, T.; Saeki, S.; Sugahara, Y.; Kuroda, K. *Langmuir* 1999, **15**, 2794.

(14) Kimura, T.; Kuroda, K.; Sugahara, Y.; Kuroda, K. *J. Porous Mater.* 1998, **5**, 127.

(15) Yamamoto, K.; Tatsumi, T. *Microporous Mesoporous Mater.* 2001, **44-45**, 459.

(16) Sayari, A.; Hamoudi, S. *Chem. Mater.* 2001, **13**, 3151.

(17) Tatsumi, T.; Koyano, K. A.; Tanaka, Y.; Nakata, S. *Chem. Lett.* 1997, 469-470.

(18) Tatsumi, T.; Koyano, K. A.; Tanaka, Y.; Nakata, S. *J. Porous Mater.* 1999, **6**, 13-17.

(19) Ishikawa, T.; Matsuda, M.; Yasukawa, A.; Kandori, K.; Inagaki, S.; Fukushima, T.; Kondo, S. *J. Chem. Soc., Faraday Trans.* 1996, **92**, 1985.

(20) Antochshuk, V.; Jaroniec, M. *Chem. Mater.* 2000, **12**, 2496.

(21) Wouters, B. H.; Chen, T. H.; Dewilde, M.; Grobet, P. J. *Microporous Mesoporous Mater.* 2001, **44-45**, 453.

(22) Zhao, X. S.; Lu, G. Q.; Hu, X. *Microporous Mesoporous Mater.* 2000, **41**, 37.

(23) Impens, N. R. E. N.; Voort, P. v. d.; Vansant, E. F. *Microporous Mesoporous Mater.* 1999, **28**, 217.

(24) Price, P. M.; Clark, J. H.; Macquarrie, D. J. *J. Chem. Soc., Dalton Trans.* 2000, **2**, 101.

(25) Tripp, C. P.; Hair, M. L. *J. Phys. Chem.* 1993, **97**, 5693.

(26) Yanagisawa, T.; Kuroda, K; Kato, C. *React. Solids* 1988, **5**, 167.

(27) Shimojima, A.; Mochizuki, D.; Kuroda, K. *Chem. Mater.* 2001, **13**, 3603.

(28) Koyano, K. A.; Tatsumi, T.; Tanaka, Y.; Nakata, S. *J. Phys. Chem. B* 1997, **101**, 9436.

Tabel 5-1. Characteristics of mesoporous silica KSW-2 and the silylated derivatives.

	BET surface area/ (m_2 g^{-1})	pore volume/ (mL g^{-1})	width of pore[a] / nm	carbon content/ (wt %)	nitrogen content/ (wt %)	number of silyl group per 1 mol SiO_2
KSW-2	1190	0.60	2.7	—	—	—
TMS-precursor	800	0.31	2.2	12.7	0.06	0.25
TMS-KSW-2	770	0.29	2.1	9.2	0.06	0.17
ODMS-precursor	470	0.12	1.6	25.6	0.09	0.17
ODMS-KSW-2	430	0.10	1.5	21.5	0.08	0.14
Calcined TMS-precursor	1110	0.48	2.3	—	—	—
Calcined TMS-KSW-2	1000	0.40	2.1	—	—	—

[a] The width of pore was determined by the equation of $4V/S$, where V is pore volume and S is inner surface area.

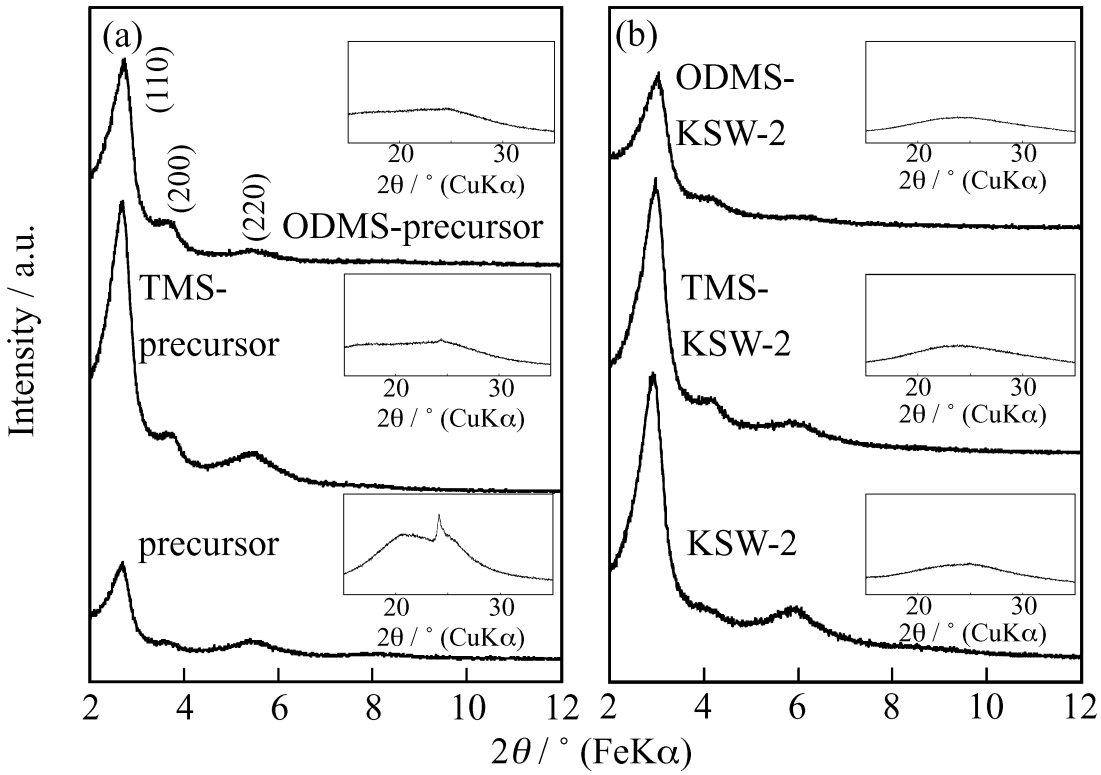

Figure 5-1. XRD patterns of (a) precursor and the silylated derivatives; (b) KSW-2 and the silylated derivatives.

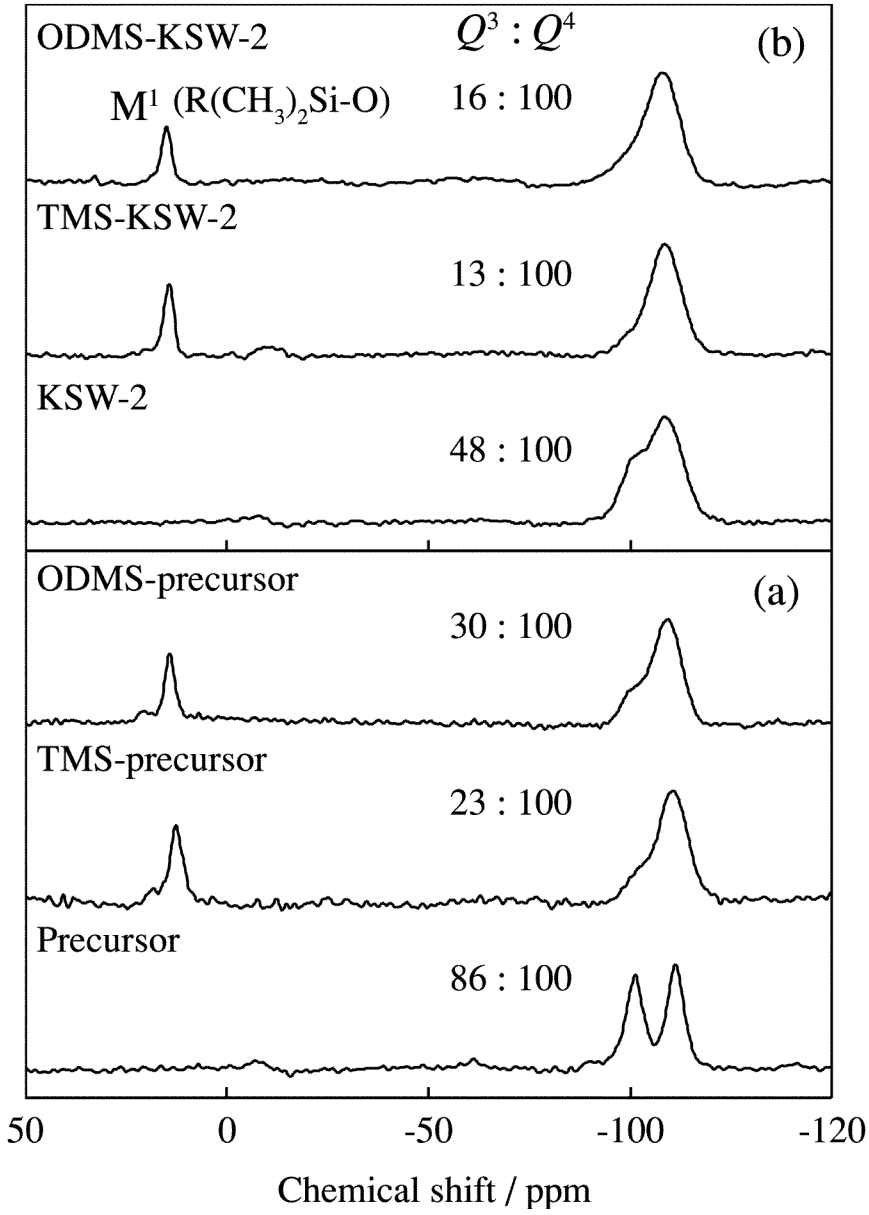

Figure 5-2. ^{29}Si MAS NMR spectra of (a) precursor and the silylated derivatives; (b) KSW-2 and the silylated derivatives.

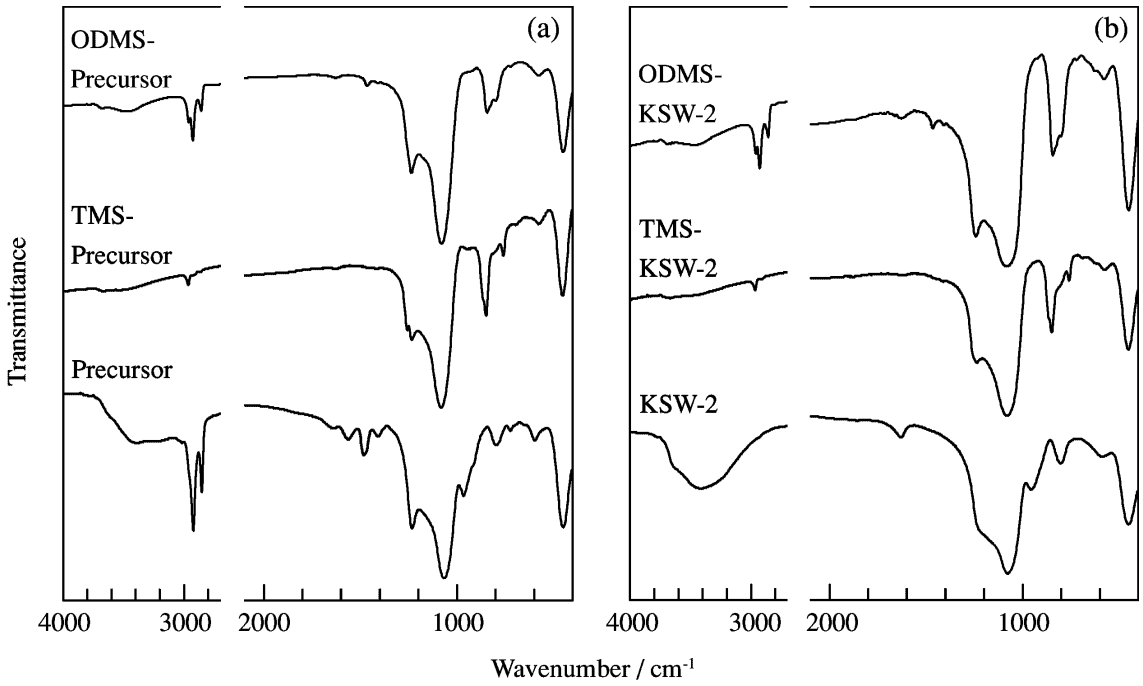

Figure 5-3. IR spectra of (a) precursor and the silylated derivatives; (b) KSW-2 and the silylated derivatives.

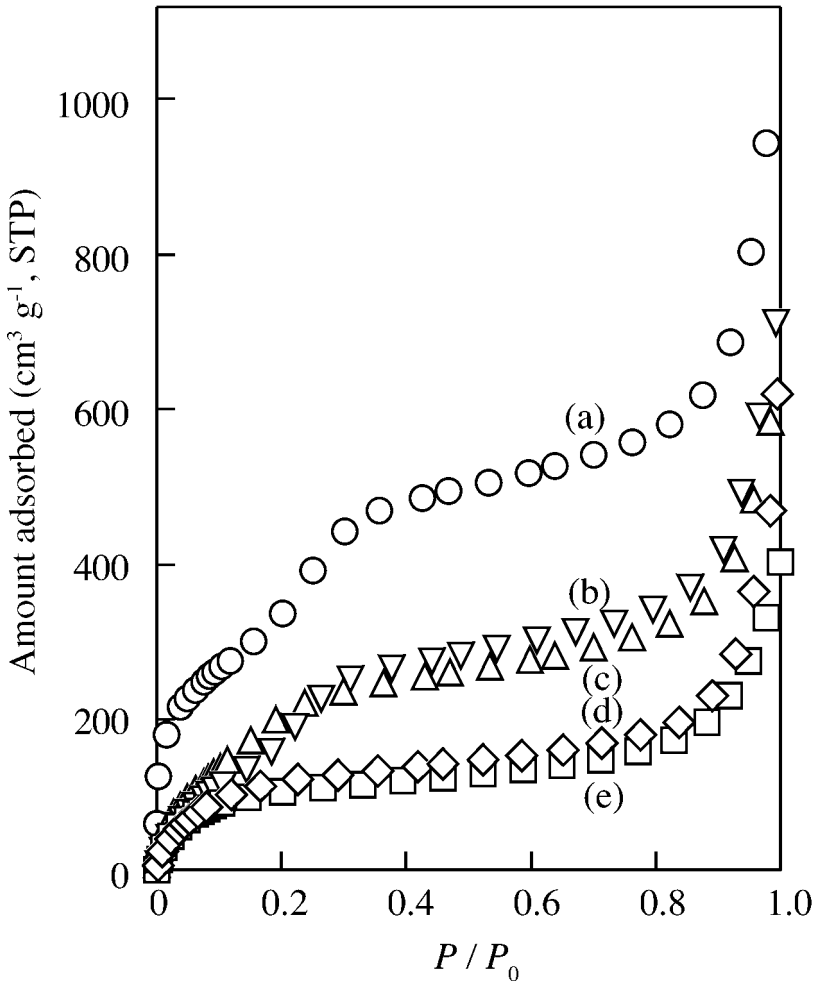

Figure 5-4. Nitrogen adsorption isotherms of (a) KSW-2 (○), (b) TMS-precursor (▽), (c) TMS-KSW-2 (△), (d) ODMS-precursor (◇), and (e) ODMS-KSW-2 (□).

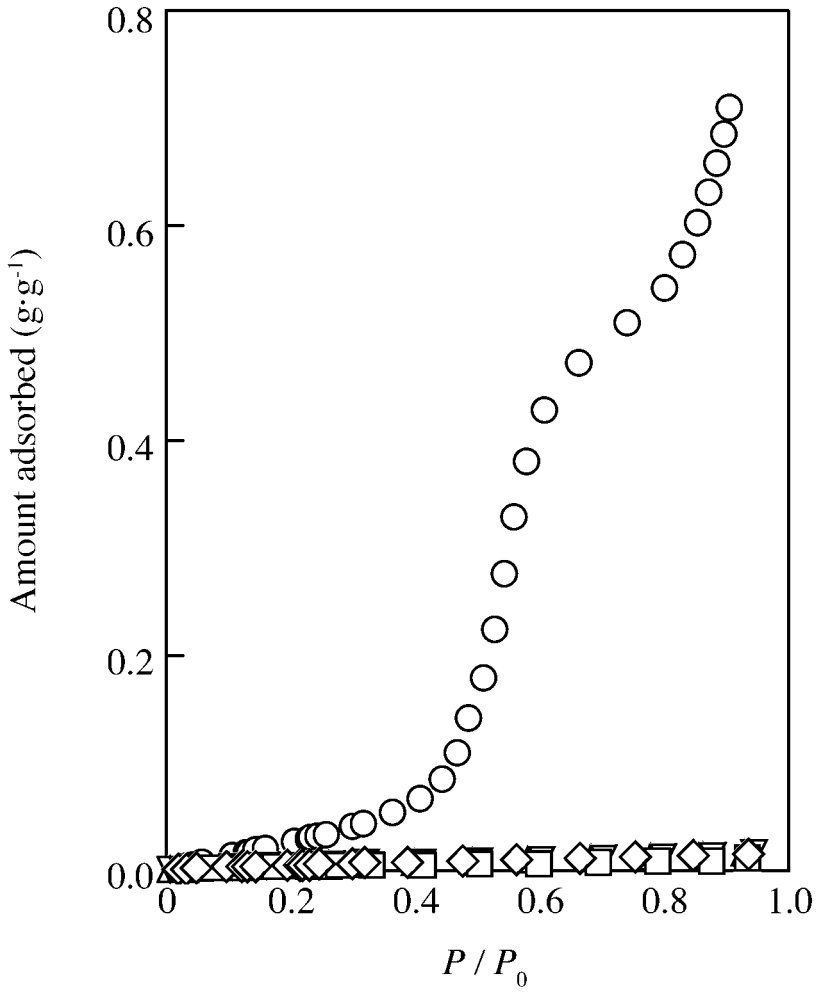

Figure 5-5. Adsorption isotherms of water vapor on KSW-2 (○), TMS-precursor (▽), TMS-KSW-2 (△), ODMS-precursor (◇), and ODMS-KSW-2 (□).

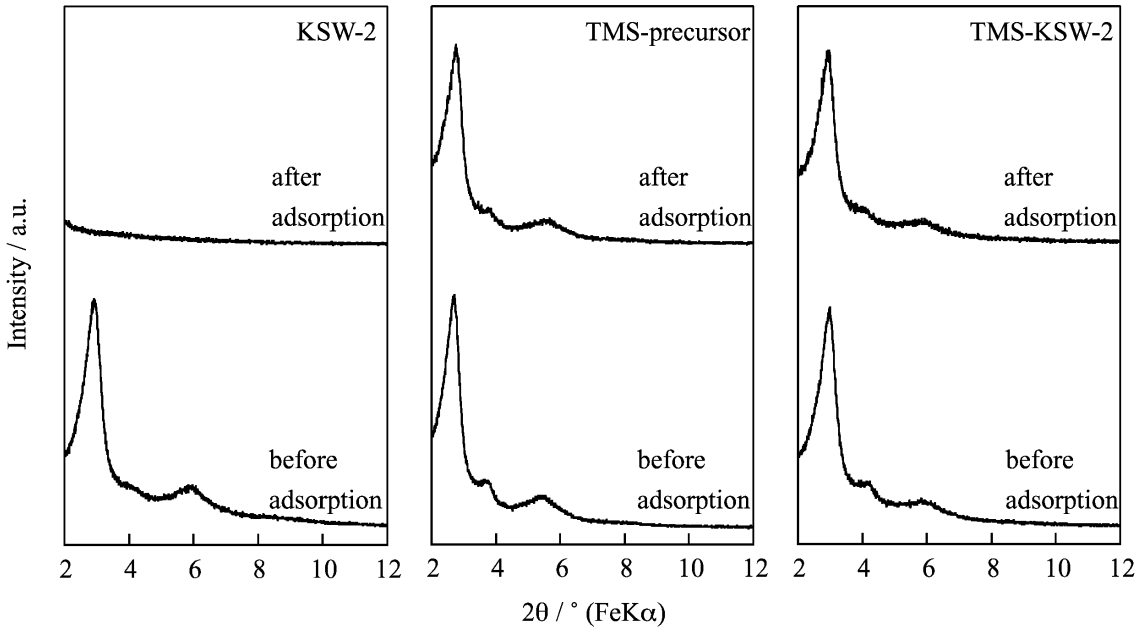

Figure 5-6. Changes in XRD patterns of KSW-2, TMS-precursor, and TMS-KSW-2 by water vapor adsorption.

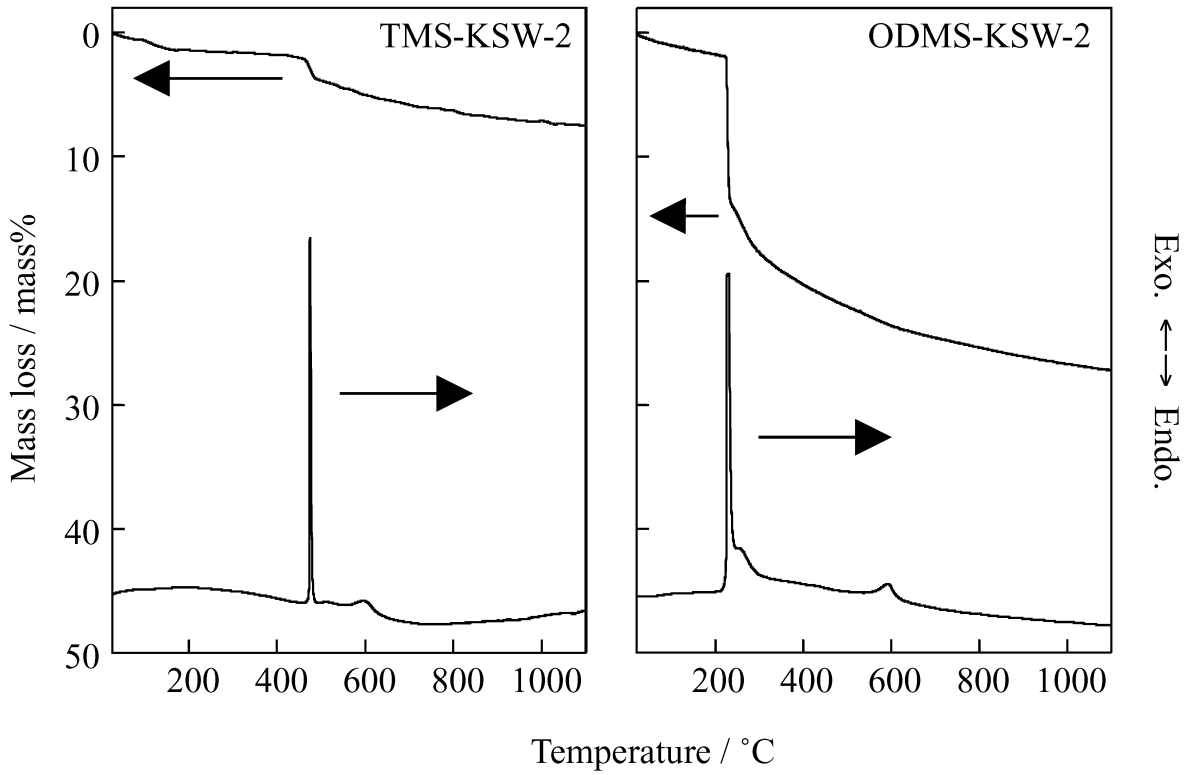

Figure 5-7. **TG-DTA** curves of silylated derivatives derived from KSW-2.

Chapter 6

Effects of the kind of layered disodium disilicates on the formation of silica-organic mesostructured materials

6.1 Introduction

Silica-organic mesostructured materials can be prepared by the reaction of a layered polysilicate kanemite ($NaHSi_2O_5 \cdot 3H_2O$)[1–3] with surfactant molecules as templates.[4] By calcining the mesostructured materials, mesoporous silica with narrow pore size distribution (denoted as KSW-1 at a later stage[5]) was obtained. FSM-16 (2-d hexagonal mesoporous silica derived from kanemite) was also formed by optimizing the reaction conditions.[6] Since the report on M41S mesoporous silicas such as 2-d hexagonal MCM-41 by the Mobil group,[7,8] a huge number of papers on this type of materials have been reported in this decade. The characteristic points of ordered mesoporous materials are controllable morphology, structure, and composition, which makes the materials very promising in diverse fields of applications including not only separation and adsorption but also photonics and electronics materials.

Davis *et al*. compared MCM-41 with mesoporous silica derived from kanemite (KSW-1) and reported that the thermal and hydrothermal stabilities of KSW-1 are higher than those of MCM-41.[9] Inaki *et al*. also compared both types of the materials from the point of photometathesis of propene in mesopores and reported that the activity of FSM-16 is higher than that of MCM-41 because of the unique arrangements of surface Si–OH groups originated from kanemite.[10] The *in-situ* XRD analysis of mesostructured materials also clarified that the formation process of the as-synthesized precursor for FSM-16 is different from that of MCM-41.[11] It has been described several times that fragmented silicate sheets wrap rod-like micelles to form a 2-d hexagonal structure in the formation of FSM-16.[9,11,12] Recently I have reported the presence of fragmented silicate sheets in the formation process of mesostructured materials for FSM-16,[13] and the finding is consistent with the report by O'Brien *et al*.[11] On the other hand, structurally different mesoporous silica called KSW-2 is also formed from kanemite.[5] An intercalation compound composed of kanemite-derived silicate sheets and hexadecyltrimethylammonium ($C_{16}TMA$) ions [14] can be transformed into silica-based mesostructured materials containing squared mesopores by acid treatment which induces the structural deformation. This reaction uses surfactant assemblies but the porous structures are not governed by the packing, which is only observed for the unique kanemite system. The powder XRD patterns of mesostructured precursors for

KSW-2 exhibit several peaks at higher diffraction angles, suggesting the partial retention of the silicate framework of kanemite. Based on these findings, it is reasonable to say that mesoporous silicas derived from layered disilicate are structurally superior to those using soluble silicate species in thermal and hydrothermal stabilities as well as catalytic activity, and that the formation mechanisms between them are different. However, kanemite has never retained its intact crystalline structure after the formation of mesoporous materials. Therefore, it would be quite interesting to survey the influence of the diversity of the crystalline silicate structures on the formation of mesostructured materials.

Layered disodium disilicates have several crystal structures which are composed of single-layered silicate sheets with interlayer sodium ions, and the silicate layers consist of six-membered rings of SiO_4 tetrahedra with only Q^3 environments of Si ($OSi(OSi)_3$).[15–17] Among them, α-$Na_2Si_2O_5$ (precursor for kanemite) and β-$Na_2Si_2O_5$ have different framework structures; the α phase has silicate sheets with boat-type 6-membered rings whereas the β phase possesses silicate sheets with chair-type 6-membered rings (Figure 6-1).[17,18] Therefore, it can be expected that the degree of condensation during the formation of mesostructured materials should be different and that the assembling structure of surfactants should also be different, which may affect the structure of mesoporous silica after calcination.

However, there have been no reports on the formation of mesostructured materials derived from β-$Na_2Si_2O_5$ and related materials, though Lagaly *et al.* reported that acid-treated $H_2Si_2O_5$-I reacted with some alkylamines to form intercalation compounds.[19,20] In the present study, based on the synthetic procedure established for FSM-16, hydrated β-sodium disilicate was used as a starting layered polysilicate for the formation of mesostructured materials and the products were characterized to find the influences of the different structural features of layered disodium disilicates on the formation of mesostructured materials.

6.2 Experimental

6.2.1 Materials

An aqueous solution of NaOH (2 M) was added to a high purity sodium silicate solution (SiO_2/Na_2O = 3.51, Nissan Chemical Ind. Ltd.) to adjust the ratio of Na/Si to be 1.0. The mixed solution was stirred at room temperature for one day. After drying the solution, the resultant solid was pulverized and then heated at 800 °C for 12 h in an air atmosphere to form α-$Na_2Si_2O_5$. According to the method of preparing kanemite from α-$Na_2Si_2O_5$, 1 g of α-$Na_2Si_2O_5$ was dispersed in 50 ml of water and the mixture was stirred for 30 min. The suspension was then centrifuged and air-dried to form hydrated α-sodium disilicate. Wet slurries of hydrated α-sodium disilicate were used without drying when mesostructured materials were synthesized. Disilicic acid ($H_2Si_2O_5$-I) was prepared by treating α-$Na_2Si_2O_5$ (1 g) with HCl (2 M) at room temperature for 3 h, centrifuged, and air-dried.

6.2.2 Formation of hydrated a-sodium disilicate-C16TMA mesostructured materials.

Wet slurries of hydrated α-sodium disilicate were added to a hexadecyltrimethylammonium chloride (C_{16}TMACl) solution (0.1 M) with the C_{16}TMA/Si molar ratios of 2.0. The mixture was stirred at room temperature (for 3 h to 7 d) or 70 °C (for 3 to 6 h). Stirring at 70 °C for 6 h was needed to complete the reaction. The suspensions were then centrifuged, washed with distilled water, and air-dried to form hydrated α-sodium disilicate-C_{16}TMA mesostructured materials. A different C_{16}TMA/Si molar ratio of 4.0 was also employed to form a hydrated α-sodium disilicate-C_{16}TMA mesostructured material. The resultant solids were calcined at 550 °C for 6 h in an air atmosphere (heating rate: 5 °C min^{-1}).

The lower ratios of C_{16}TMA/Si (0.2, 0.5, 0.7, and 1.0) were also applied for the formation of hydrated α-sodium disilicate-C_{16}TMA mesostructured materials. Wet slurries of hydrated α-sodium disilicate were reacted with C_{16}TMACl solutions and the mixtures were stirred at 70 °C for 3 h. The suspensions were treated similarly, as described above. The resultant solid at the C_{16}TMA/Si molar ratio of 0.2 was calcined at 550 °C for 6 h in an air atmosphere (heating rate: 5 °C min^{-1}).

6.2.3 Formation of kanemite-C_{16}TMA mesostructured materials.

Kanemite was synthesized according to the report by Kimura *et al*.[14] Wet slurries of kanemite were used without drying when mesostructured materials were synthesized. Kanemite was added to C_{16}TMACl solutions (0.1 M) with the C_{16}TMA/Si molar ratios of 0.2, 0.5, 0.7, 1.0, and 2.0. The mixtures were stirred at 70 °C for 3 h. The suspensions were then centrifuged, washed with distilled water, and air-dried to form kanemite-C_{16}TMA mesostructured materials.[14] The resultant solids at the C_{16}TMA/Si molar ratios of 0.2 and 2.0 were calcined at 550 °C for 6 h in an air atmosphere (heating rate: 5 °C min^{-1}).

6.2.3 Characterization

Powder XRD patterns were recorded on Mac Science MXP^3 (Cu K□) and M03XHF^{22} (Fe K□) diffractometers with a scanning speed of 2°/min. The diffraction angles were calibrated by using phlogopite as a reference. Solid-state ^{29}Si MAS NMR spectra were measured by a JEOL CMX-400 spectrometer, using a resonance frequency of 79.4 MHz, a rotation speed of 5 kHz, accumulation of 500–800 scans, pulse delays of 200 sec for the inorganic substances (disilicates and their hydrates) and 100 sec for mesostructured materials, and a pulse angle of 45°. Tetramethylsilane was used as a reference (0 ppm). Nitrogen adsorption desorption isotherms were obtained by a BELSORP 28SA (Japan Bel Co.) and samples were outgassed at 120 °C under 10^{-2} mmHg for 3 h prior to the measurement. Specific surface areas, pore volumes, and pore size distributions were calculated by the BET method,[21] the *t*-plot method, and the BJH method using adsorption isotherms.[22] TEM images were taken by a JEM2010EX electron microscope (JEOL) at an accelerating voltage of 200 kV. Powdery samples were dispersed in acetone and mounted on microgrids. The chemical compositions were determined by ICP, CHN, and TG. ICP analysis was performed with an IRIS-AP spectrometer (Jarrell Ash) and samples were prepared by a melting method with lithium metaborate. The surfactant/silicon ratio (C_{16}TMA/Si) was determined by CHN analysis using a Perkin-Elmer PE-2400II instrument. Thermogravimetry was

conducted by a TG-DTA2000S apparatus (Mac Science Co.) in the temperature range from RT to 1000 °C at a heating rate of 10 °C min^{-1} and an air flow of 200 ml min^{-1}.

6.3 Results and Discussion

6.3.1 δ-$Na_2Si_2O_5$ and its hydrate.

All the powder XRD peaks of δ-$Na_2Si_2O_5$ (Figure 6-2(a)) are consistent with those reported by Williamson[23] and no impurity phases were observed. The ^{29}Si MAS NMR spectrum of δ-$Na_2Si_2O_5$ (Figure 6-3(c)) shows a single signal at –95 ppm due to Si atoms with a Q^3 environment, which coincides with the report by Heidemann.[24] The Na/Si ratio, determined by ICP, was 1.03. All these data confirm the formation of δ-$Na_2Si_2O_5$.

Figure 6-2(b) shows the powder XRD pattern of hydrated δ-sodium disilicate obtained by dispersing δ-$Na_2Si_2O_5$ in water. The pattern is different from those of δ-$Na_2Si_2O_5$ and $H_2Si_2O_5$-I.[25] The appearance of the new peak at d = 0.96 nm (2θ = 9.2°) indicates the expansion of the interlayer spacing. The composition of hydrated δ-sodium disilicate prepared here was $Na_{1.2}H_{0.8}Si_2O_5 \cdot 2.5H_2O$. Ai *et al*. also reported the formation of a hydrated product of δ-$Na_2Si_2O_5$ by allowing the disilicate to stand under the humidity of 35–50 % at room temperature for 6 months.[26] The XRD pattern shows a peak at d = 0.94 nm with some peaks due to unreacted δ-$Na_2Si_2O_5$ and some other peaks inconsistent with those observed by me. They do not provide the crystal structure of the substance.

Figure 6-3 shows the ^{29}Si MAS NMR spectra of δ-$Na_2Si_2O_5$, β-$Na_2Si_2O_5$, and their hydrates. Kanemite exhibits a sharp signal ascribable to the Q^3 units at –97 ppm. The spectrum of hydrated δ-sodium disilicate (Figure 6-3(d)) shows several signals in the region of Q^2 and Q^3 units, indicating the diversity of Si environments, which is basically consistent with the previous reports.[26,27] The hydrated behavior is quite different from that of kanemite. The previous papers[26,27] report the presence of the peaks at –110 ppm due to Q^4 that I did not observe, possibly because of the differences between the hydration conditions. The Raman spectra of δ-$Na_2Si_2O_5$ and hydrated δ-

sodium disilicate (Figure 6-4) show similar patterns, suggesting the retention of the original silicate framework in the hydrated form.

The layered nature of the hydrate was also supported by the intercalation behavior with $C_{16}H_{33}NH_2$. The powder XRD pattern of the reaction product (Figure 6-5) shows the peaks at d = 5.55, 2.76, and 1.86 nm assignable to (001), (002), and (003) reflections, respectively, indicating the large expansion by the intercalation, which confirms the lamellar structure of hydrated □-sodium disilicate.

6.3.2 Mesostructured products derived from hydrated □-sodium disilicate and kanemite.

The powder XRD patterns of the reaction products of hydrated □-sodium disilicate or kanemite with C_{16}TMA ions, prepared at the ratio of C_{16}TMA/Si = 2.0, are shown in Figures 6-6 and 7, respectively. When kanemite was used, the peak at d = 3.22 nm and the higher order peaks are observed (Figure 6-7(a)). These peaks disappeared after calcination, which means the formation of a lamellar mesophase, as reported previously by Kimura *et al*.[14] On the other hand, the peak at d = 4.23 nm and a broad peak at 2□ = 4–6° (Figure 6-6(a)) are observed when hydrated □-sodium disilicate was used. These peaks were preserved after calcination, (Figure 6-6(b)), indicating the formation of a three-dimensional (3-d) silica network. The finding that the formation of the 3-d silica network at the C_{16}TMA/Si ratio of 2.0 is important because the C_{16}TMA/Si ratio induces the formation of a lamellar mesophase from kanemite.

The ^{29}Si MAS NMR spectrum (Figure 6-8) revealed the degree of condensation of the silicate network of the hydrated □-sodium disilicate-C_{16}TMA compound (C_{16}TMA/Si = 2.0) before calcination and the ratio of $Q^4/(Q^3+Q^4)$ was 0.57. Though the compound was not acid-treated, the value is quite high, being similar to that found for the pH-adjusted precursor for FSM-16. Consequently, the structure of the compound was retained after calcination without pH adjustment. Compared with the pH of the solution before acid treatment in the synthesis of FSM-16 (higher than 11.5),[28] the pH of the solution at the C_{16}TMA/Si ratio of 2.0 was relatively low (10.2). Therefore, the silicate sheets do not tend to be fragmented by dissolution and the

interlayer condensations are liable to occur, leading to a stable 3-d silica network. This is the reason for the high degree of condensation of the silicate network under the high C_{16}TMA/Si ratio.

The surfactant/silicon ratio (C_{16}TMA/Si) was 0.20 in the hydrated □-sodium disilicate-C_{16}TMA compound when the starting ratio of C_{16}TMA/Si was 2.0, while the contents were 0.24–0.28 in lamellar mesophases derived from kanemite under the same C_{16}TMA/Si ratio. The smaller organic content of the hydrated □-sodium disilicate-C_{16}TMA compound results from a higher degree of condensation of the silicate network, that is, there are many Q^4 environments of Si which do not interact with C_{16}TMA.

The nitrogen adsorption isotherm of the porous material derived from the hydrated □-sodium disilicate-C_{16}TMA compound (C_{16}TMA/Si = 2.0) after calcination (denoted as SSW-1 hereafter) is shown in Figure 6-9. A type IV isotherm is observed,[29] and the pore size is 2.7 nm though the pore size distribution is broad .

The TEM image of SSW-1 is shown in Figure 6-10. A disordered structure (Figure 6-10(a)) is observed, which corresponds to the broadness of the diffraction peaks shown in Figure 6-6(b). On the other hand, when I look at the arrangement of the channels, the uniformly arranged straight channels are observed (Figure 6-10(b)). This is characteristic of the system using hydrated □-sodium disilicate which should bend along the *a* axis.[30] Even under the higher C_{16}TMA/Si ratio of 4.0, the XRD peak of the solid after calcination at 550 °C was observed (Figure 6-11), showing the formation of a 3-d silica network in the case of hydrated □-sodium disilicate.

To examine the initial stage of the formation of the hydrated □-sodium disilicate-C_{16}TMA compound (C_{16}TMA/Si = 2.0), the reaction was conducted at room temperature and the XRD patterns of the resultants are shown in Figure 6-12. A broad peak with *d* value of *ca*. 4 nm began to appear in the XRD pattern of the product at 6 h. As shown in Figures 6-6 and 7, when C_{16}TMA was used as a template, the peak with *d* value of *ca*. 3 nm was observed in the lamellar mesostructure, whereas the peak with *d* value of *ca*. 4 nm in a less ordered hexagonal structure. Therefore, the appearance of the peak with *d* value of *ca*. 4 nm even at very initial stage of 6 h indicates that the hydrated □-sodium disilicate forms a 3-d silica network at the initial stage. In the formation of hexagonal mesostructured silica from kanemite, it is reported that a 3-d

silica network is formed by way of a lamellar mesophase at the initial stages,[13] though hydrated δ-sodium disilicate-C_{16}TMA does not take such a process. Moreover, the peak at 2θ of 11.6° due to hydrated δ-sodium disilicate was observed at the initial stages and the peak intensity gradually weakened as the reaction proceeded. The pH values of the reaction solutions were less than 11 at any reaction conditions, therefore, the possibility of dissolution of hydrated δ-sodium disilicate is low. However, only a halo peak resulting from the very poorly crystalline structure was observed at higher diffraction angles in the XRD pattern (Figure 6-13), indicating that the intact crystal structure was not preserved in the hydrated δ-sodium disilicate-C_{16}TMA compound. Several peaks at 2θ of 9°, 24°, and 28° were also observed, and these were due to a very small amount of unreacted hydrated δ-sodium disilicate detectable by a high power XRD apparatus (50 kV, 300 mA).

The powder XRD patterns of the reaction products of hydrated δ-sodium disilicate and kanemite with C_{16}TMA ions, prepared at the C_{16}TMA/Si molar ratios less than 2.0 (C_{16}TMA/Si = 0.2, 0.5, 0.7, and 1.0) are shown in Figures 6-14 and 15. When kanemite was used, four diffraction peaks were observed at the C_{16}TMA/Si molar ratios of 0.2 (Figure 6-15(a)). These are characteristic of a hexagonal structure, corresponding to (100), (110), (200), and (210) reflections. At the C_{16}TMA/Si molar ratio of 0.5, in addition to the four peaks characteristic of the hexagonal structure, a peak at *d* value of 3.18 nm and the higher order peaks were observed (Figure 6-15(b)). This shows the mixture of the hexagonal and lamellar structures. At the ratios of 0.7 and 1.0, only lamellar mesophases were formed (Figure 6-15(c) and (d)). In the report by Kimura *et al.*,[14] the diffraction peaks resulting from a lamellar structure are observed though a hexagonal structure is mainly formed at the ratio of 0.2. The slight difference between these reports is supposed to be due to the reaction conditions.

On the other hand, when hydrated δ-sodium disilicate was used, four peaks characteristic of 2-d hexagonal structures were observed in all the XRD patterns at the C_{16}TMA/Si molar ratios of 0.2–1.0 (Figure 6-14). No clear diffraction peaks were observed at higher diffraction angles (Figure 6-16), indicating the substantial loss of the crystal structure of the framework. When the ratio was 1.2, the structure was less ordered, which is similar to the results on the product at the ratio of 2.0.

The relation between the C_{16}TMA/Si molar ratio and the structural variation is shown in Figure 6-17. A lamellar mesostructure was formed at the C_{16}TMA/Si molar ratios higher than 0.5 in the case of kanemite, whereas 2-d hexagonal structures were formed at the C_{16}TMA/Si molar ratios of 0.2–1.0 in the case of hydrated □-sodium disilicate. The reason for this difference will be discussed later. When hydrated □-sodium disilicate-C_{16}TMA prepared at the C_{16}TMA/Si molar ratio of 0.2 was calcined at 550 °C, no diffraction peaks were observed, meaning the collapse of the mesostructure (Figure 6-18(b)). The reason of the collapse is that this mesostructured material was not acid-treated and the degree of condensation was low ($Q^4/(Q^3+Q^4)$ = *ca.* 0.35). The collapse of the mesostructure was prevented by acid treatment, as in the case of FSM-16, and the stability was higher than that of FSM-16, which is under investigation and will be reported in near future.

From these results, it is easier for hydrated □-sodium disilicate to form mesoporous materials than for kanemite. The reason why hydrated □-sodium disilicate tend to form mesoporous materials is discussed here. The ^{29}Si MAS NMR spectra of the wet slurries of hydrated □-sodium disilicate and kanemite, as well as their integrated intensity ratios, are shown in Figure 6-19. The signals due to Q^3 environment were observed mainly in both of them, suggesting hydrated □-sodium disilicate did not dissolve completely, though the ratios of Q^1 and Q^2 were higher for the hydrated □-sodium disilicate than for kanemite.

Inagaki *et al*. have recently reported the successful preparation of ordered mesoporous materials with uniform organic-inorganic hybrid frameworks.[31] They commented that the low anion charge density plays a role in making the headgroups of alkyltrimethylammonium (C_nTMA) ions apart and that a 3-d hexagonal structure is formed. In our report, lamellar mesostructures were formed at the C_{16}TMA/Si molar ratios higher than 0.5 in the case of kanemite, whereas 2-d hexagonal structures were obtained at the C_{16}TMA/Si ratios of 0.2–1.0 in the case of hydrated □-sodium disilicate. This is probably due to the fact that the distances between Si–O^- sites along the bending direction are longer for the hydrated □-sodium disilicate than those for kanemite. The distances between the Si–O^- sites for sodium disilicate are shown in Figure 6-20. These layers are considered to bend along the *a* axis,[30] and the distance between Si–O^-

along the *a* axis is longer for β-sodium disilicate (Figure 6-20(b)) than for α-sodium disilicate (Figure 6-20(a)). If I assume that the structures similar to the parent silicates are preserved in the hydrates, the headgroups of C_{16}TMA ions become larger, as shown in Figure 6-20(d), in the case of hydrated β-sodium disilicate, leading to the formation of a hexagonal structure.

Although the distance between Si–O^- is longer along the bending direction, the hexagonal structure of the product obtained from the hydrated β-sodium disilicate at the C_{16}TMA/Si molar ratio of 2.0 was less ordered. Because the pH value of the reaction solution was not high enough to fragment the silicate sheets, obviously those sheets cannot form an ordered hexagonal structure due to their structural restriction. When C_nTMA ions are used as a template, a highly ordered 2-d hexagonal structure is formed at various pH values from soluble silicate species,[7,8,32,33] whereas it is not formed from a layered silicate unless the pH of the solution is high enough to fragment the sheets. This is a distinctive difference between a layered disilicate and soluble silicate species as the silica sources.

The most important thing for using hydrated β-sodium disilicate is that mesoporous silica can be prepared at lower pH than in the case of kanemite and without acid treatment when the ratio was increased to 2.0. From this point of view, it is expected that the silicate structure would be retained partly in the framework of mesostructured silica when hydrated β-sodium disilicate is used. Further structural control during the formation remains to be tackled. If the *intra*layer condensation observed for the C_nTMA-kanemite systems[5,14] is ideally controlled depending on both the kind of layered polysilicates and the reaction conditions, the deformation of the silicate frameworks would be suppressed. Introduction of heterogeneous atoms such as Al into the framework will also be one of the most interesting themes.

6.4 Conclusions

Silica-based mesostructured materials were formed using two different disilicates of hydrated β-sodium disilicate and kanemite as the silica sources. The influence of the

different structural features of layered disodium disilicates on the formation of mesostructured materials was verified. The original silicate framework of δ-$Na_2Si_2O_5$ is probably preserved in its hydrated δ-sodium disilicate. In the C_{16}TMA/Si molar ratios of 0.2–1.0 (C_{16}TMA/Si = 0.2, 0.5, 0.7, and 1.0), 2-d hexagonal structures were formed from hydrated δ-sodium disilicate though a less ordered structure was formed when the ratio was 2.0. The uniformly arranged straight channels are observed in the TEM image. This is characteristic of the system using hydrated δ-sodium disilicate which should bend along the *a* axis. On the other hand, in the case of kanemite, lamellar mesostructures were formed at the ratios higher than 0.5, while a 2-d hexagonal structure was formed only at the ratio of 0.2. Longer distance between $Si–O^-$ sites along the bending direction in hydrated δ-sodium disilicate than that in kanemite, making the headgroups of C_nTMA ions apart, may be the reason for these differences. Mesoporous silica (SSW-1) derived from hydrated δ-sodium disilicate is prepared at lower pH than from kanemite at the C_{16}TMA/Si ratio of 2.0. More importantly, the acid treatment, which is normally required for the preparation of mesoporous silica from kanemite, was not needed for the formation of 3-d silica network from hydrated δ-sodium disilicate at the ratio of 2.0. These findings are quite useful for future design of the framework of mesostructured silica because, by an appropriate selection of disilicate, mesostructured materials can be prepared under lower pH conditions that are advantageous for retaining the original silicate structures to some extent.

6.5 References

1) Johan, Z.; Maglione, G. F. *Bull. Soc. Fr. Mineral. Cristallogr.* **1972**, *95*, 371.
2) Beneke, K.; Lagaly, G. *Am. Mineral.* **1977**, *62*, 763.
3) Vortmann, S.; Rius, J.; Marler, B.; Gies, H. *Eur. J. Mineral.* **1999**, *11*, 125.
4) Yanagisawa, T.; Shimizu, T.; Kuroda, K.; Kato, C. *Bull. Chem. Soc. Jpn.* **1990**, *63*, 988.
5) Kimura, T.; Kamata, T.; Fuziwara, M.; Takano, Y.; Kaneda, M.; Sakamoto, Y.; Terasaki, O.; Sugahara, Y.; Kuroda, K. *Angew. Chem. Int. Ed.* **2000**, *39*, 3855.
6) Inagaki, S.; Fukushima, Y.; Kuroda, K. *J. Chem. Soc., Chem. Commun.* **1993**, 681.
7) Kresge, C. T.; Leonowicz, M. E.; Roth, W. J.; Vartuli, J. C.; Beck, J. S. *Nature* **1992**, *359*, 710.
8) Beck, J. S.; Vartuli, J. C.; Roth, W. J.; Leonowicz, M. E.; Kresge, C. T.; Schmitt, K. D.; Chu, C. T.-W.; Olson, D. H.; Sheppard, E. W.; McCullen, S. B.; Higgins, J. B.; Schlenker, J. L. *J. Am. Chem. Soc.* **1992**, *114*, 10834.
9) Chen, C. Y.; Xiao, S. Q.; Davis, M. E. *Microporous Materials* **1995**, *4*, 1.
10) Inaki, Y.; Yoshida, H.; Kimura, K.; Inagaki, S.; Fukushima, Y.; Hattori, T. *Phys. Chem. Chem. Phys.* **2000**, *2*, 5293.
11) (a) O'Brien, S.; Francis, R. J.; Price, S. J.; O'Hare, D.; Clark, S. M.; Okazaki, N.; Kuroda, K. *J. Chem. Soc.*, *Chem. Commun.* **1995**, 2423.
(b) O'Brien, S.; Francis, R. J.; Fogg, A.; O'Hare, D.; Okazaki, N.; Kuroda, K. *Chem. Mater.* **1999**, *11*, 1822.
12) Inagaki, S.; Sakamoto, Y.; Fukushima, Y.; Terasaki, O. *Chem. Mater.* **1996**, *8*, 1499.
13) Kimura, T.; Itoh, D.; Shigeno, T.; Kuroda, K. *Langmuir* **2002**, *18*, 9574.
14) Kimura, T.; Itoh, D.; Okazaki, N.; Kaneda, M.; Sakamoto, Y.; Terasaki, O.; Sugahara, Y.; Kuroda, K. *Langmuir* **2000**, *16*, 7624.
15) Pant, A. K.; Cruickshank, D. W. J. *Acta Crystallogr.* **1968**, *B24*, 13.
16) Pant, A. K. *Acta Crystallogr.* **1968**, *B24*, 1077.
17) Kahlenberg, V.; Dorsam, G.; Wendschuh-Josties, M.; Fischer, R. X. *J. Solid State Chem.* **1999**, *146*, 380.
18) Fleet, M. E. *J. Solid State Chem.* **1995**, *199*, 400.

19) Lagaly, G. *Adv. Colloid Interface Sci.* **1979**, *11*, 105.

20) Lagaly, G.; Beneke, K.; Dietz, P.; Weiss, A. *Angew. Chem. Int. Ed.* **1974**, *13*, 819.

21) Sing, K. S. W.; Everett, D. H.; Haul, R. A. W.; Moscou, L.; Pierotti, R. A.; Rouquerol, J.; Siemieniewska, T. *Pure Appl. Chem.* **1985**, *57*, 603.

22) Barret, E. P.; Joyner, L. G.; Halenda, P. P. *J. Am. Chem. Soc.* **1951**, *73*, 373.

23) Williamson, J.; Glasser, F. P. *Phys. Chem. Glasses* **1966**, *7*, 127.

24) Heidemann, D.; Hubert, C.; Schwieger, W.; Grabner, P.; Bergk, K. H.; Sarv, P. *Z. Anorg. allg. Chem.* **1992**, *617*, 169.

25) Liebau, F. *Z. Kristallographie* **1964**, *Bd. 120*, S. 427.

26) Ai, X.; Deng, F.; Dong, J.; Chen, L.; Ye, C. *J. Phys. Chem. B* **2002**, *106*, 9237.

27) Wieker, W.; Heidemann, D.; Ebert, R.; Tapper, A. *Z. Anorg. Allg. Chem.* **1995**, *621*, 1779.

28) Inagaki, S.; Koiwai, A.; Suzuki, N.; Fukushima, Y.; Kuroda, K. *Bull. Chem. Soc. Jpn.* **1996**, *69*, 1449.

29) Kruk, M.; Jaroniec, M. *Chem. Mater.* **2001**, *13*, 3169.

30) The bending direction is limited to the *a* axis. Our recent calculation of the stiffness of kanemite sheet shows that the energy required to strain the sheet in kanemite is much higher in the *c* axis than that in the *a* axis. This finding is in good agreement with our experience using a structural model kit. The same tendency was observed for hydrated □-sodium disilicate.

31) Inagaki, S.; Guan, S.; Fukushima, Y.; Ohsuna, T.; Terasaki, O. *J. Am. Chem. Soc*. **1999**, *121*, 9611.

32) Huo, Q.; Leon, R.; Petroff, P. M.; Stucky, G. D. *Science* **1995**, *268*, 1324.

33) Huo, Q.; Margolese, D. I.; Stucky, G. D. *Chem. Mater.* **1996**, *8*, 1147.

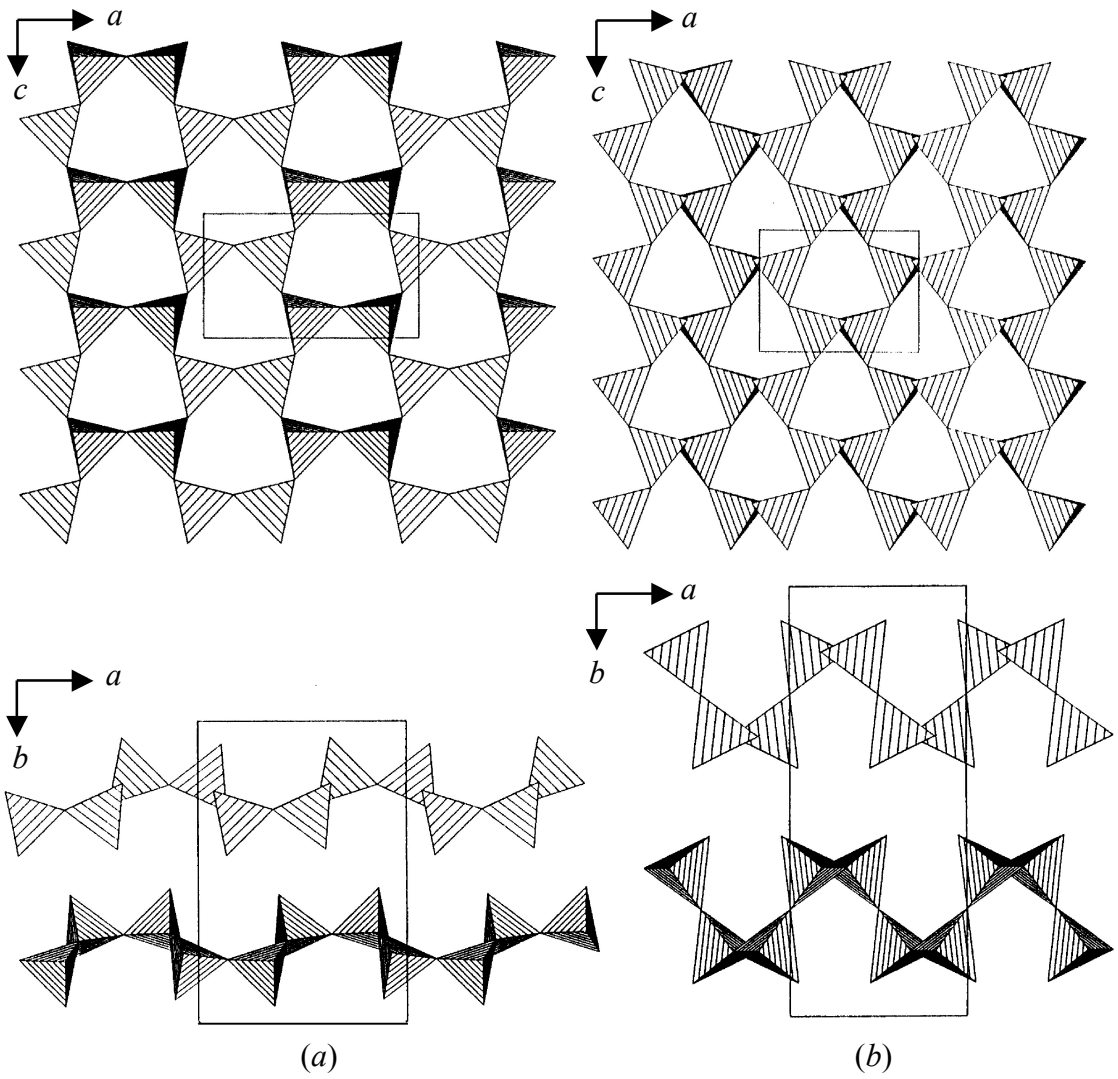

Figure 6-1. Crystal structures of □- and □-disodium disilicates.[17] (a) □-$Na_2Si_2O_5$ and (b) □-$Na_2Si_2O_5$.

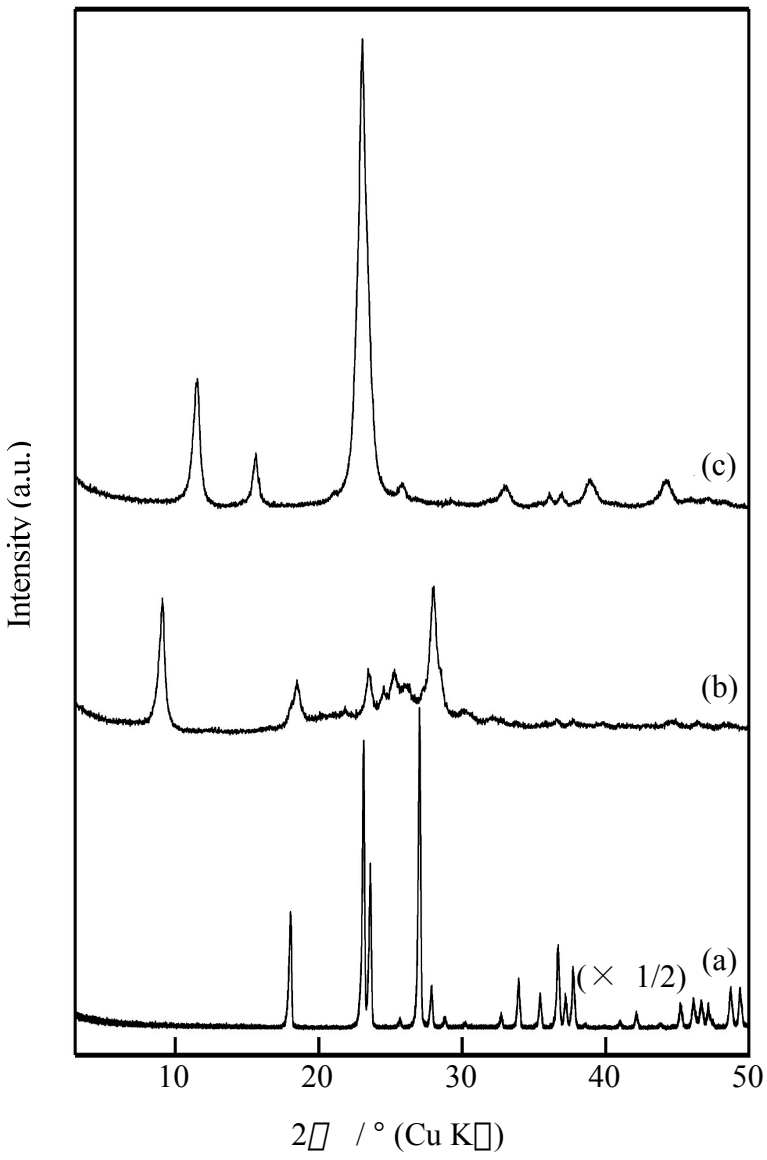

Figure 6-2. XRD patterns of (a) α-$Na_2Si_2O_5$, (b) hydrated β-sodium disilicate, and (c) $H_2Si_2O_5$-I.

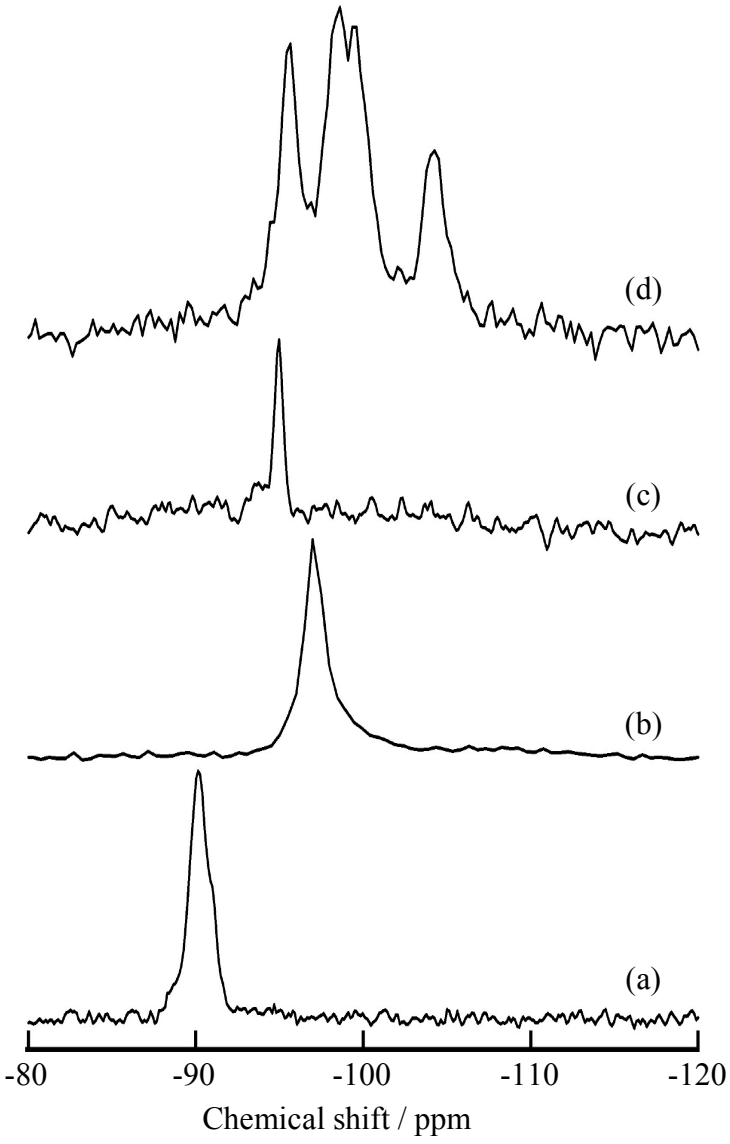

Figure 6-3. ^{29}Si MAS NMR spectra of □- and □-$Na_2Si_2O_5$ and their hydrates
(a) □-$Na_2Si_2O_5$, (b) kanemite, (c) □-$Na_2Si_2O_5$, and (d) hydrated □-sodium disilicate.

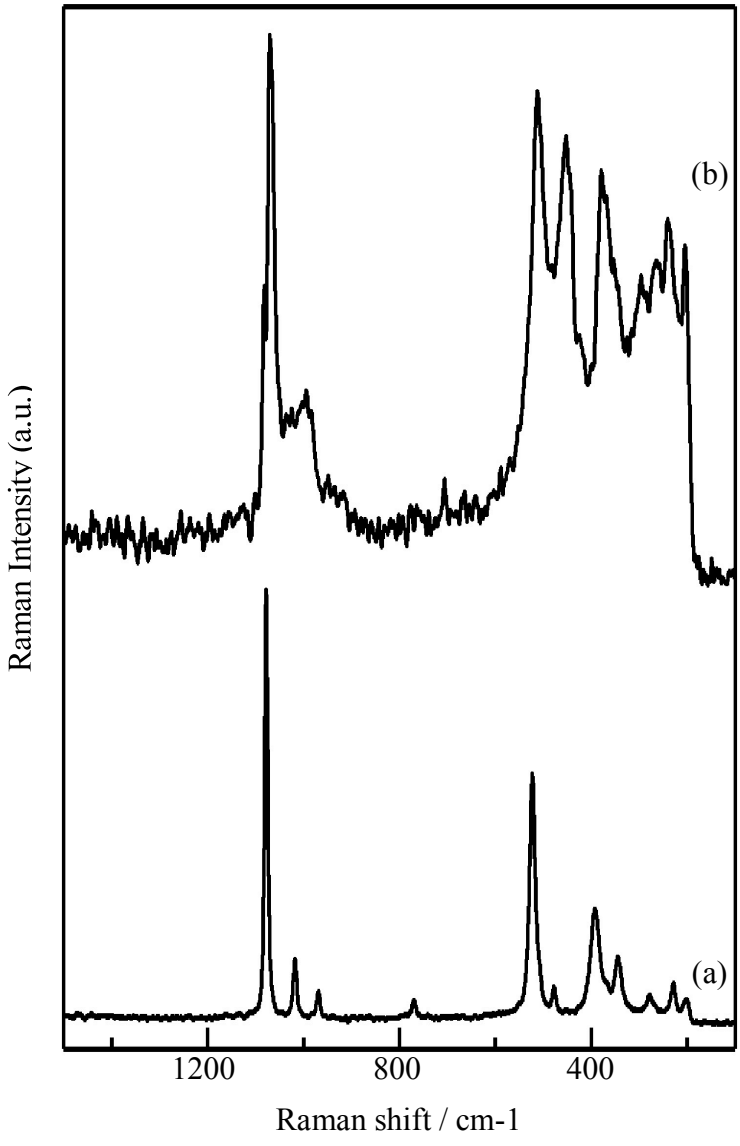

Figure 6-4. Raman spectra of (a) δ-$Na_2Si_2O_5$ and (b) hydrated δ-sodium disilicate.

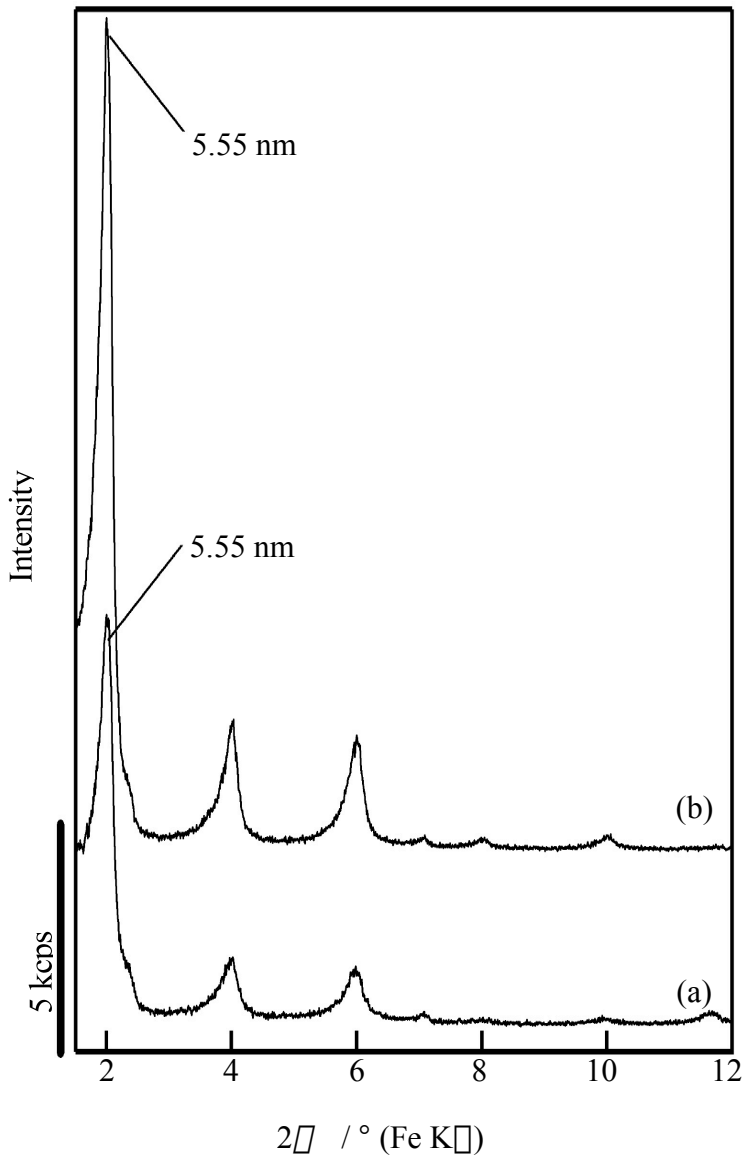

Figure 6-5. XRD patterns of (a) hydrated α-sodium disilicate-$C_{16}H_{33}NH_2$, (b) kanemite-$C_{16}H_{33}NH_2$.

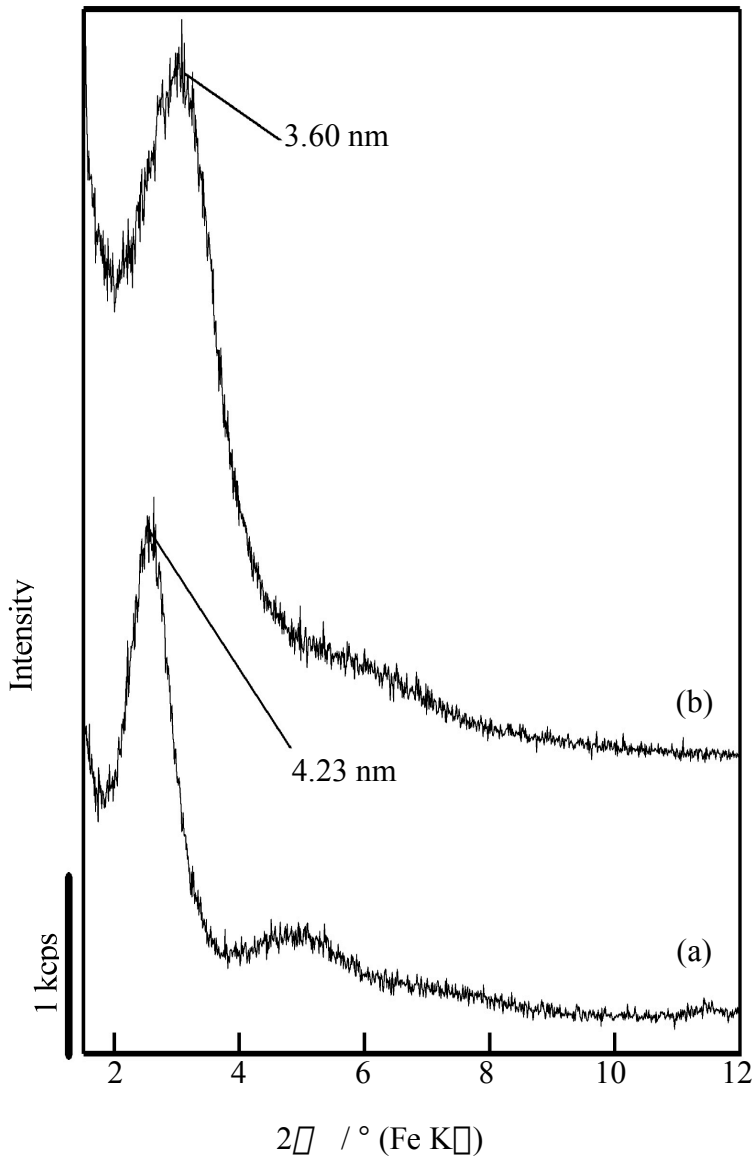

Figure 6-6. XRD patterns of (a) the hydrated α-sodium disilicate-C_{16}TMA compound and (b) the product after calcination of (a) (C_{16}TMA/Si = 2.0).

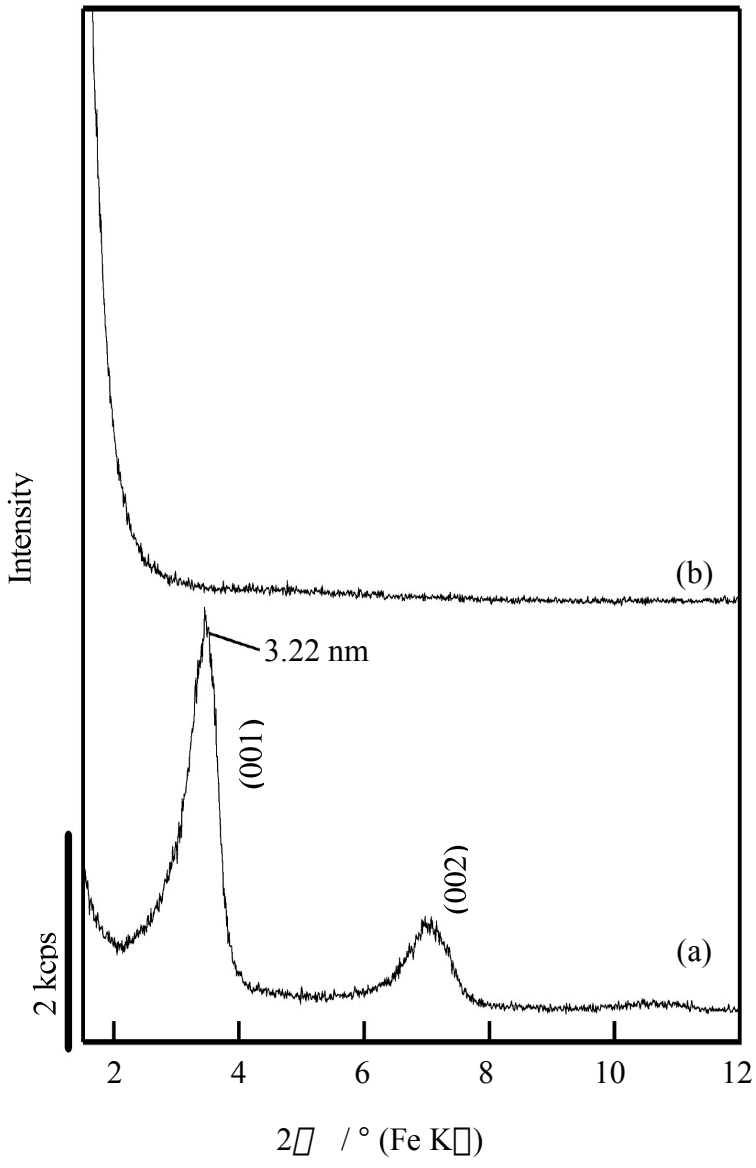

Figure 6-7. XRD patterns of (a) kanemite-C_{16}TMA intercalated compound and (b) calcined product of (a) (C_{16}TMA/Si = 2.0).

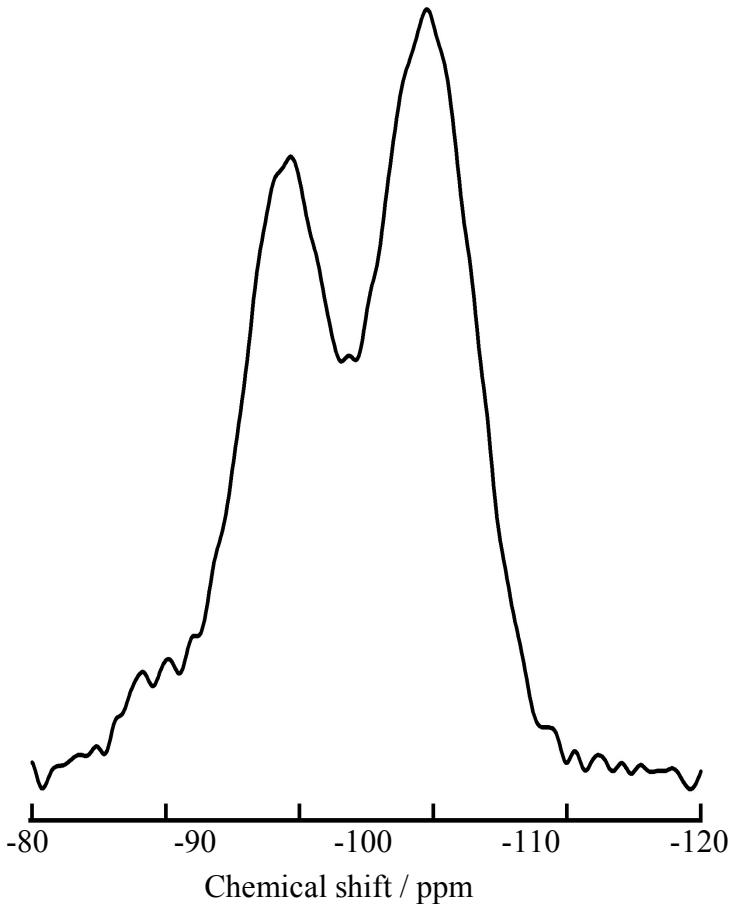

Figure 6-8. ^{29}Si MAS NMR spectrum of the hydrated □-sodium disilicate-C_{16}TMA compound (C_{16}TMA/Si = 2.0).

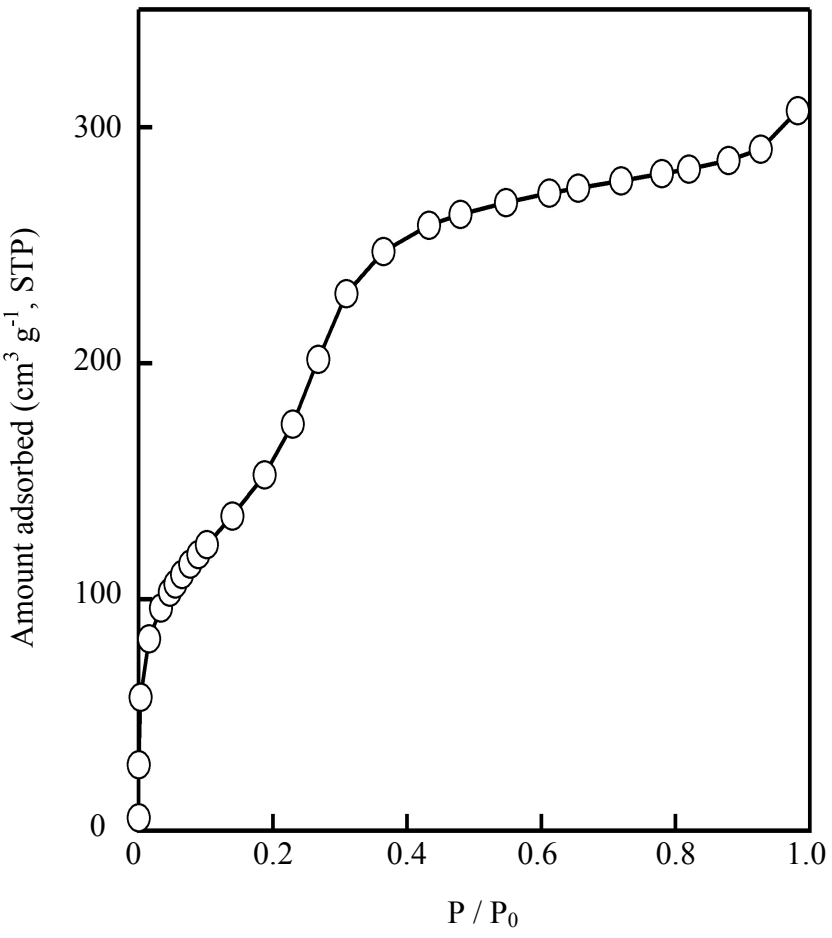

Figure 6-9. N_2 adsorption isotherm of the hydrated □-sodium disilicate-C_{16}TMA compound (C_{16}TMA/Si = 2.0) after calcination (SSW-1).

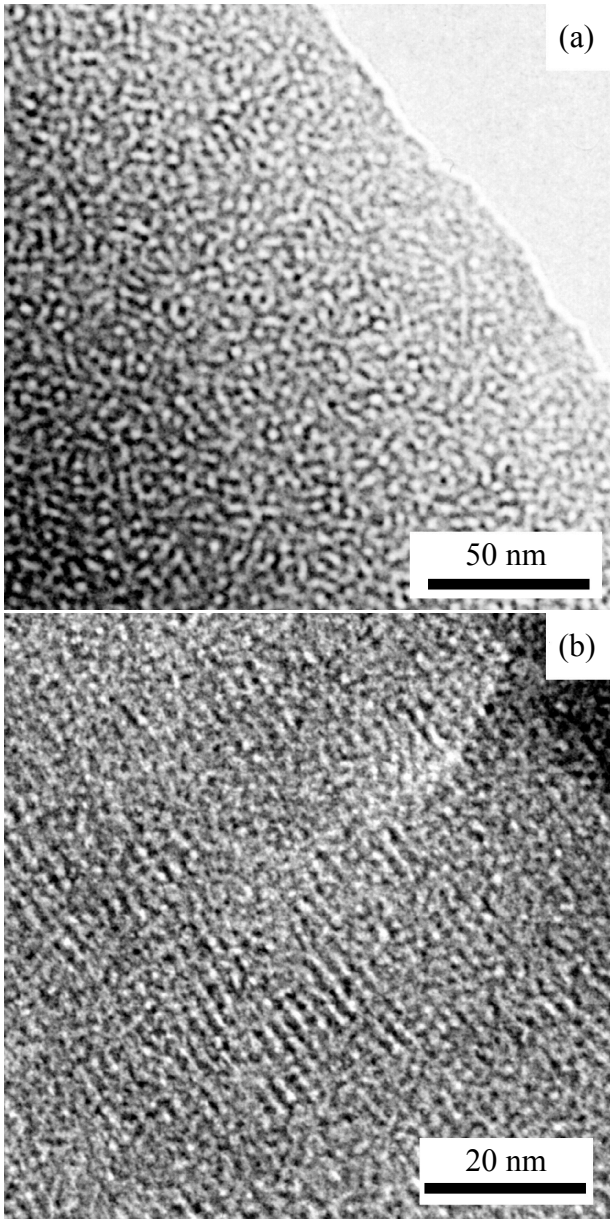

Figure 6-10. TEM images of the hydrated □-sodium disilicate-C_{16}TMA compound (C_{16}TMA/Si = 2.0) after calcination (SSW-1).

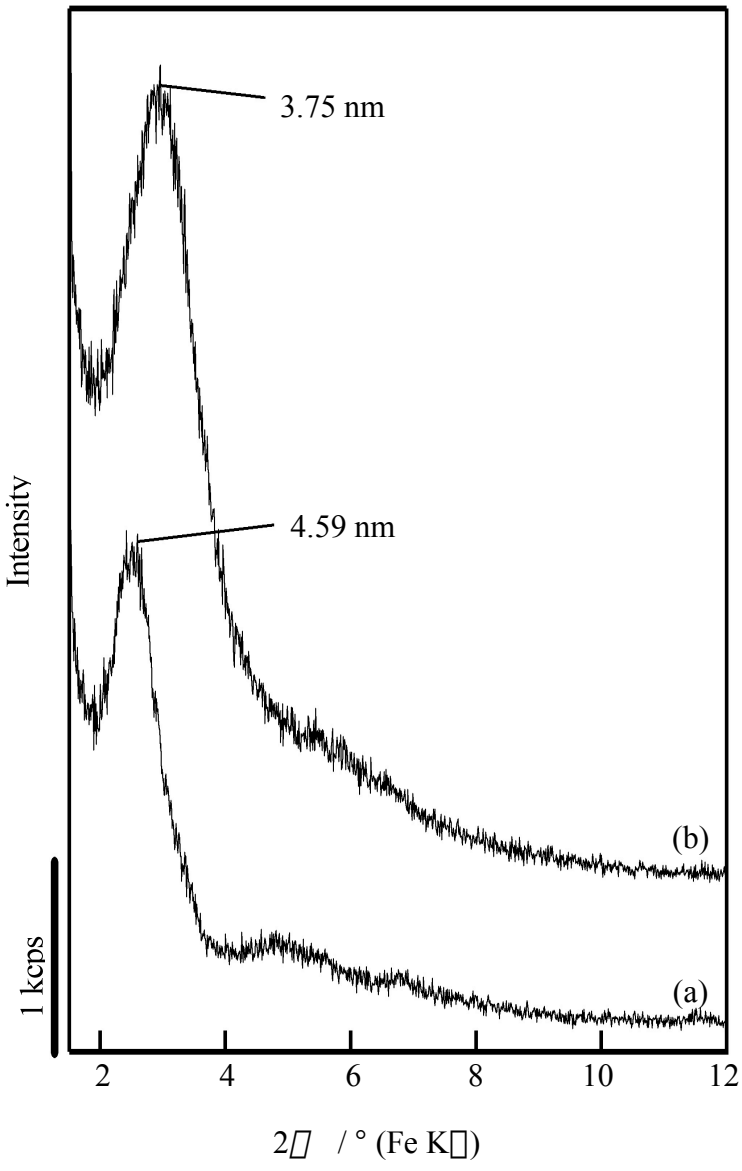

Figure 6-11. XRD patterns of (a) hydrated α-sodium disilicate-C_{16}TMA, (b) calcined product of (a) (C_{16}TMA / Si = 4.0).

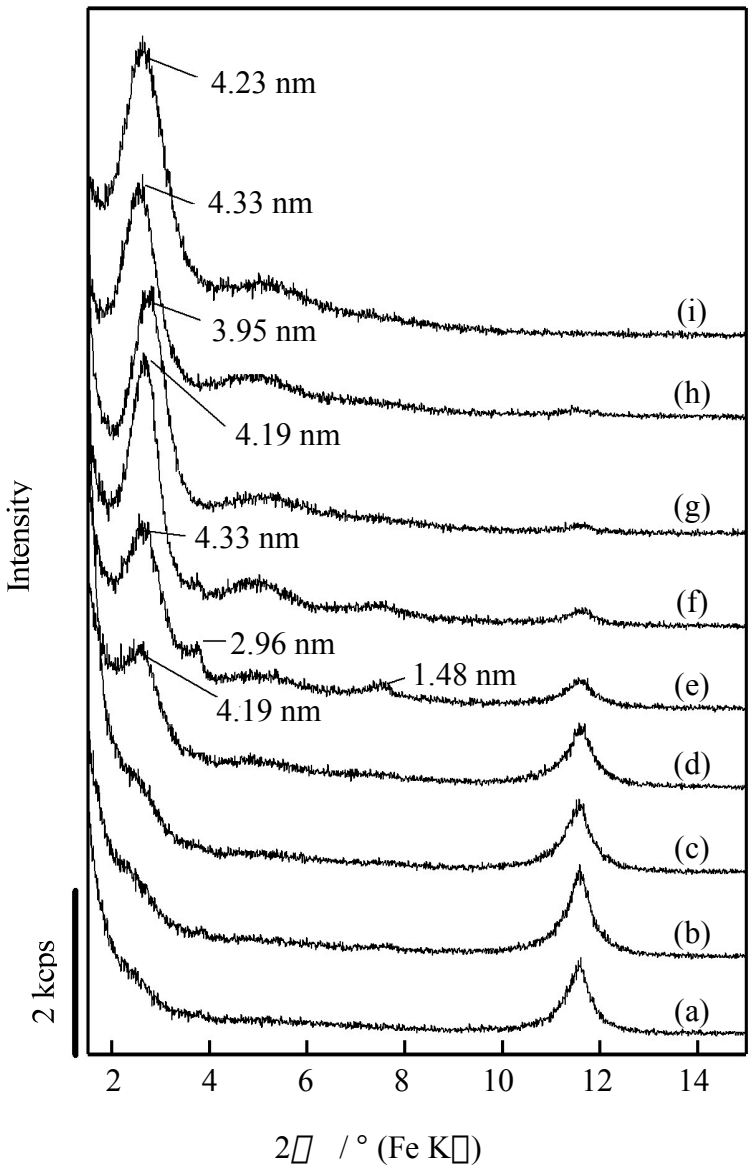

Figure 6-12. XRD patterns of the hydrated □-sodium disilicate-C_{16}TMA compound (C_{16}TMA/Si = 2.0) prepared at R.T. for (a) 3 h, (b) 6 h, (c) 12 h, (d) 1 d, (e) 3 d, (f) 5 d, (g) 7 d, and 70 ˚C for (h) 3 h and (i) 6 h.

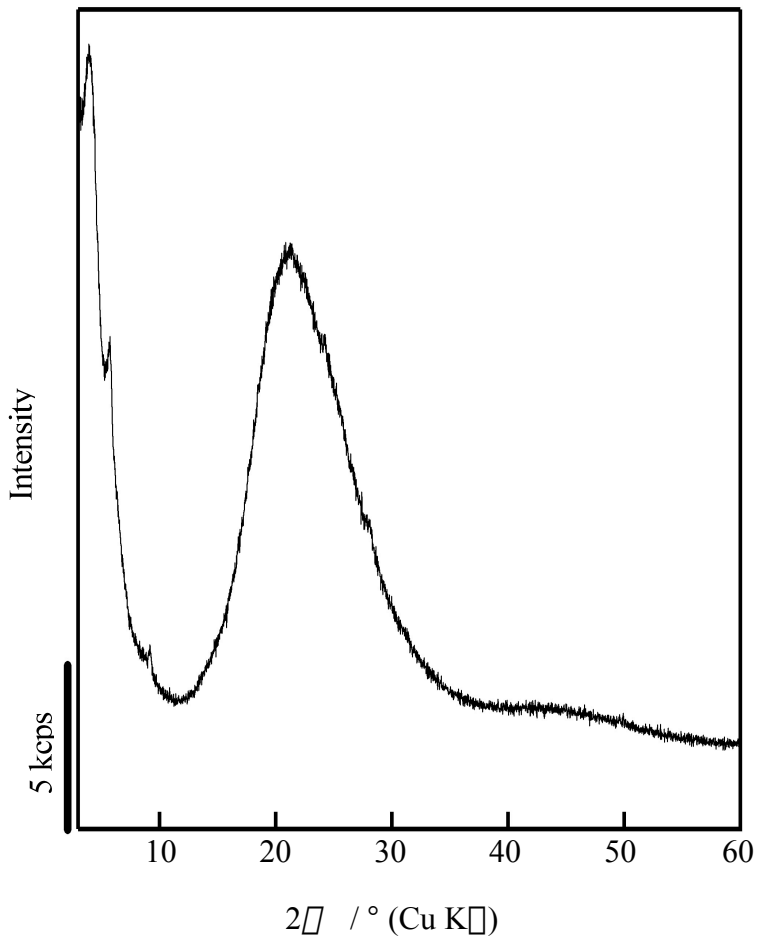

Figure 6-13. XRD patterns of hydrated α-sodium disilicate – C_{16}TMA mesostructured silica (C_{16}TMA / Si = 2.0).

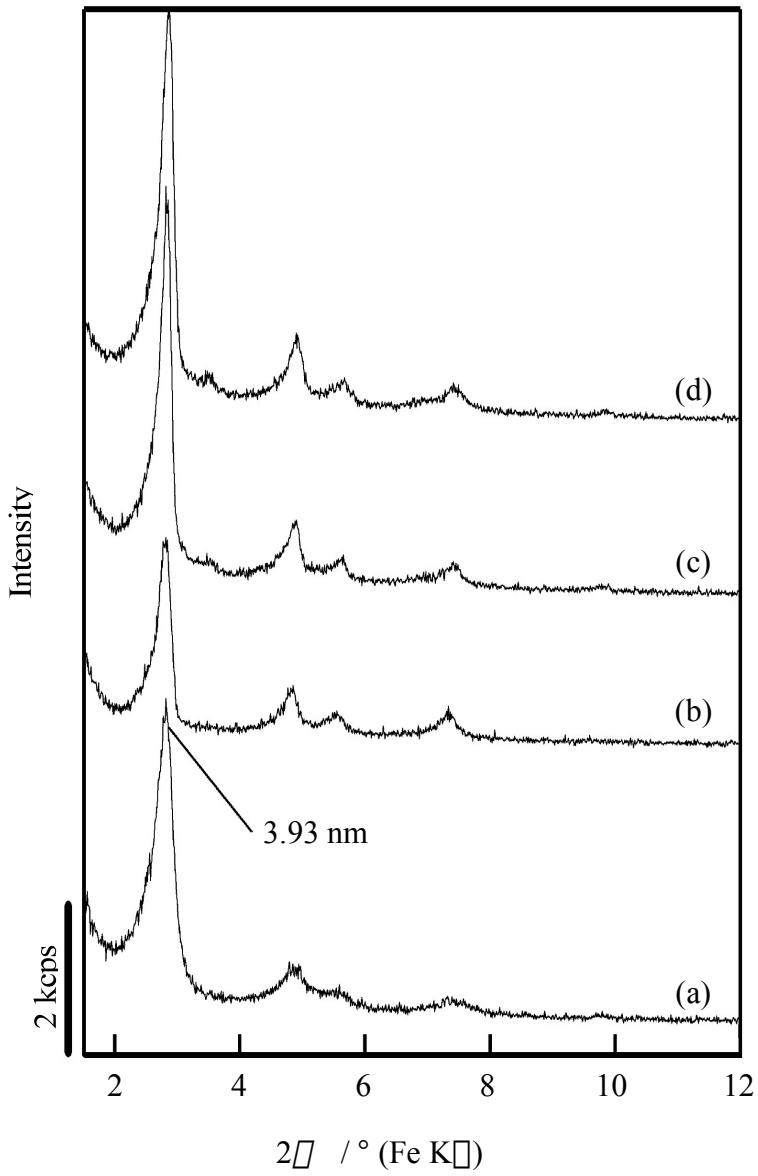

Figure 6-14. XRD patterns of the hydrated α-sodium disilicate-C_{16}TMA compound at the C_{16}TMA/Si ratios of (a) 0.2, (b) 0.5, (c) 0.7, and (d) 1.0.

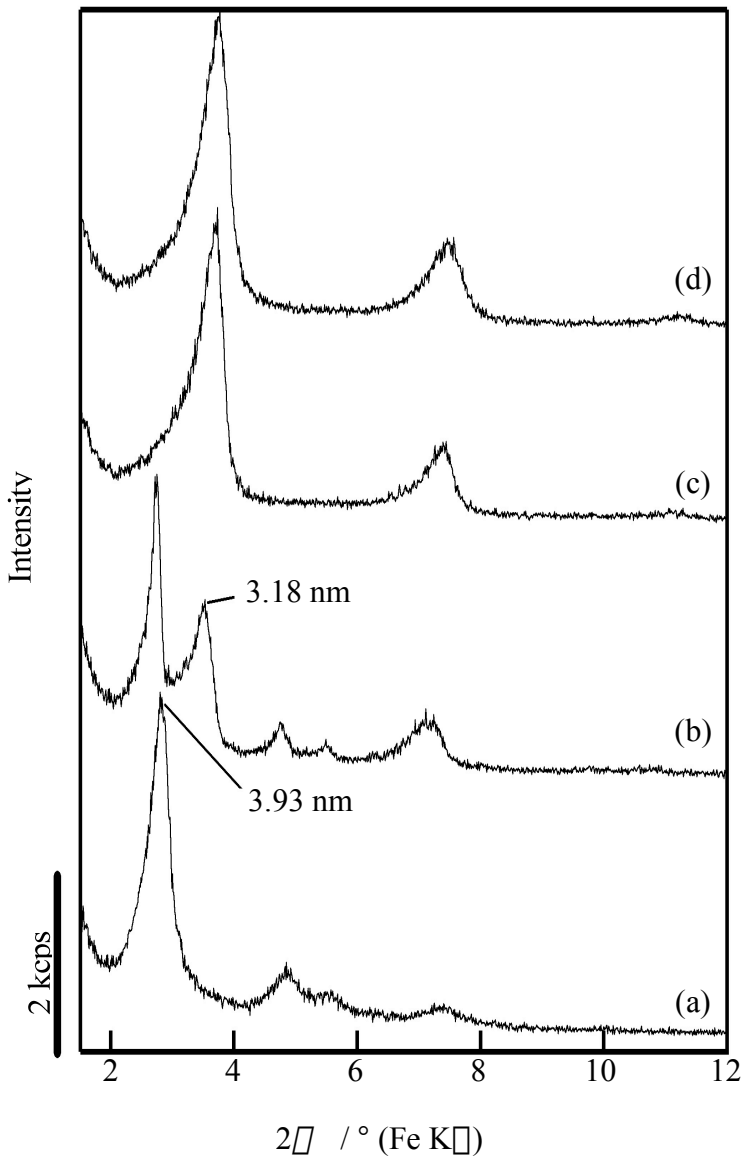

Figure 6-15. XRD patterns of kanemite-C_{16}TMA mesostructured compound at the C_{16}TMA/Si molar ratios of (a) 0.2, (b) 0.5, (c) 0.7, and (d) 1.0.

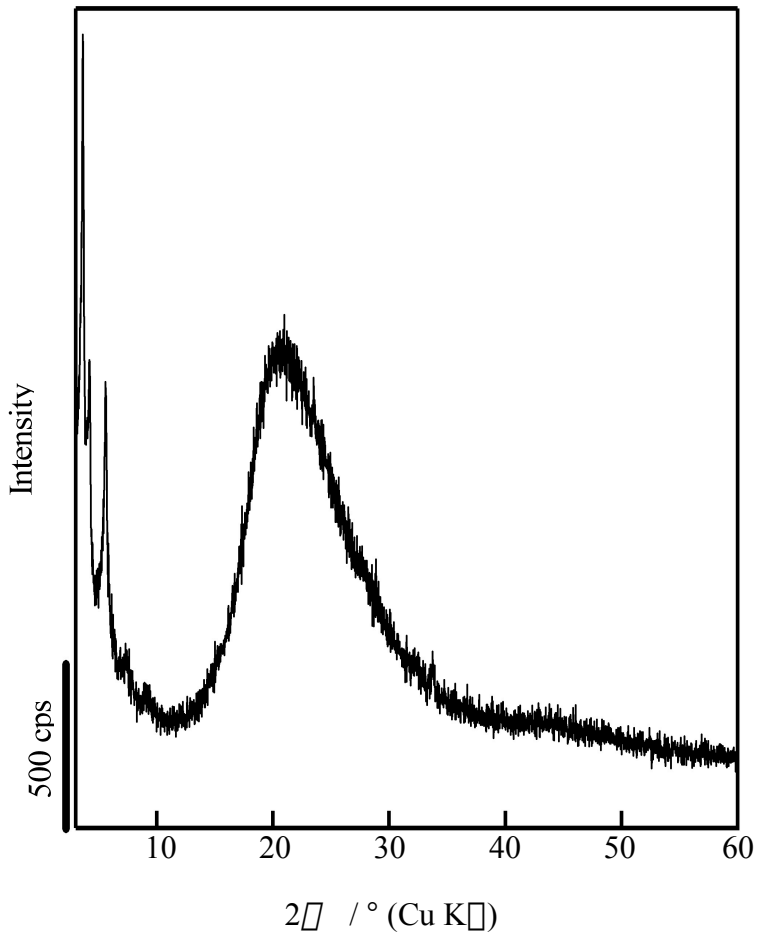

Figure 6-16. XRD patterns of hydrated α-sodium disilicate – C_{16}TMA mesostructured silica (C_{16}TMA / Si = 0.2).

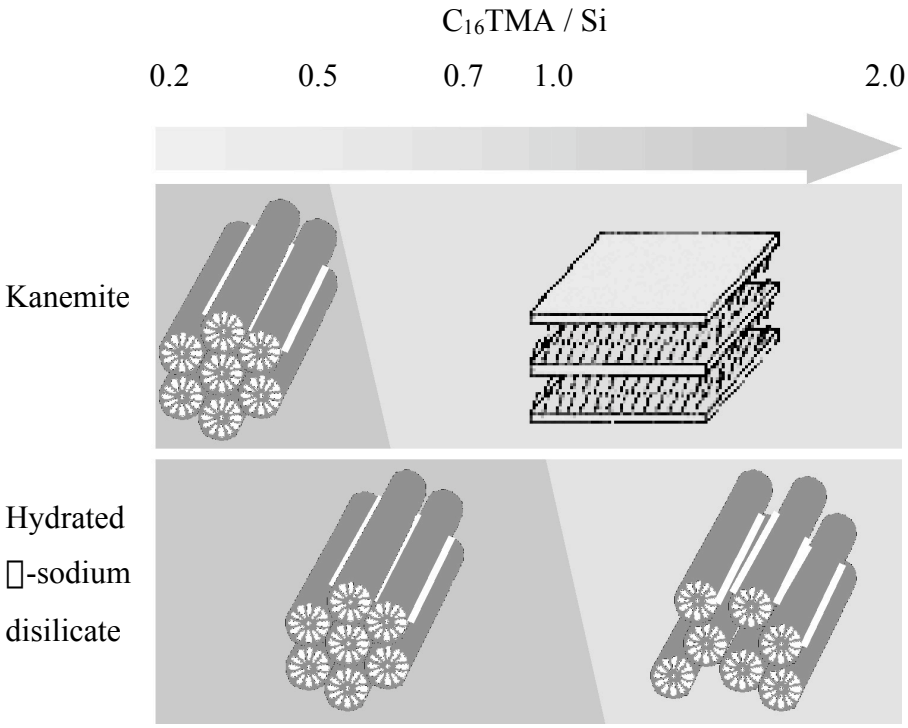

Figure 6-17. Structural variation with the C_{16}TMA/Si ratio.

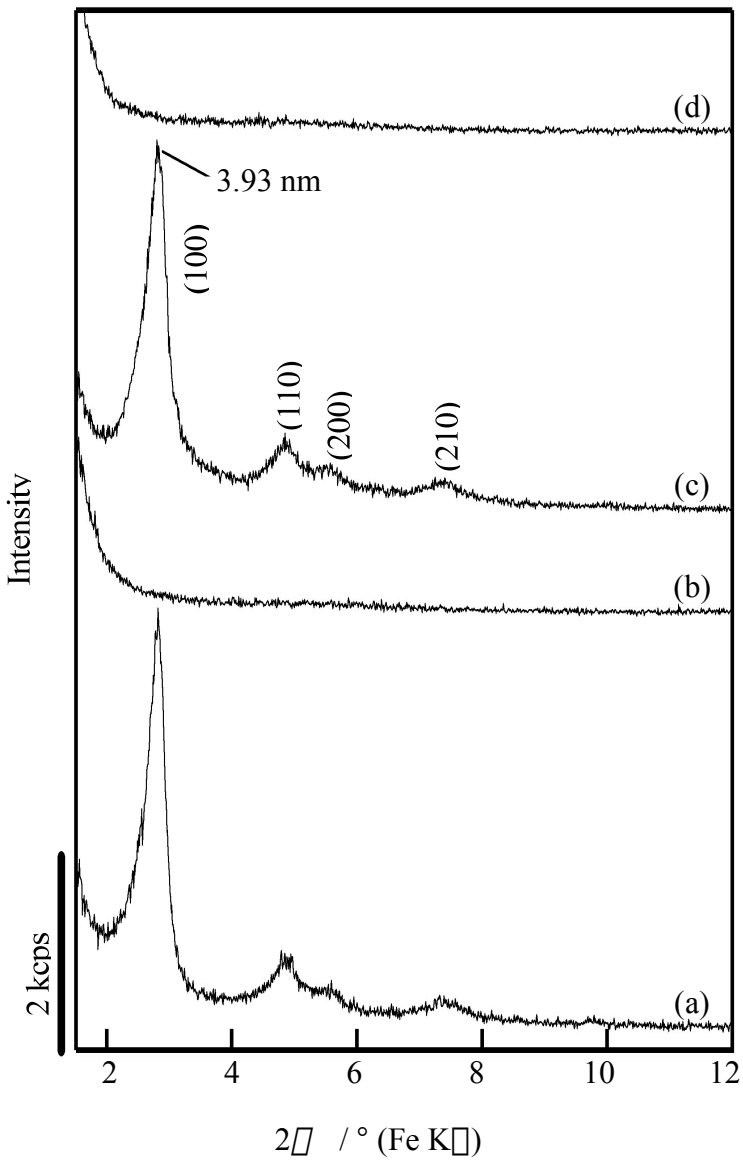

Figure 6-18. XRD patterns of (a) the hydrated α-sodium disilicate-C_{16}TMA compound (C_{16}TMA/Si = 0.2), (b) the calcined product of (a), (c) the kanemite-C_{16}TMA compound (C_{16}TMA/Si = 0.2), and (d) the calcined product of (c).

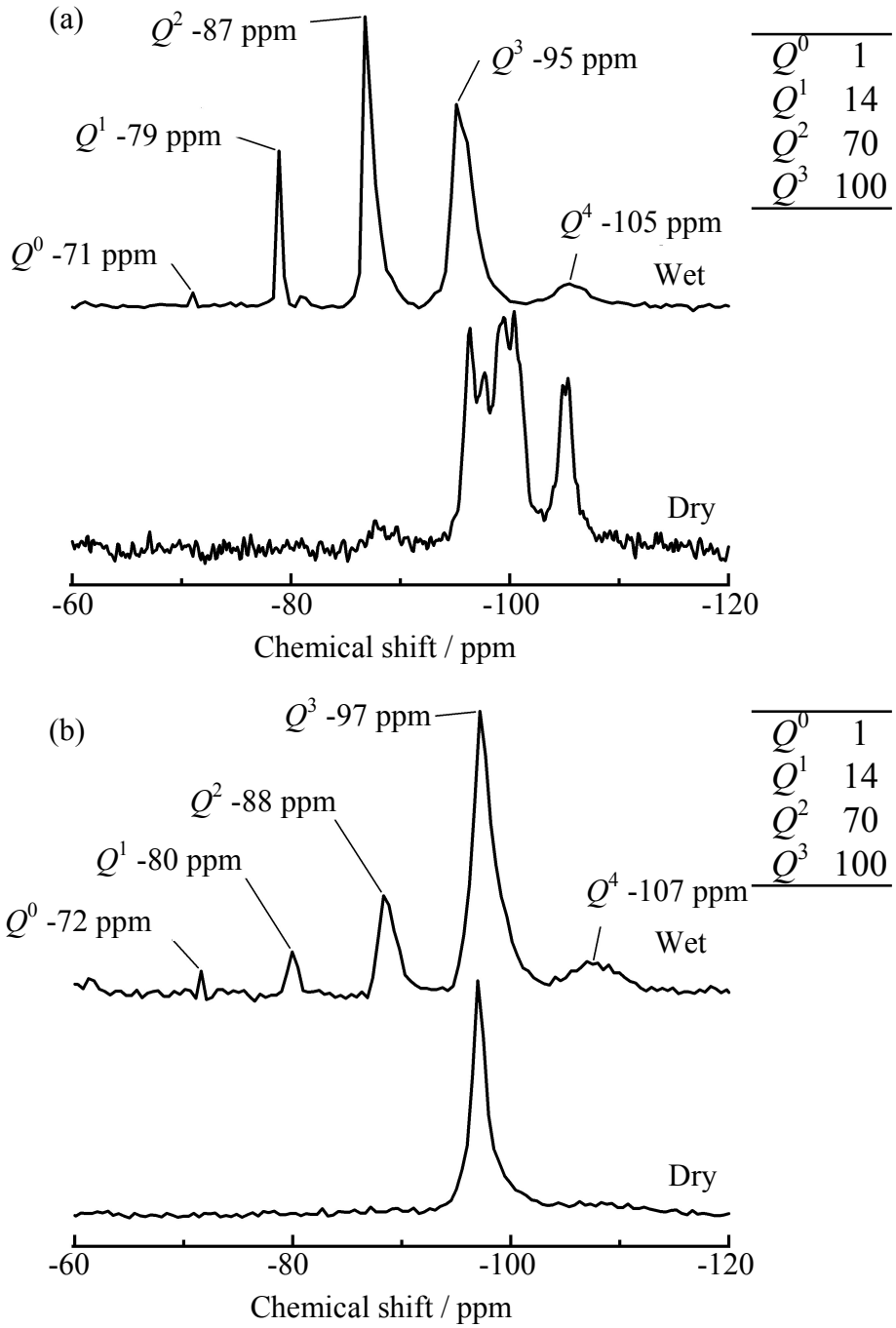

Figure 6-19. ^{29}Si MAS NMR spectra and the integrated intensity ratios of wet slurries of (a) hydrated □-sodium disilicate and (b) kanemite.

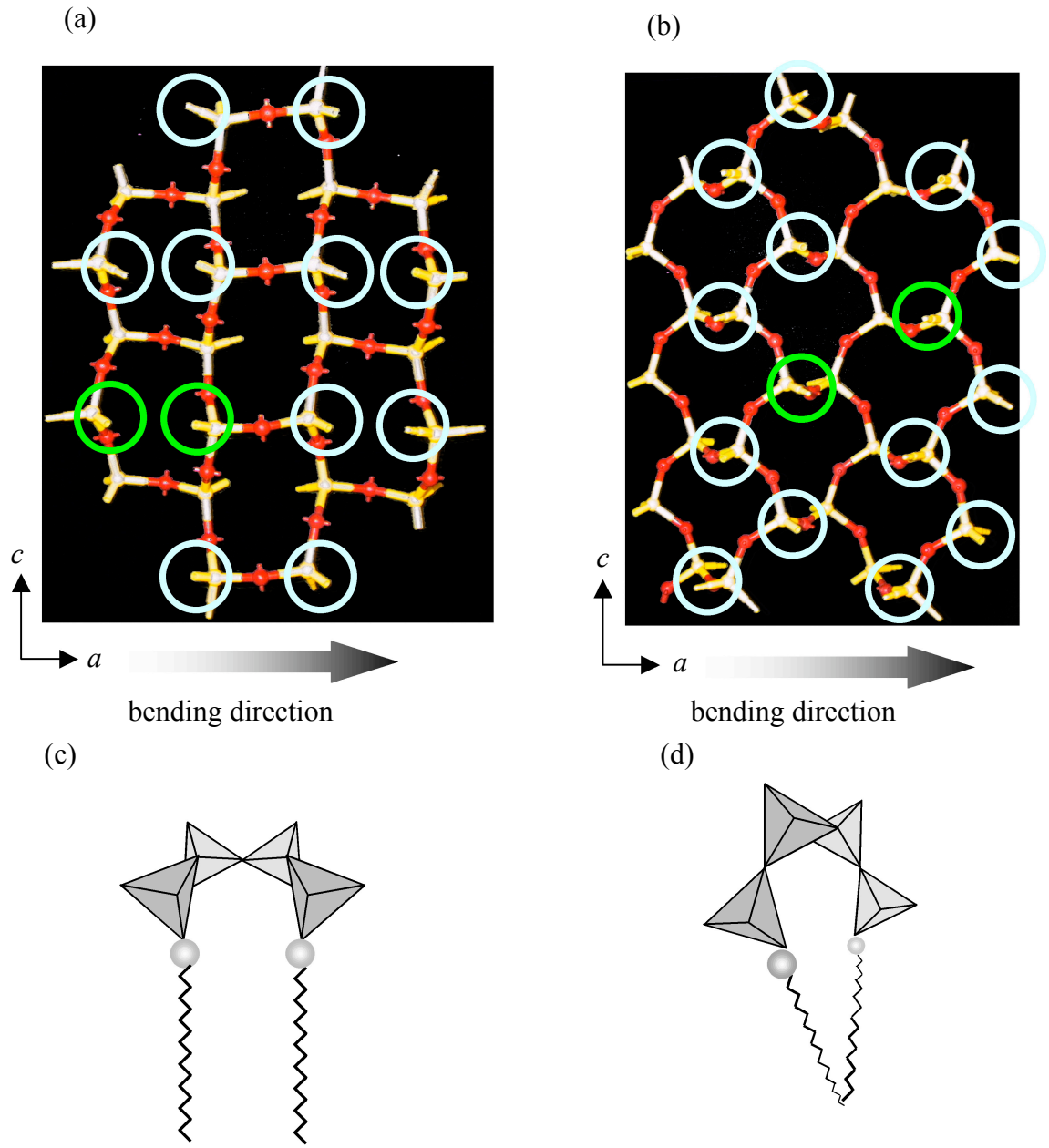

Figure 6-20. The distances between the Si–O^- sites of (a) kanemite and (b) hydrated □-sodium disilicate and the difference of the mesostructures derived from (a) and (b) (c,d).

Chapter 7

Conclusions

Silica-based mesostructures are derived from a layered polysilicate kanemite, and the formation is induced by the reactions with various cationic surfactants with different geometrical packings. In the surfactant-kanemite systems, several reactions such as the interactions of cationic surfactants with the silicate sheets, the fragmentation or bending of the silicate sheets, and the geometrical packing of surfactant molecules are complicated. However, the formation of ordered (lamellar, 2-d hexagonal, and 2-d orthorhombic) and disordered mesostructured materials can be simply summarized on the basis of the presence of layered surfactant-silicate intermediates. The obtained insights are potentially applicable for simultaneous control of short (framework) and long range orderings (mesostructure) in mesostructured materials obtained from layered polysilicates. Several research groups have challenged the transformation of silicate frameworks of MCM-41 into crystallized frameworks. However, the mesostructural orderings of MCM-41 was lost by crystallization though catalytic performance and hydrothermal stability of MCM-41 were enhanced by post-treatment. In contrast, silicate frameworks of lamellar mesophase silicates can be successfully transformed into molecularly ordered inorganic frameworks by hydrothermal post-treatment. The molecularly ordered inorganic frameworks are formed depending on the shapes of head groups in cationic surfactants. Therefore, the sheet-like silicate framework in KSW-2 constructing semi-squared mesopores is especially attractive to realize the preparation of mesostructured and mesoporous materials with truly crystallized silicate frameworks.

KSW-2 is a novel mesoporous silica with semi-squared mesopores and is obtained by mild acid treatment of layered alkyltrimethylammonium silicate mesostructured materials in which the silicate is derived from kanemite, a single layered sodium polysilicate. The effect of the carbon chain length of the alkyltrimethylammonium cations on the mesostructures was investigated. Hexadecyl- and tetradecyl-trimethylammonium exchanged silicate mesophases are successfully converted to the precursors with higher ordering, whereas the mesophase with

octadecyltrimethylammonium cations exhibit a strong tendency to hold the layered nature. On the other hand, the mesophase containing dodecyltrimethylammonium cations tends to be converted to less ordered three dimensional structure at relatively higher pH region. The width of the semi-squared pore of KSW-2 derived from hexadecyltrimethylammonium cations is larger than that from tetradecyltrimethyl-ammonium cations. The structure of the mesophase containing C_{18}TMA cations collapsed after the heat treatment at 550 °C for 6 h. The mesophase derived from C_{12}TMA cations was calcined under the same conditions and the product was porous with a very disordered structure.

Layered sodium disilicate □-$Na_2Si_2O_5$ containing four-coordinated Al was successfully prepared by heating treatment at appropriate temperatures, depending on the Al contents. Al-containing □-$Na_2Si_2O_5$ were transformed into Al-kanemite without the variation of Al coordination. By the reaction of Al-kanemite with C_{16}TMA, 2-d orthorhombic mesoporous silica (KSW-2) containing AlO_4 units can be obtained. This synthetic route was useful for the isomorphous substitution of Al atoms within the silicate framework of KSW-2. The incorporation of Al affords the acid sites that are more effective for the adsorption of cationic dyes than siliceous KSW-2. This study reveals that the incorporation of other metal oxides into starting layered silicates is feasible for realizing the compositional variation of ordered mesoporous silicas derived from layered silicates, which would be applicable to various catalytic and adsorptive reactions.

Mesoporous silica KSW-2 and the precursor are silylated by the reaction with chlorotrimethylsilane and octyldimethlchlorosilane without the collapse of the mesostructures. The semi-squared mesopores found only for KSW-2 and the precursor are retained after silylation. The grafted numbers for the silylated derivatives derived from the precursor are larger than those from KSW-2. All the silylated derivatives show

the lower values of BET surface area, pore volume, and width of the mesopore than those for KSW-2 and the values for ODMS derivatives are lower than those for TMS derivatives because of the steric hindrance. The hydrophobicity and the stability against water vapor significantly increase by silylation. The calcined products of the silylated derivatives have shorter widths of the mesopores than KSW-2. The wall thickness and the width of the pore of KSW-2 can be tunable if silylating agents are properly chosen. Therefore, the present results suggest possible molecular design based on this mesoporous silica. Novel silica-organic hybrids are obtained by silylation of mesoporous silica KSW-2 and the precursor. Because KSW-2 has a very unique shape of mesopores, the organic derivatives should afford distinctive characteristics, such as specific reaction media and adsorption sites, which other mesoporous silicas cannot provide. Although the regularity of the silicate framework retained in the precursor was not found for the silylated derivatives by powder XRD, there should be some ordering in the framework because restructuring of the skeleton cannot occur during the silylation. Further researches are required toward the construction of organically modified mesoporous silicas with retaining a higher ordered silica network close to the original structure, which would be realized under milder reaction conditions by using well designed reagents.

On the basis of the reaction between kanemite and C_{16}TMA, mesostructured materials were synthesized by using δ-$Na_2Si_2O_5$ as a starting material. The effect on the formation of mesostructured materials by the structural difference of sodium disilicate as a starting material was studied.

In the system of C_{16}TMA/Si = 2.0, wormhole like mesoporous material formed from hydrated δ-$Na_2Si_2O_5$, while lamellar mesostructure material formed from kanemite. In regarding to organic content, hydrated δ-$Na_2Si_2O_5$ has less anion charge density than kanemite. Thus, C_{16}TMA ions with hydrated δ-$Na_2Si_2O_5$ forms micelle structure more easily than with kanemite and the hydrated δ-$Na_2Si_2O_5$ with the micelle structure tends

to form mesostructure.

On the other hand, in the system of C_{16}TMA/Si = 2.0, ordered hexagonal mesostructure forms from both hydrated □-$Na_2Si_2O_5$ and kanemite. The calcined product, FSM-a, has higher thermal stability at 1000 ℃ than FSM because of the condensation of silica framework.

This thesis shows synthetic strategy towards the variation of novel mesoporous silica system derived from layered polysilicate by using surfactants with various alkyl chain length, difference of structure in starting materials, and surface modification. The formation mechanism of KSW-2 projected here is based on the bending of intralayer-condensed silicate sheets of kanemite. Although the units are not fully retained after calcination, this approach introduced here is promising to incorporate inorganic structural units to mesostructured materials. The synthetic methods reported in this thesis are applicable to the intended materials design, such as control of pore diameter, hydrophobicity, catalytic property, for actual application in the area of molecular sieve, catalysts, catalyst supports, adsorbents, inclusion vessels, and so on.

Acknowledgments

I would like to express my sincere appreciation to Professor Kazuyuki Kuroda in Waseda University for kind encouragement, philosophical suggestions, careful reviewing of the manuscript as well as giving me the opportunities to study pioneered and exciting research topics. I also deeply appreciate to Professor Tetsuya Osaka and Professor Yoshiyuki Sugahara in Waseda University for reviewing and discussing on the dissertation.

I wish to express my gratitude to Dr. Tatsuo Kimura, Dr. Atushi Shimojima, and Dr. Tetsuro Itagaki for their valuable advices. I also acknowledge Messrs. Daigo Ito, Koji Inoue, Munetaka Kato, and Masatsune Nagao in Waseda University. Thanks to their supports, I have accomplished my thesis.

I am also grateful to Professor Miki Niwa, and Professor Naonobu Katada in Tottori University for their collaboration and useful discussion on the acidity of KSW-2 and Al-KSW-2 proved by TPD of ammonia.

Finally, I am truly grateful to my family, my mother, father, sister and brother for their boundless supports.